EDAC 175-070.02

STRUCTURAL CONDITION DOCUMENTATION AND STRUCTURAL CAPACITY EVALUATION OF THE ATOMICS INTERNATIONAL NUCLEAR MATERIALS DEVELOPMENT FACILITY AT SANTA SUSANA, CALIFORNIA

FOR

EARTHQUAKE AND FLOOD

TASK II -- STRUCTURAL CAPACITY EVALUATION

SEISMIC EVALUATION

prepared for
Nuclear Test Engineering Division
LAWRENCE LIVERMORE LABORATORY
Livermore, California

August 1978

1361 191

EDAC
ENGINEERING DECISION ANALYSIS COMPANY, INC.
480 CALIFORNIA AVE., SUITE 301, PALO ALTO, CALIF. 94306
2400 MICHELSON DRIVE, IRVINE, CALIF. 92715
BURNITZSTRASSE 34, 6 FRANKFURT 70, W. GERMANY

LIST OF TABLES

Table	Title	Page
3-1	System Damping Ratios and Ductility Factors for NMDF Building Analysis	3-20
3-2	Element Damping Ratios and Ductility Factors for Roof Girder Vertical Analysis and Wall Panel Transverse Analysis	3-20
3-3	Summary of Seismic Capacities Affecting Confinement Barriers	3-21
4-1	Summary of Seismic Capacities Affecting Critical Equipment	4-7
5-1	Summary of Critical Seismic Capacities	5-4

LIST OF FIGURES

Figure	Title	Page
2-1	NMDF Building Floor Plan	2-5
2-2	Foundation Plan	2-6
2-3	NMDF Major Structural Elements	2-7
2-4	Exterior Elevations	2-8
2-5	Typical Wall Panel Details	2-9
2-6	Typical Wall Panel Connection Details	2-10
2-7	Typical Roof Diaphragm Connection at Walls	2-10
2-8	Vault Section	2-11
2-9	Mezzanine Details	2-11
3-1	Lateral Force Resisting Systems	3-22
3-2	Finite Element Model of South Wall	3-23
3-3	South Wall Critical Regions and Deflected Shape	3-24
3-4	Analysis Response Spectra	3-25
3-5	North-South Lateral Force Resisting System Model	3-26
3-6	East-West Lateral Force Resisting System Model	3-27
3-7	Equivalent Frame Model of South Wall	3-28
3-8	Basic Structure Collapse Mode	3-29
4-1	Location of Critical Glove Boxes and Equipment within Glove Box Room	4-8
4-2	Basic Glove Box Assembly	4-9
4-3	Location of Ductwork and Exhaust Filters	4-10
4-4	Pipeway Support and Bracing	4-11

SYNOPSIS - TASK II

This report presents the results of the Task II -- Structural Capacity Evaluation of the Atomics International Nuclear Materials Development Facility (NMDF), located at Santa Susana, California. The purpose of the Task II effort was to evaluate the structural capacity of those building structures and critical equipment components which could potentially release hazardous chemicals into the environment from the NMDF facility as a result of damage or failure during an earthquake or flood. The NMDF site, however, is not subject to flooding. Therefore, the structural capacity evaluation is limited to seismic loading conditions.

The Task II effort focused primarily on the building structure as representing the final confinement barrier for release of hazardous chemicals. The designated process equipment such as glove boxes and exhaust ducting were also evaluated for structural capacity. The loss of primary confinement due to (1) direct glove box failure, or from (2) indirect glove box damage caused by interaction with adjacent equipment and connections, is identified as the ultimate mode of release resulting from extreme earthquake hazard. The structural capacity of the building structure and associated equipment systems as related to the ultimate mode of release are addressed in this report. Operational and functional aspects of the facility are not addressed in this report.

The NMDF is a one-story windowless tilt-up concrete building with a lightweight concrete-fill steel roof deck with roof beam support, and a concrete floor slab on grade. The building is rectangular in plan with a length-to-width ratio of 3.25:1 (Figure 2-1). Deviations from structural symmetry include the vault, mezzanine, and difference in wall thickness for the north wall. The vault is located on the exterior side

of the west wall and is a cast-in-place concrete box. The small mezzanine (partial second floor) area is located adjacent to the west wall.

The lateral force resisting system is a shear wall box system tied together by a relatively flexible steel roof diaphragm. The diaphragm consists of light weight concrete-fill on steel decking welded to the main roof beams and is connected to the shear walls by welds to the peripheral steel chord members which are anchored to the walls at the roof line. The structure may be considered to resist seismic forces as two independent systems; one for each major building direction, north-south and east-west. Due to the diaphragm flexibility and large length-to-width ratio, torsional coupling of the two systems will be negligible. For both systems, the roof and the tributary wall inertia is transferred to the active panel shear walls by the diaphragm acting as a deep beam with chord flanges. The vault is weakly coupled to the east-west system through flexure of the above vault wall panel (See Figure 2-3). The in-plane wall seismic shear forces are transferred to grade through the individual spread footings and through the building floor slab. The slab is positively connected to the wall panels near the wall base for this purpose.

The evaluation of the structure, in terms of ground acceleration capacity, utilized simple finite element dynamic models to assess the component stress levels associated with a given level of ground motion. The controlling collapse capacities (0.60 - .87g) were all associated with loss of diaphragm support for the west and east walls. Once the diaphragm resistance is lost, the roof girder/column pin-jointed frames with attached wall panels will progressively collapse after only a few cycles of motion. The median seismic capacity of the east-west force resisting system is 0.60g. Based upon the statistical uncertainty bound analysis, the estimated 1σ standard deviation upper and lower bound seismic capacities are 0.88g and 0.4g respectively.

The interior partitions and secondary architectural systems in the critical areas do not sustain major damage prior to diaphragm failure and, therefore, are not themselves critical in terms of release of hazardous material.

The equipment items exhibit a higher structural capacity than the structural system and are generally only affected by total facility collapse or by the large relative displacements between the floor and the roof which occur just prior to collapse.

1. INTRODUCTION

This document presents the results of the structural evaluation of the Atomics International Nuclear Materials Development Facility (NMDF), located at Santa Susana, California. The report is submitted in accordance with Contract No. 5453703, dated 2 May 1977, between Lawrence Livermore Laboratory (LLL) of the University of California and Engineering Decision Analysis Company, Inc. (EDAC). The Task II Structural Evaluation and prior Task I Condition Documentation by EDAC (as defined in the referenced contract) are part of an overall natural hazards evaluation (Reference 1) performed by a group of consultants expert in the various hazard fields. The study is sponsored and directed by the Fuel Reprocessing and Recycle Branch of the United States Nuclear Regulatory Commission (USNRC). The natural hazards study includes evaluation of several facilities at different locations within the United States. EDAC is responsible for the structural evaluation of these facilities for both earthquake and flood induced loadings.

Atomics International (AI) maintains and operates the Nuclear Development Field Laboratory (NDFL). The NDFL is located at the site of the Liquid Metals Engineering Center at Santa Susana, California in the Simi Hills of Ventura County, approximately 29 miles northwest of downtown Los Angeles. The building of interest for the Natural Hazards Study within the NDFL is Building 055, denoted as the Nuclear Materials Development Facility (NMDF). The NMDF was constructed within the period 1966-67.

The evaluation of possible flooding at the NMDF site (Reference 2) has indicated that the site is not subject to flooding. Consideration of local precipitation flooding indicates that a depth of flow less than six inches should be expected due to a one-hour

Probable Maximum Precipitation event. Existing drainage facilities are assumed adequate to handle such a flow. Therefore, the analyses discussed in this report consider only seismic loading conditions and focus on those portions of the structure and designated critical equipment items which can result in the loss of a confinement barrier for hazardous chemicals.

The structural evaluation effort was broken into two phases or tasks. The Task I effort encompassed the documentation of the present condition of the NMDF facility including a review of drawings and specifications related to the structure and critical equipment. The Task I report (Reference 3) identified the critical locations within the facility, presented details of the critical process equipment, the structural systems which are able to carry lateral loads, and described the analysis procedures which would be subsequently used in the Task II seismic capacity evaluation of the NMDF facility. In addition to providing a data base for structural evaluations by EDAC, the Task I condition documentation is intended to provide structural data for the extreme wind load evaluation by other consultants.

The Task II effort encompasses the analysis of the building structure and all critical equipment in order to establish the ground motion acceleration which causes the structural or critical component to collapse or to result in loss of confinement of hazardous chemicals. This report describes the results of the Task II analyses which are presented in the following sections.

Section 2. Facility and Site Description
Section 3. Evaluation of Structural Behavior
Section 4. Evaluation of Critical Equipment
Section 5. Structural Damage Scenario

Section 2 presents a brief discussion of the Atomics International facility layout, its critical areas and general structural description, together with a brief discussion of the general seismicity of the region. Section 3 presents the seismic capacity evaluation of the building structure including a description of the structural systems, a discussion of the analysis procedures used in the seismic evaluation, and a description of each of the structural behavior models together with the analysis results pertaining to the collapse or confinement breach of the building structure. Similarly, Section 4 presents the evaluation of the critical equipment items, again describing the analysis procedures and the results. Section 5 summarizes the capacity evaluation of the NMDF facility by means of the presentation of a seismic structural damage scenario which describes the potential damage to the facility at various acceleration levels of seismically induced ground motion.

2. FACILITY AND SITE DESCRIPTION

This section of the report presents a brief discussion of the structural information pertinent to the Task II seismic capacity evaluation of the Atomics International NMDF Facility. A general structural description of the NMDF building is given together with an identification of the critical areas and a discussion of the site seismicity. The interested reader is directed to the Task I Report (Reference 3) where information concerning the structural condition of the facility is given in more detail.

2.1 GENERAL STRUCTURAL DESCRIPTION

The NMDF is a one-story, windowless tilt-up concrete building with a lightweight concrete-fill steel roof deck with roof beam support, and a concrete floor slab on grade. The building is rectangular, approximately 62 feet by 202 feet in plan dimension and 17 feet high (above grade). The general layout of the building is indicated in Figure 2-1. All of the work directly related to fuel processing is carried out in the large glove box room which is separated from the remaining portion of the building by gypsum board/steel stud partitions. The vault is located on the exterior side of the west wall and is a cast-in-place concrete box extending approximately 11 feet above the finished floor line. A small mezzanine (partial second floor) area is located adjacent to the west wall.

The primary vertical load resisting system of the NMDF building is a steel roof deck supported by transverse steel roof beams spaced at 20 foot intervals which are simply supported by steel building columns along the east and west exterior walls. The columns in turn bear upon reinforced concrete spread footings resting on the natural soil materials. The footings are founded at least 1.5 feet below the natural soil surface. Floor slabs are supported on compacted fill. The foundation plan of the building is shown in Figure 2-2.

The lateral force resisting system is a shear wall box system tied together by a relatively flexible steel roof diaphragm. The diaphragm consists of light weight concrete fill on steel decking welded to the main roof beams and is connected to the shear walls by welds to the peripheral steel chord members which are anchored to the walls at the roof line. The major structural elements of the NMDF building are identified in the isometric view of the strucutre shown in Figure 2-3.

The concrete tilt-up panels are tied together to form continuous shear walls by means of concrete insert connections welded to the main building columns. The tilt-up panels also bear on the main building column isolated spread footings. The wall panels are not supported on foundation beams or walls, but rather span between each footing. However, ties between each wall panel and the floor slab are provided around the entire building periphery. Exterior building elevations are shown in Figure 2-4 with a typical precast wall panel and section shown in Figure 2-5. Typical roof diaphragm/wall connection details are shown in Figure 2-7.

Although the vault and mezzanine are not part of the primary wall/diaphragm lateral force system, their effect on overall system dynamic response must be considered. A section of the vault is shown in Figure 2-8. The portion of the vault precast panel above the vault roof is six inches thick while the portion below the roofline is nine inches thick. The remainder of the vault enclosure is nine-inch cast-in-place reinforced concrete. The mezzanine floor is a seven-inch concrete slab supported by steel decking which spans across the beam and pipe column support system shown in Figure 2-9. It should be noted that the lateral force resistance for the mezzanine floor and vertical support frame is provided entirely by the exterior columns and attached wall panels.

2.2 CRITICAL AREAS

The NMDF has been used in the past for a number of different processes related to fuel development which involve hazardous chemicals. Both mixed oxide and mixed carbide fuels have been handled within the facility. The most extensive past program involved development of mixed carbide

fuels and the current process configuration is for fabrication and processing of mixed carbide fuels. For purposes of the overall natural hazards study, critical areas are those locations in which hazardous chemicals are processed or stored in a dispersible form which makes loss to the outside possible should the confinement barriers be breached. Similarly, critical equipment is equipment which is used to process materials which include hazardous chemicals in dispersible form and whose structure serves as a primary confinement barrier.

The primary focus of the Task II effort is upon the building structure (final confinement barrier), architectural walls or partitions (secondary confinement barrier), and glove box equipment (primary confinement barrier) associated with the critical areas. The loss of primary confinement due to (1) direct glove box failure, or from (2) indirect glove box damage caused by interaction with adjacent equipment and connections, collapsing structural elements, or structure supported equipment components, is identified as the ultimate mode of release resulting from extreme earthquake hazard. The structural capacity of the building structure and associated equipment systems as related to the ultimate mode of release are addressed in this report. The continuity of operation of the facility and other functional aspects (safety related) affected by earthquake hazard are not discussed.

The areas of the NMDF identified as critical (Reference 4) for the handling of hazardous chemicals are the glove box room and the storage vault. The location of these critical areas are shown in Figure 2-1. The vault area is of secondary concern, with the prime concern being focused upon the glove boxes which process the hazardous chemicals in dispersible form. The confinement barriers for the glove box room consist of the process glove boxes as primary confinement barriers, the building walls and roof as final barriers, and nonstructural gypsum board/steel stud partitions as secondary barriers. Within the vault area, primary and secondary confinement is provided by the storage canisters in which the

hazardous chemicals are stored. The canisters are supported on racks anchored to the vault wall and floor. Final confinement for the storage vault is provided by the vault walls and roof.

2.3 SITE SEISMICITY

The NMFL site is situated in an isolated pocket in the Simi Hills of Ventura County, California. The site may be generally described as an irregular plateau covered by a thin layer of alluvial deposits with rock outcroppings above the more level patches and with peripheral eroded gullies. The area surrounding the site is rugged terrain typical of mountain areas of recent geological age. The NMDF building site is at an elevation of 1814 feet above sea level and is underlain by approximately 14 feet of silt-clay soil on sandstone.

A seismic risk analysis of the NMFL site was conducted by other consultants in order to define the ground motions which the facility could be expected to encounter. The results of this risk analysis are presented in Reference 5 and indicate that the site is in a region which historically has a high level of seismic activity. Based upon a probabilistic approach (Reference 5) peak seismic ground acceleration levels within the range of 0.18-0.25g are associated with a return period of 10 years, 0.28-0.41g are associated with a return period of 100 years, and 0.53-0.75g are associated with a return period of 1000 years. The shaking effects of ground motion were considered by specifying the general shape of statistically-based response spectra. The median spectra presented in WASH 1255 (Reference 18) for rock sites were judged (Reference 5) to be appropriate for the structural evaluation of the AI facility.

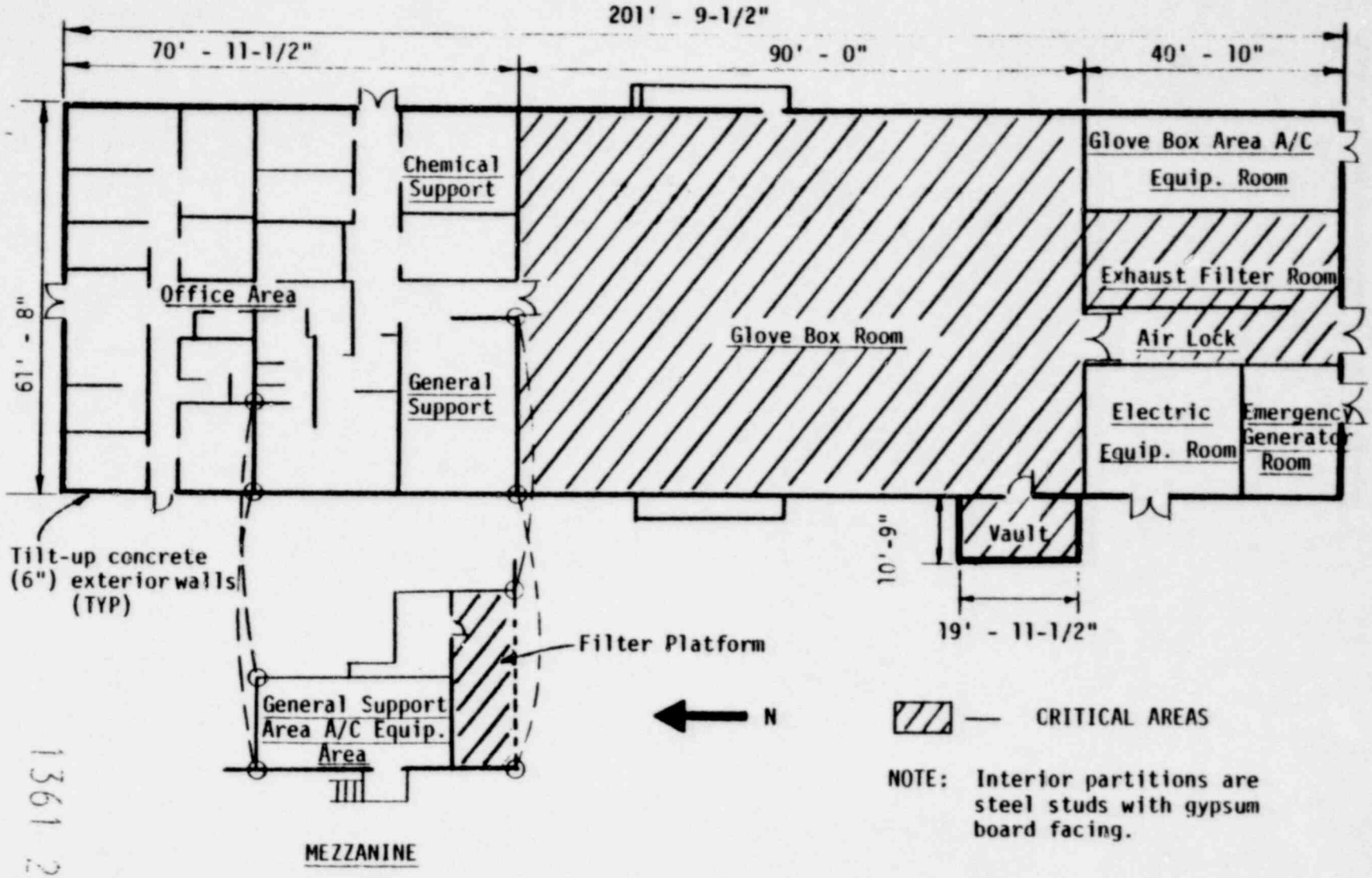

FIGURE 2-1 NMDF BUILDING FLOOR PLAN

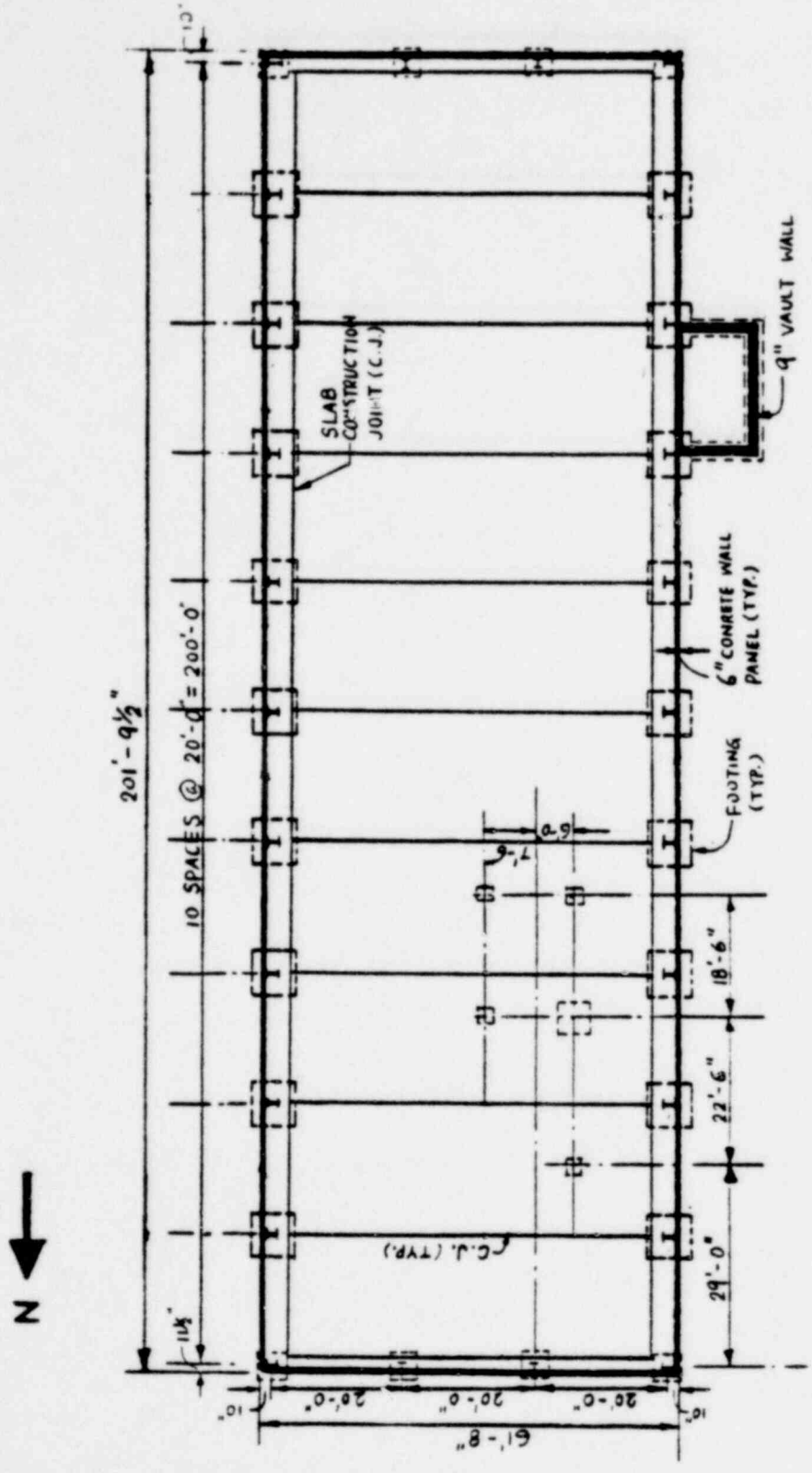

FIGURE 2-2. FOUNDATION PLAN

EDAC

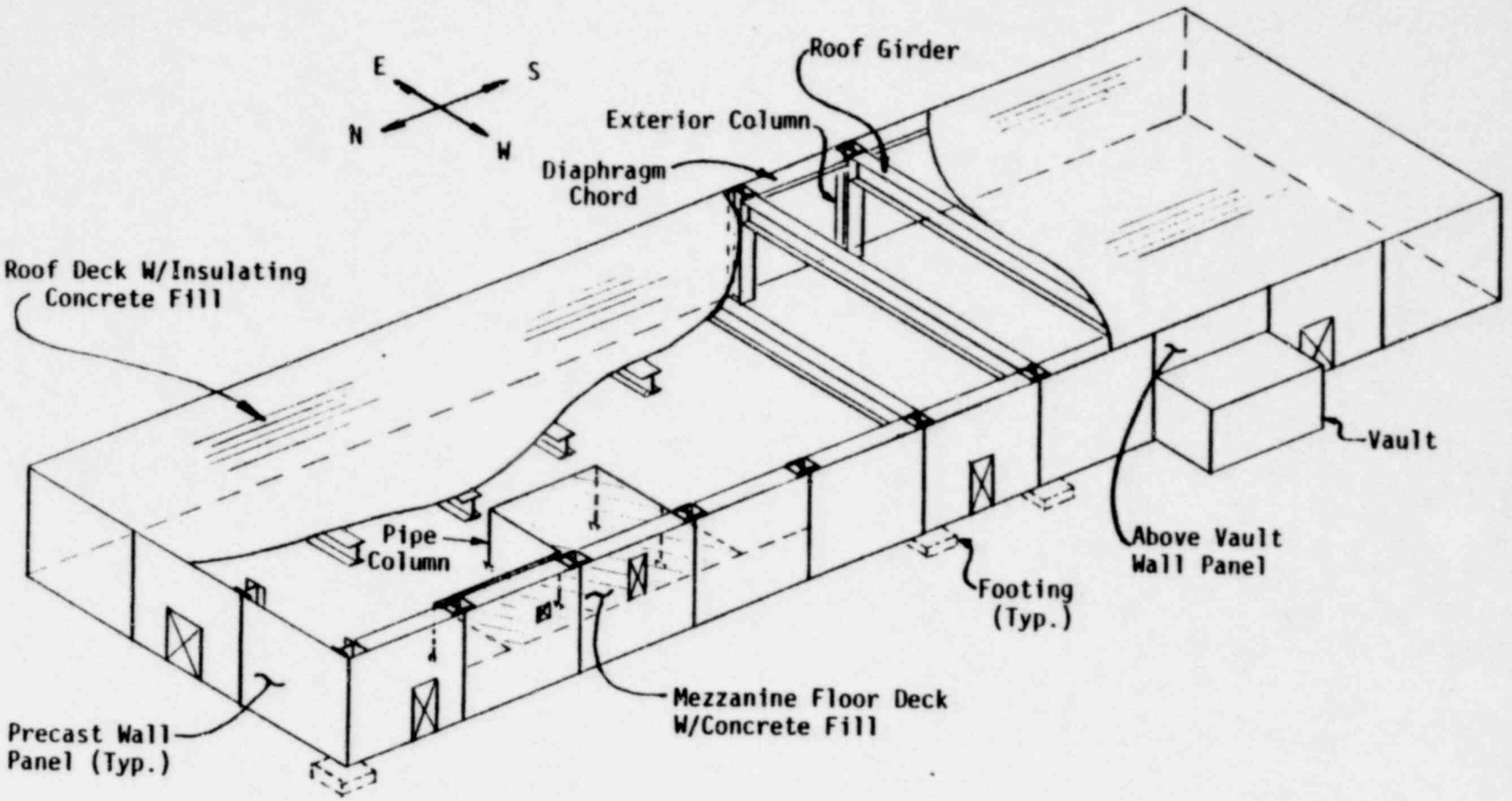

FIGURE 2-3. NMDF MAJOR STRUCTURAL ELEMENTS

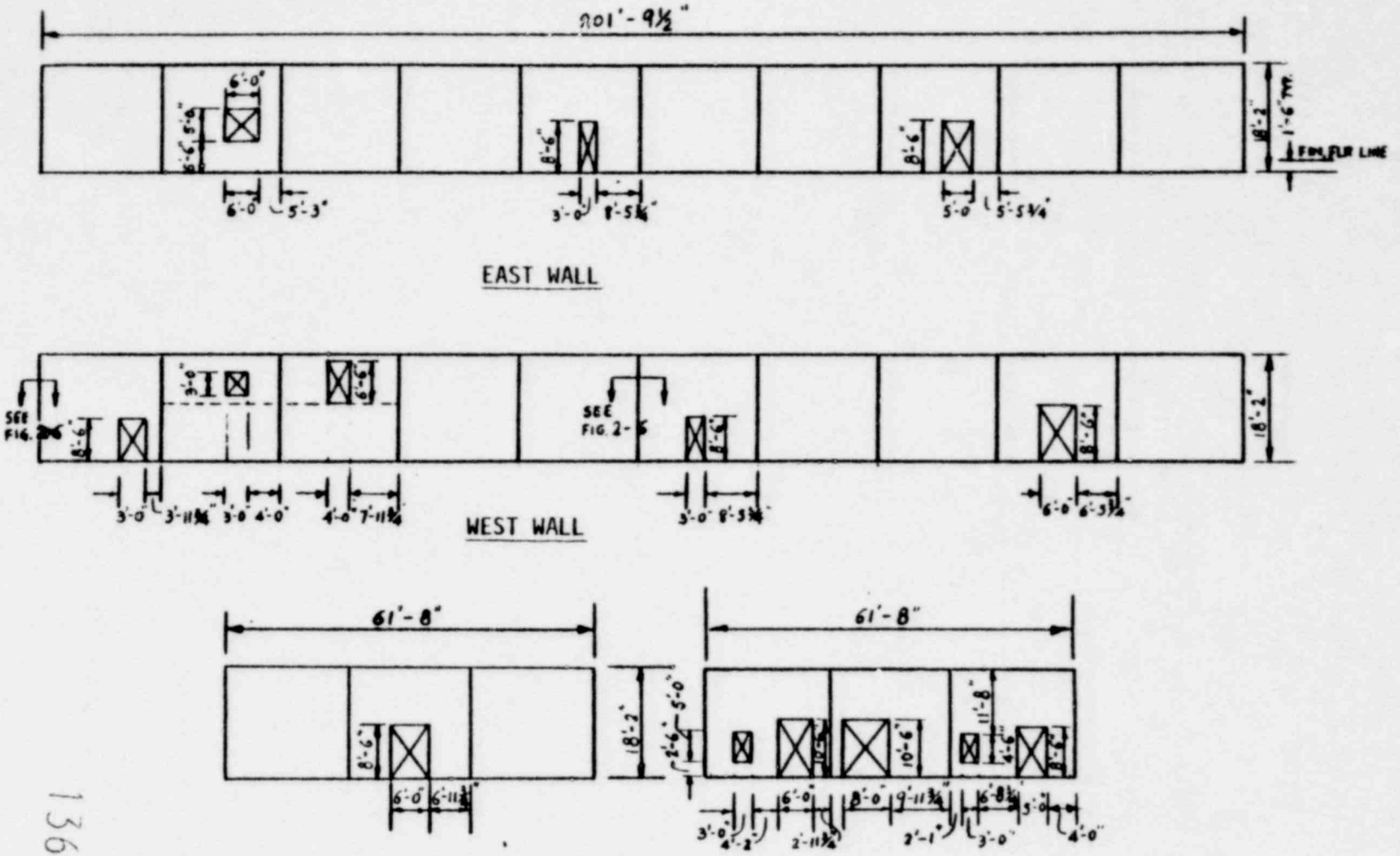

FIGURE 2-4. EXTERIOR ELEVATIONS

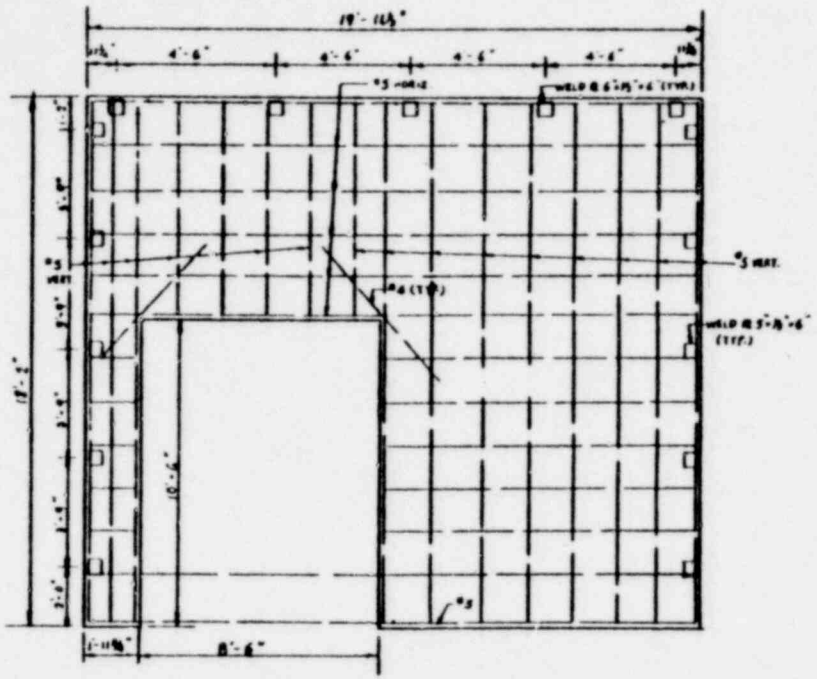

a) Wall Panel

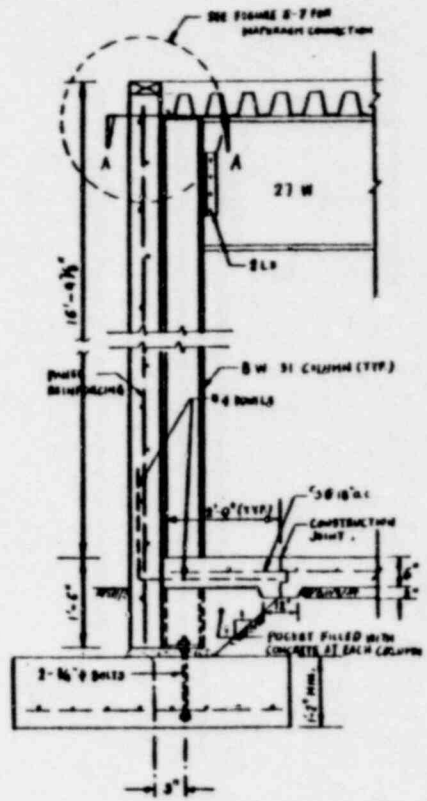

b) Wall Section

FIGURE 2-5. TYPICAL WALL PANEL DETAILS

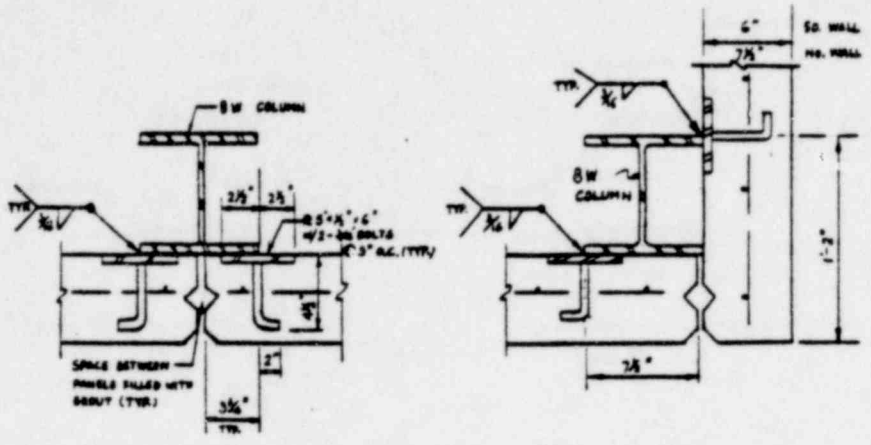

FIGURE 2-6. TYPICAL WALL PANEL CONNECTION DETAILS

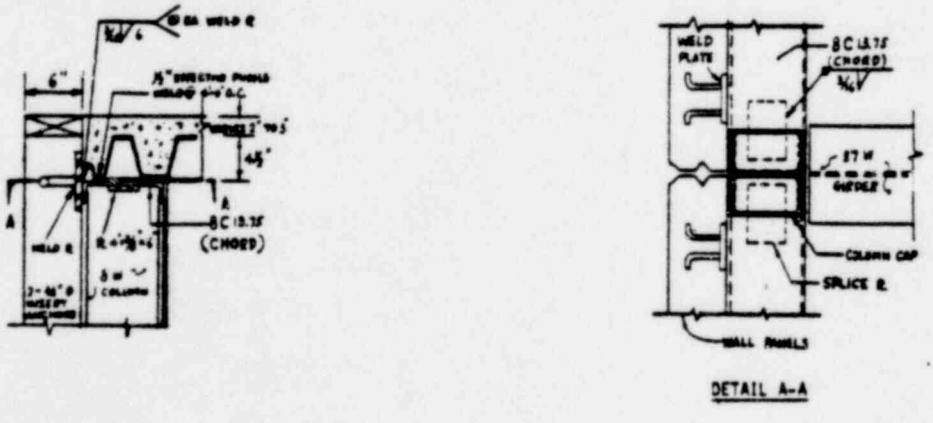

FIGURE 2-7. TYPICAL ROOF DIAPHRAGM CONNECTION AT WALLS

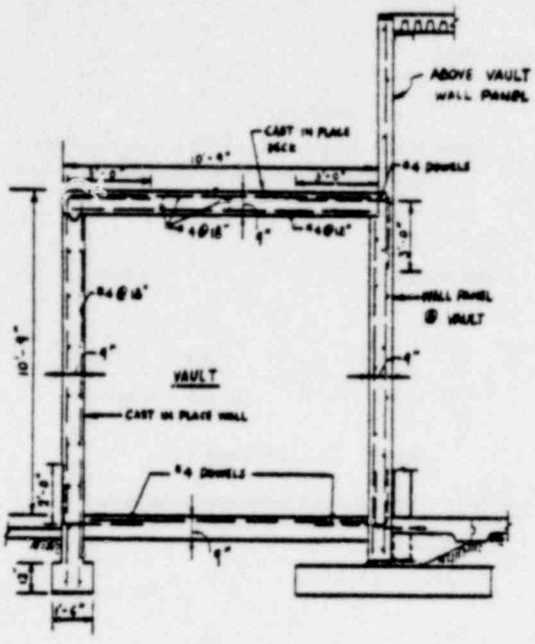

FIGURE 2-8. VAULT SECTION

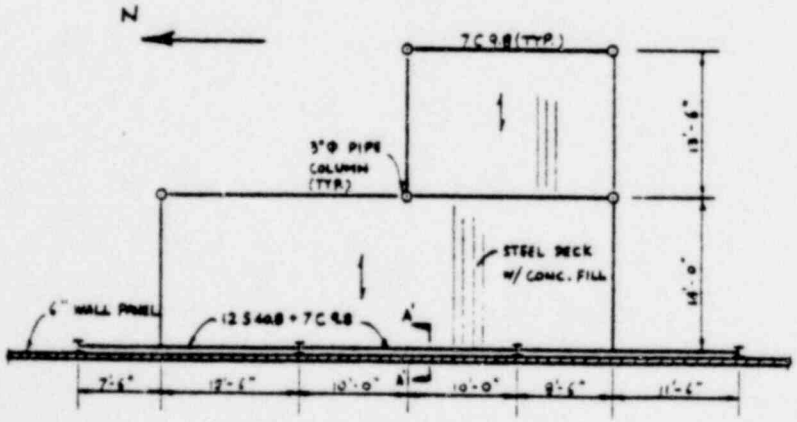

a) Mezzanine Framing Plan

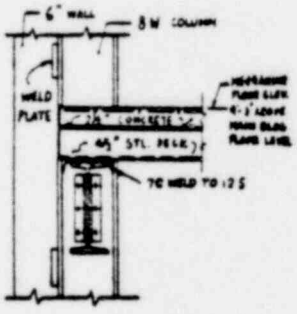

b) Side Wall Section A'-A'

1361 210

FIGURE 2-9. MEZZANINE DETAILS

3. EVALUATION OF STRUCTURAL BEHAVIOR

This section of the report presents a discussion of the analysis of the NMDF building structure including an identification of the lateral force resisting systems and the analysis procedures used in the evaluation. Again the interested reader is directed to the Task I Report (Reference 3) where information concerning the key structural details is given in more detail. A description of the structural models utilized for analysis together with the analysis results is presented in this section.

3.1 STRUCTURAL SYSTEMS

The seismic lateral force resistance of the NMDF building structure is provided by a shear wall box system tied together by a steel roof diaphragm. The building is rectangular in plan with a length-to-width ratio of 3.25:1. Deviations from structural symmetry include the vault, mezzanine, and difference in wall thickness for the north wall. The structure may be considered to resist seismic forces as two independent systems; one for each major building direction, north-south and east-west. Due to the diaphragm flexibility and large length-to-width ratio, torsional coupling of the two systems will be negligible. These two systems are shown in schematic plan-view in Figure 3-1. For both systems, the roof and tributary wall inertia is transferred to the active panel shear walls by the diaphragm acting as a deep beam with chord flanges. The vault is weakly coupled to the east-west system through flexure of the above vault wall panel. For north-south motion, the vault provides additional shear stiffness to the west wall but also provides considerable additional mass which must be resisted for north-south ground motion. The in-plane wall seismic shear forces are transferred to grade through the individual spread footings and through the building floor slab. The slab is positively connected to the wall panels near the wall base for this purpose. In-plane wall seismic overturning (bending) forces are transmitted to the footings

as axial forces through the column base connections. The necessary soils data required for estimation of the soil compliance due to the footing and slab reactions was discussed in the Task I Report. It may be generally observed that for east-west ground motion, a much smaller length of shear wall must resist approximately the same level of seismic inertial forces as would occur in the north-south direction. Thus, based upon geometric layout considerations alone, the east-west resisting system will be the controlling-lowest capacity system.

Both tributary gravity roof load and vertical seismic forces are transferred directly to the columns by roof girders (27 inches deep) which span the width of the structure without intermediate support

3.2 STRUCTURAL ANALYSIS PROCEDURES

A general discussion of the analytical approach used in the Task II analyses of the building structure follows. The procedure relating to the determination of uncertainty bounds is presented in Appendix A and is discussed more extensively since it was not included in the Task I Report.

3.2.1 Modeling Considerations

The synthesis of a mathematical model which represents the physical behavior of a building structure subjected to earthquake ground motion requires the idealization of the effective structural behavior of an assemblage of structural components and the appropriate lumping of distributed building mass (weight). As previously discussed, the NMDF building lateral force resisting system may be idealized as a shear wall box system tied together by a flexible roof diaphragm. The precast exterior panel walls may be idealized as monolithic shear walls. The discrete modeling of box-type structures with low height-to-width ratio must consider the effects of shear-lag (Reference 6) on overall wall resistance to in-plane lateral force. Application of the relationships outlined in Reference 6 allows the effective wall flanges to be defined for each of the primary lateral force systems as shown in Figure 3-1. Thus, each

wall tends to behave as a short cantilever channel section with negligible influence on the structure response in the orthogonal horizontal direction.

The roof diaphragm may be idealized as a two-flange deep beam spanning between the cantilever shear walls. The beam web is the metal roof decking (and insulating lightweight concrete fill) with the perimeter steel chords and an effective portion of transverse wall acting as the beam flange. The precise determination of diaphragm flexibility cannot be accomplished, since metal diaphragms are not designed using principles of structural mechanics, but rather are qualified by static testing to failure (Reference 7). Design values of allowable in-plane shearing forces are obtained by dividing the ultimate test load at failure by an appropriate factor of safety (usually taken as FS = 4.0). The stiffness (inverse of flexibility) of diaphragms has been estimated (References 8 and 9) using empirical relationships developed from qualification testing conducted on a wide range of metal diaphragm types. The stiffness of the AI steel roof deck with lightweight insulating concrete fill was estimated using the formulas given in Reference 9. Using the definitions of Reference 9, the AI roof deck was judged to be "flexible" in functioning as a diaphragm to distribute lateral forces in the plane of the roof. Because of the diaphragm flexibility and general symmetry of the NMDF building with regard to mass and structural rigidity, overall torsional effects will be minimized and building response to ground motions can be evaluated independently for each major orthogonal horizontal direction of the building, north-south and east-west.

The behavior of cantilever single story concrete shear walls with numerous openings is an area which has not been addressed adequately in recent earthquake engineering research (Reference 10). In design practice, one-story shear walls are often idealized as an assemblage of fixed base piers tied together with a deep spandrel beam (References 11 and 12). Finite element studies (Reference 13) of one-story shear walls have shown that the flexibility and stress distribution within walls with

several openings differs considerably from the assumptions of pier behavior governed by beam theory. For the east-west resisting system, the south wall will be the controlling wall (lowest collapse capacity) because of the largernumber of openings it has as compared to the north wall (Figure 2-4) and also because it is thinner. Since the support conditions of the walls differ considerably from fixed base conditions (vertical support of the panel walls is provided only at each footing), an independent finite element static analysis of the south wall was conducted using the EDAC/MSAP computer program which is a version of the general structural analysis computer program SAP IV (Reference 14). The wall model and shear loading is shown in Figure 3-2 while the exaggerated deflection shape and the critical regions resulting from the uniformly distributed shear force applied at the roof line, is shown in Figure 3-3. A more complete discussion of this subsidiary analysis is presented in Appendix D. As indicated in Figure 3-3, the critical wall component is the equivalent "tee" shaped frame formed by the spandrel and pier which connect two relatively rigid wall segments.

For low rise shear wall structures, foundation soil compliance can influence the overall dynamic response. The more dominant effect, however, is the relaxation of wall base fixity at the foundation level. A reasonable procedure to adjust the stiffness of an otherwise fixed base model is to consider the distribution and compliance of the individual wall footings represented by a series of equivalent translational and vertical soil springs. The stiffness of the individual soil springs may be estimated using relationships such as presented in Reference 15 for rectangular footings resting on the soil surfaces. For the NMDF building, the equivalent soil springs under the individual spread footings were based upon the estimated elastic properties of the supporting soil developed in the Task I report. The effects of footing embedment (References 16 and 17) were included in the compliance estimate. It should be noted that the soil springs were included in the models to assess the effect on wall stress distribution, not to model soil-structure interaction feedback effects.

The distribution of mass was accounted for in the NMDF building models by simple discrete lumping. The equivalent lumped masses were assigned to the model node points, formed by the structural element idealizations, in proportion to the tributary area of building components supported (in terms of lateral force support) by the structural elements. The diaphragm is sufficiently flexible so that horizontal response amplification occurs for the roof and its contributing inertia. Therefore, a model for east-west shaking was developed which considered both the north and south walls and the connecting flexible diaphragm. The effect of the flexible diaphragm on the out-of-plane support at the top of the east and west walls was included as well as the interaction of the vault and mezzanine. For north-south shaking it may be observed that the capacity of the west wall is lower than that of the east wall due to greater tributary mass and more wall openings resulting in less net shear area. Thus, only the west wall was modeled with one-half of the flexible diaphragm. Because of the relative simplicity of the structural systems, simple lumped mass models were used to approximately determine dynamic response. The second order effect of rotary inertia of the wall elements was not included in the models.

In two cases, elements were considered to act independently of the overall building response. First, the vertical response of the roof beams (girders) subjected to vertical ground motion accelerations at their supports were analyzed assuming a simple beam dynamic model. Second, transverse (out of the plane) bending response of the wall panels was considered based on the model of a plate (wide beam) simply supported on two edges.

3.2.2 Inelastic Behavior

In order to determine the seismic ground accelerations which could cause failure or collapse, behavior in the inelastic range must be considered. The nonlinear response of shear wall systems is generally small compared with other structural systems due to fewer energy absorption and ductility mechanisms. Sources of nonlinear response prior to collapse of such systems come from cracking of concrete and yielding of steel and from working or tearing of connections. Where significant cracking of concrete and steel yielding is involved prior to collapse; energy absorption is enhanced. For the NMDF building, local failure of connections governs the failure of the precast wall-roof system with corresponding low ductility. Significant degradation is not expected in the system under repetitions of earthquake motions.

The modal spectral method of dynamic analysis is appropriate for the determination of response of the NMDF building as represented by lumped mass models. A non-degrading system such as described, with low energy absorption capacity and geometrically no particular weak point (i.e., a relatively uniform system), is well suited to analysis by the approximate nonlinear spectral-method (References 20 - 26). In this method, the elastic response spectra which define seismic input (and are used to calculate elastic system response) are modified to account for hysteretic energy absorption in the nonlinear system. The nonlinear analysis procedure is the same as for an elastic spectral analysis except for the utilization of the reduced or nonlinear spectra. The hysteretic energy absorption capacity is measured by the ductility factor which is the ratio of the maximum response deflection of a single-degree-of-freedom structure to its yield point deflection. The procedure for altering elastic response spectra to account for nonlinear behavior was illustrated in the Task I report and further background

may be found in References 23-25. The spectral acceleration reduction factor, R, is a function of the system ductility factor, μ, within each spectral region. The factor R is taken as unity for the ground accelerations portion of the response spectrum, $1/\sqrt{2\mu-1}$ for the amplified acceleration spectral region and $1/\mu$ for the spectral velocity and spectral displacement regions.

Many references are available to assist in judging appropriate damping and ductility levels to represent response at the point of incipient collapse in the nonlinear analysis. In particular, References 24 and 26 report values of ductility and damping for various systems which may be used as guideline values. On the basis of values found in these references and engineering judgement, upper and lower bound (one standard deviation) and median values for ductility and damping were selected. The selection of these factors involved a comparison of the NMDF shear wall system with standards systems for which the referenced values are tabulated. The selected damping and ductility factors are given in Table 3-1.

Table 3-2 provides damping ratios and ductility factors which are appropriate for the independent analysis of the roof girders and wall panels considered as separate structural elements. Again the selection is based on judgement using the referenced values as guidelines.

It should be noted that the ductility method of analysis is an approximate method for assessing nonlinear response and capacity of structural systems. The method was judged in Reference 24 as the most practical state-of-the-art method for nonlinear analysis of buildings. The justification of the method for multi-degree-of-freedom systems is, however, on a heuristic basis. The values of "system ductility" selected must be interpreted as a means of allowing the overall hysteretic energy dissipation of the structural system to be included in the response analysis. The values of "system damping" selected represent the non-hysteretic mechanisms of energy dissipation in dynamic response and are associated with stress levels at or just below yield point values.

The definition of the seismic ground motion input for the NMDF site is provided (Reference 5) by elastic response spectra. The horizontal and vertical spectra used in the analysis were based upon the median data for a rock site resulting from the earthquake ground motion study presented in Reference 18. The resulting analysis response spectra, normalized to 1.0g peak horizontal ground motion, for ductility ratios of 1.0 (elastic), 2.0, and 4.0 are shown in Figure 3-4. Also included in Figure 3-4 is the vertical response spectrum, normalized to 0.67g peak ground motion, for a ductility factor of 6.5.

3.2.3 Seismic Capacity Estimates

Given a capacity criteria in terms of internal stress or deflection for a selected key structural element or connection, a capacity force resultant F_C, was directly obtainable using relations of engineering mechanics. For most of the details and elements investigated for structural capacity, the seismic response to ground motion was obtained from the overall dynamic analysis of the building. The forces within key elements (or connections) due to a ground acceleration of 1.0g were obtained from the modal spectral analysis of the building models using the spectrum (median) given in Figure 3-4 for damping, β, and ductility factor, μ. The modal components of force within an element, $F_{m,1g}$, were combined using the square-root-sum-of-square (SRSS) procedure to obtain an estimate of the element median resultant force due to dynamic response:

$$F_{SRSS,1G} = \sqrt{\sum_m (F_{m,1g})^2} \qquad (3\text{-}1)$$

The ground acceleration capacity, A_g, for the element or connection under consideration, is then given by:

$$A_g = F_C \Big/ F_{SRSS,1g} \qquad (3\text{-}2)$$

For components or connections affected by ground motion orthogonal to the principal direction of each lateral force system or affected by vertical ground motion, consideration of concurrent ground motion was necessary to allow for additional stress effects. For those elements affected by concurrent motion from various directions, the procedure suggested in Reference 19 was utilized. The median element force resultant corresponding to 100 percent of the motion in one direction of response was combined with 40 percent of the resultant due to response in the other orthogonal directions by addition of the absolute values. This procedure of superimposing reduced element force resultants, caused by concurrent motion, reflects the fact that input excitations in the three directions are not necessarily of the same magnitude, and that the response maxima do not occur simultaneously. Thus, since peak vertical motions are on the order of 1/2 to 2/3 of peak horizontal motions (Reference 19), a maximum value of vertical motion of 25 percent of the peak horizontal motion was considered to act concurrently with each component of horizontal ground motion for the evaluation of each lateral force system.

The determination of the ultimate element or connection capacity F_C, was generally based upon the ultimate stress distribution for the given material in the mode of element response considered. For assemblages of structural elements, the formation of collapse mechanisms due to regions of localized yielding was also considered. The formation of the hinging regions was governed by the yield strength of the given material and the geometry of the assemblage of structural elements. The determination of the structural material properties for the structural elements of the NMDF building was part of the Task I effort. The estimated upper bound, median, and lower bound values of material strength are tabulated in Reference 3 (see also Appendix E).

The determination of concrete element capacity was, in general, based upon the ultimate strength design provisions of References 31 and 32. The failure criteria for ultimate flexure and/or shear capacity

for a concrete element was the same as utilized in Reference 31 with an increase to a median value corresponding to the increase from the nominal design value to the median value of ultimate compressive strength f'_c. However, the capacity reduction factor, ϕ, was assigned a value of unity for the NMDF evaluation. This factor is a safety factor to account for effects of material properties and construction practice in design. The effect of construction variables on actual concrete capacity was considered by utilizing a correction factor centered on a median value of unity, with a lower bound and upper bound value of 90 percent and 111 percent, respectively.

The ultimate static pull-out and shear criteria, including proximity and free-edge effects, for concrete inserts was based upon relationships and test data presented in References 32-34. The dynamic (seismic) ultimate capacities for concrete inserts were taken as 80 percent of the single cycle static ultimate value. Tests have indicated that no significant degradation in strength occurs under cyclic loadings below 80 percent of the static ultimate but that degradation and failure are rapid for loadings above the 80 percent level (References 36-38). Combined pull-out and shear capacity of inserts was estimated using the ultimate strength interaction relation given in Reference 34.

The ultimate interface shear transfer (shear friction) capacity at concrete-to-concrete joints was estimated after review of References 36-45. Tests have shown that interface shear transfer capacity is a function of the parameter, ρf_y, where ρ is the ratio of net reinforcing steel area crossing the joint to the gross concrete area and f_y is the reinforcement yield strength. However, very few tests have been conducted for low steel/concrete ratios ($\rho \approx 0.001$) typical of the NMDF building concrete joints. Thus, based upon the relationships suggested in Reference 39, an estimate of the shear transfer capacity was assumed to be given by the relationship,

$$v_u = 1.4\rho f_y$$

where v_u is the equivalent ultimate concrete shear stress for the interface joint. Cyclic loading tests (Reference 37) have indicated that no significant degradation in interface shear transfer capacity occurs below 80 percent of the static ultimate capacities. Thus, the dynamic (seismic) ultimate shear transfer capacities across concrete joints were taken as 80 percent of the estimated static capacity bounds.

The ultimate strength capacities of structural steel elements and connections were estimated using the requirements of Reference 46 and the general recommendations and guidelines given in Reference 47. The capacity of column anchor bolts in combined tension and shear was estimated using the classical elliptical interaction curve (Reference 47).

As discussed previously, the ultimate capacity of diaphragms is determined by prototype testing to failure. However, no tests have been conducted on diaphragms with the extreme length-to-width ratio of the NMDF building nor have tests been conducted on diaphragms with insulating concrete fill (35 ~ 40 lb/cu ft). Thus, the capacities of all internal connections and details of the diaphragm were assessed and compared to the design shear, q_d, (expressed in terms of a shear flow or lbs/ft for a bare deck without fill) multiplied by a factor of safety, FS, of four. The longitudinal seam welds of the diaphragm were found to control the internal capacity of the diaphragm with a capacity estimate approximately given by $q_d \times 4.32$. Comparison of computed shear values using relationships given in Reference 8 for similar diaphragm decks, with and without lightweight concrete fill, indicated that the presence of the fill increased the shear capacity of the diaphragm by a factor of 4.48 compared to the design shear for bare decking. Thus, an estimate of internal diaphragm shear capacity was taken as the average of the above,

$$q_{CAPACITY} = q_d \times 4.40$$

for the NMDF building roof. The capacity of the diaphragm peripheral connection welds and diaphragm chords (acting as beam flanges) were assessed independently as structural steel connections (Reference 48).

The racking damage threshold for the interior partitions (architectural elements) due to imposed relative displacement between the roof and floor slab was estimated based on the test data summarized in Reference 49.

3.2.4 Uncertainty Bound Determination

As previously stated, the seismic capacity evaluation herein is part of an overall natural hazards risk analysis. In order to provide compatability with this overall analysis, results are required in terms of estimated median capacities and estimated one standard deviation (one sigma, σ) upper and lower bound capacities. Thus, the results presented in this report give estimated upper bound, median, and lower bound values for the seismic capacity of the building structure and critical equipment. Median capacity results were obtained for structures and equipment utilizing the procedures described herein with median values of parameters associated with the analysis. A probabilistic approach was utilized to obtain the one standard deviation upper and lower bound variation of each random function or parameter which affects the results. The parameters which affect the capacity estimates include material properties, analysis procedures and seismic input definition. The expected variation in the values of the important parameters, such as yield strength, damping, and ductility, which affect the determination of collapse capacity were developed during the Task I effort and presented in the Task I report. The parameters were considered to be log-normally distributed for purposes of the approximate uncertainity bound analyses performed under the Task II evaluations.

The probablistic approach adopted was based upon the general statistical properties of a lognormal distribution (Reference 30). For a lognormal distribution, the mean value does not have a physical interpretation, thus the median value is used as the characteristic parameter (i.e., 50% of the values are above the median value and 50% are below the median value). The structural capacity analysis procedure described above was employed to determine a median value for seismic capacity using the median values of the important contributing variables. The upper and lower bound capacities were estimated to represent a one standard deviation variation and are based upon engineering judgement concerning the variation of the contributing variable values rather than on detailed statistical studies. Thus, the lower and upper bound values represent the estimated 16% and 84% percentile values, respectively, with 68% of all values falling between the upper and lower bound values. The probabilistic procedure used in this analysis is described in Appendix A along with a sample calculation.

3.3 STRUCTURAL MODELS AND RESULTS

As discussed in Section 3.1 of this report, the east-west and north-south structural systems were analyzed as independent lateral force systems. Therefore, the models and results of each are presented separately in the subsections which follow. A description of the secondary architectural systems and an assessment of their potential effect upon the critical areas is also included. For convenient reference, selected data and structural details which are most pertinent to the key structural systems analyzed are abstracted from the Task I Report (Reference 3) in Appendix E.

3.3.1 North-South Lateral Force Resisting System

The dynamic model used to evaluate the response of the NMDF building for north-south ground motion reflects the general assessment, noted previously, that the structure response in the north-south direction will not be the controlling response mode. Sufficient detail was provided in the model only to estimate the diaphragm and gross wall shear

forces due to ground motion. The finite element model used to evaluate the north-south direction is shown in Figure 3-5 along with an outline drawing of the structure. The finite element mathematical idealization of the diaphragm, shear walls, and foundation compliance was formulated employing the EDAC/MSAP computer code which is a version of the general structural analysis computer program SAP IV (Reference 14). The three-dimensional elastic beam element and boundary spring elements were utilized to construct the model with the necessary kinematic constraints to achieve the element stiffnesses desired. The diaphragm element is constrained to provide only shear displacement between nodes (i.e., a shear spring). The wall elements are constrained to act as a shear-flexure cantilever. The mass lumping is also indicated in Figure 3-5. The input data for the stiffness, mass and constraints are given in Appendix C.

The capacity of the diaphragm is controlled by the peripheral puddle weld connections to the edge chord at the junction of the west wall. The shear capacity of the west wall was based on a nominal estimate of ultimate concrete shear stress given by relationship, $v_u = 2\sqrt{f'_c}$, and was found not to govern.

Using the median element force response (SRSS) obtained from a modal dynamic analysis of the finite element idealization and the median element capacities, the median ground acceleration capacities, Ag, were computed as indicated by Equation 3-3. The median ground acceleration capacity for the NMDF building walls given ground motion in the north-south direction was determined to be $(Ag)_m = 2.9g$. The median ground acceleration capacity for the roof diaphragm given ground motion in the north-south direction was determined to be $(Ag)_m = 0.83\text{-}0.87g$. This capacity estimate includes the effect of concurrent east-west shaking on diaphragm shear. Assuming that the north-south system was controlling the failure of the diaphragm boundary connections along the west (and east) wall would remove the wall lateral support provided by the diaphragm, and the walls would collapse in the east-west direction as shown in Figure 3-8.

3.3.2 East-West Lateral Force Resisting System

The dynamic model used to evaluate the response of the NMDF building for east-west ground motion is shown in Figure 3-6 along with an outline drawing of the structure. As can be noted, the additional detail provided by this model reflects the assessment that the east-west system will be controlling. Again, the finite element idealization of the shear walls, diaphragm, transverse walls, and foundation compliance was formulated with the EDAC/MSAP computer code using the three-dimensional beam and boundary spring elements with appropriate kinematic constraints. The diaphragm element is constrained to act as a shear spring between nodes. The wall elements are constrained to act as equivalent shear-flexure cantilevers. The effective stiffness assigned to the south wall element was based upon the results of the static wall study shown in Figures 3-2 and 3-3 and further discussed in Appendix D. The effective transverse walls were included in the model, as indicated in Figure 3-6, to account for the additional mass provided by the mezzanine area and the additional resistance provided by the vault. Note that the effective transverse walls are modeled as pin-pin beam elements which transfer only the forces required for lateral support by the diaphragm and the footing/slab foundation. The numerical values assigned to the element stiffnesses and lumped masses for the east-west model are given in Appendix C along with the results of the modal analysis.

For the east-west lateral force system, the ultimate capacities for several major structural elements and associated connections were determined. The major structural elements evaluated for the NMDF are the diaphragm and precast panels acting as shear walls. Other items considered were the interface shear transfer capacity of the slab joints, column anchor bolt capacity in combined tension and shear, footing flexural capacity, initiation of footing uplift, and wall panel insert capacities.

The capacity of the diaphragm is controlled both by a chord splice detail and the internal seam welds. Chord channel compressive strength was evaluated and found not to be controlling. Once diaphragm resistance is lost, building collapse is probable.

A considerable amount of effort was expended to determine the collapse capacity of the south wall to insure that the capacity estimate was not biased by conservative design approximations. As noted previously, the behavior of long, one-story walls with numerous openings is a problem which has not been adequately addressed in the literature. The finite element model shown in Figure 3-2, was used (static loading) to assess the equivalent wall stiffness utilized in the dynamic model of the E-W system. In addition, the distribution of stress within the wall was determined (see Appendix D), allowing the critical regions of shear and flexure to be identified. The detailed wall study allowed the determination of insert reaction forces and also provided the distribution of base shear resisted by each footing and the wall shear transferred to the floor slab. After evaluation of the wall stress distribution, an equivalent frame model of the wall, as shown in Figure 3-7 was proposed to allow the collapse behavior of the wall to be evaluated. To achieve approximate correspondence between the detailed model of Figure 3-2 and the equivalent frame model shown in Figure 3-7, the pseudo-spandrel transition stiffnesses of each pier were adjusted until the overall displacement and distribution of wall shear within each pier and critical spandrel were in approximate agreement with the detailed finite element model. Again the EDAC/MSAP code using beam and boundary spring elements was utilized for the frame model. The purpose of the frame model was to allow the evaluation of the flexural and shear behavior of the critical spandrel and pier regions. Using the equivalent frame model, the final collapse mechanism shown in Figure 3-7 was identified. After initial yield hinge formation at the top of pier No. 2, the wall can carry approxiamtely 50% more shear (static) until hinges form at the ends of the idealized spandrels, which frame into pier No. 2, and an additional hinge forms at the top of pier No. 4. For the dynamic analysis considered herein, the formation

of the first hinge was associated with elastic response (μ = 1.0) while the formation of the collapse mechanism was associated with the nonlinear response represented by a system ductility of μ = 2.0.

Re-evaluation of the Task I documentation indicated that the mezzanine east-west lateral force resistance is provided entirely by two main building columns and an effective portion of the (west) wall panel acting as a composite beam with the panel weld plates as shear connectors. The capacity of the panel-column composite behavior was determined and found to be governed by shear failure of the inserts due to beam flexure within the elastic range of stress. Thus, the capacity of the panel-column composite was associated with elastic response (μ = 1). After the inserts fail, the lateral resistance of the mezzanine floor area is provided by the steel columns independent of the panels. This fact prompted the inclusion of the mezzanine inertia in the dynamic model supported laterally by the columns only. The capacity of this subsystem, in terms of collapse, is governed by the columns forming a yield hinge at mid-height. Since the column end connections, at both the roof girder connection and at the anchor bolt detail, are essentially a pin-joint idealization (refer to Figure 2-5), building collapse would be probable once the yield mechanism is initiated. It should be noted that the ductility associated with this subsystem collapse mechanism is greater than the system ductility (μ = 2.0), however, the system factor was utilized in the evaluation to demonstrate that the mezzanine collapse mode does not govern.

The flexural capacity of the transverse wall panels acting as one-span plate elements was also determined. This capacity is directly applicable to the upper wall panel above the vault. The wall panel above the vault roof tends to act as an intermediate support for the diaphragm, acting as a cantilever effectively fixed by the vault walls. However, the flexural stiffness of the effective cantilever is insignificant compared to the diaphragm and thus the upper vault panel must essentially accommodate the imposed diaphragm displacement. A yield hinge will form at the upper panel cantilever base which effectively isolates the vault

structure from the overall structure response. The formation of this hinge was associated with elastic system response ($\mu = 1.0$).

The median force response for each element was determined from the modal analysis of the dynamic model and the stress distribution indicated by the static finite element wall and equivalent frame studies. Then, given the median element force capacities, the median ground acceleration capacities were computed using Equation 3-2. Table 3-3 presents the ground acceleration capacity determined for each of the elements or connections with major damage potential considered for the controlling east-west system. The ground acceleration capacities for the N-S system and other system considerations (independent transverse wall panel assessment, partition damage, and vertical roof response) are also tabulated for comparison. Estimated lower and upper standard deviation bounds as well as median results are presented. Lower and upper bounds were determined as described in Appendix A. The numerical values of the median element force capacities utilized are given in Appendix B for each of the major elements considered.

The controlling collapse capacities (0.60-.87g) are all associated with loss of diaphragm support for the west and east walls. Once the diaphragm resistance is lost, the roof girder/column pin-jointed frames with attached wall panels will progressively collapse after only a few cycles of motion. This basic mode of collapse for the NMDF structure is illustrated in Figure 3-8. Each of the transverse (east-west) girder/column frames may be idealized by the basic spring stabilized mechanism shown in Figure 3-8. Given that the diaphragm failure is associated with the system ductility, then the idealized support spring will fail when the system response achieves a ductility demand equivalent to the adjudged median system ductility. It should be noted that the vault structure (monolithic concrete) will not be affected by structure collapse. The above vault panel section will hinge at the vault roof, which will prevent any further interaction of the collapsing structure with the vault. The vault,

then acts as an independent box structure with high capacity. Assuming a low bound of vault wall shear capacity given by a nominal value of ultimate shear stress, $v_u = 2\sqrt{f'_c}$, the ground acceleration capacity of the vault exceeds 2.4G.

It should be noted that several of the seismic capacities listed in Table 3-3 are damage capacities and not associated with structure collapse. Damage thresholds associated with formation of effective yield mechanisms ($\mu = 1$) are listed as well as damage modes which are associated with non-key components with a ductility capacity in excess of the structural system ductility. These values should be viewed as general indicators of structural performance and as reference values to establish that the particular mode of damage is not governing. Additional items considered during the evaluation included footing uplift (1.35g), soil bearing capacity (1.65g), and footing flexure capacity (1.59g). These modes of behavior do not affect the confinement barriers.

3.3.3 Other System Considerations

The behavior of the internal gypsum board/steel stud partitions, which serve as secondary confinement barriers within the structure envelope were evaluated for the imposed displacement response of the roof diaphragm. Using the test data provided in Reference 49, the partition barrier was assumed to be significantly damaged for displacement-height ratios of 0.005. As can be noted from Table 3-3, the ground acceleration capacity (1.12g) associated with this mode of damage does not control.

The transverse wall panels and the roof girders were also considered as independent structural elements. The wall panels were evaluated in transverse flexure (simple span) for lateral inertia loading. The roof girder was evaluated as a simple span beam for the roof inertia loading caused by response to vertical ground motion. In addition, the individual roof panels between the roof girders were evaluated as simply-supported composite plates in order to determine the levels of vertical response required to fail the puddle welds and hence destroy the diaphragm capability of the roof. The diaphragm to chord shear transfer and the chord

channel comparison strength were evaluated. The capacities associated with each of these potential damage modes are not controlling although some are included in Table 3-3 for comparison with the other damage modes considered. Since low cycle fatigue strength data for the roof diaphragm to plate weld was not available, it was impossible to evaluate the number of cycles of expected life for this detail. However, sufficient ductility of the diaphragm is available to prevent localized "peeling" or corner loading of these welds and also to develop the average strength of these welds rather than as a succession of weak links.

TABLE 3-1. SYSTEM DAMPING RATIOS AND DUCTILITY FACTORS FOR NMDF BUILDING ANALYSIS

Parameter	Lower Bound	Median Value	Upper Bound
System Damping Ratio, β (percent of critical)	7	10	14
System Ductility Factor, μ	1.5	2.0	2.6

TABLE 3-2. ELEMENT DAMPING RATIOS AND DUCTILITY FACTORS FOR ROOF GIRDER VERTICAL ANALYSIS AND WALL PANEL TRANSVERSE ANALYSIS

Key Component	Element Damping Ratio, β Percent of Critical			Element Ductility Factor, μ		
	Lower Bound	Median Value	Upper Bound	Lower Bound	Median Value	Upper Bound
Roof Girder Vertical Response (27W114 steel beam)	3.5	5.0	7.0	2.5	6.5	10
Wall Panel Transverse Response (6 in. precast reinf. concrete)	7	10	14	3.0	4.0	5.3

TABLE 3-3. SUMMARY OF SEISMIC CAPACITIES AFFECTING CONFINEMENT BARRIERS

Structural Element Description	Structural Response Description	Structural Damage	Ground Acceleration Capacity, A_g (g)		
			Lower	Median	Upper
Pier #2, South Wall	Wall Shear Response (μ = 1.0) to E-W Ground Motion	Yield Hinge Formation at Pier-Spandrel Junction	0.28	0.41	0.60
Composite Wall Panel/Exterior Column, Mezzanine	Mezzanine Inertia Response (μ = 1.0) to E-W Ground Motion	Insert Shear Failure and Loss of Composite Resistance	0.28	0.41	0.59
Upper Vault Wall Panel	Cantilever Flexure Due to E-W Diaphragm Response (μ = 1.0)	Yield Hinge Formation at Panel Base	0.32	0.47	0.68
Diaphragm Chord Splice	Diaphragm Shear Response (μ = 2.0) to E-W Ground Motion	Chord Failure at East and West Walls; Building Collapse Probable	0.41	0.60*	0.88
Internal Diaphragm Connections (Seam Welds)	Diaphragm Shear Response (μ = 2.0) to Concurrent E-W and 0.4 N-S Ground Motion [N-S and 0.4 E-W]	Loss of Diaphragm Strength; Building Collapse Probable	0.42 [0.56]	0.62* [0.83]	0.91 [1.22]
Perimeter Diaphragm Connections (Puddle Welds)	Diaphragm Shear Response (μ = 2.0) to Concurrent N-S and 0.4 E-W Ground Motion	Loss of Diaphragm Strength; Building Collapse Probable	0.59	0.87*	1.28
Upper Vault Wall Panel	Cantilever Flexure due to E-W Diaphragm Response (μ = 2.0)	Yield Hinge Ductility Demand Equivalent to System Ductility	0.54	0.79	1.15
Slab Construction Joint, South Wall	Slab Shear Response (μ = 2.0) due to E-W Ground Motion	Shear Transfer Capacity; Joint Slippage	0.63	0.91	1.32
Precast Panels (West and East Walls)	Transverse Flexure due to E-W Ground Motion (μ = 2.0)	Yield Hinge (at mid-height) Ductility Demand Equivalent to System Ductility	0.65	0.94	1.37
Anchor Bolts at Corner Columns	Tension and Shear due to Wall Response (μ = 2.0)	Anchor Bolt Failure, Partial Panel Uplift	0.69	1.00	1.45
Exterior Mezzanine Column	Mezzanine Inertia Response (μ = 2.0 to E-W Ground Motion	Yield Hinge (at mid-height) Ductility Demand Equivalent to System Ductility	0.71	1.02	1.46
South Wall	Wall Shear Response (μ = 2.0) to E-W Ground Motion	Yield Hinges at Pier-Spandrel Junctions; Collapse Mechanism at System Ductility; Building Collapse Probable	0.74	1.08*	1.57
Gypsum Board/Steel Stud Partitions (Glove Box Room)	In-plane Shear Deformation due to E-W Diaphragm Response (μ = 2.0)	Partition Damage, Loss of Secondary Confinement	0.77	1.12	1.63
Wall Inserts, South Wall Spandrel	Spandrel Shear and Flexural Response (μ = 2.0) to E-W Ground Motion	Spandrel Shear Capacity, Building Collapse Probable	0.88	1.27*	1.84
Precast Panels	Transverse Flexure Considered as Independent Subsystem (μ = 4.0)	Yield Hinge (at mid-height); Collapse Mechanism at Failure Ductility; Building Collapse Probable	1.00	1.45*	2.11
Vault Wall	Wall Shear Response to E-W Ground Motion (μ = 2.0)	Nominal Shear Capacity	1.66	2.4	3.48
Roof Girder	Vertical Response Considered as Independent Subsystem (μ = 6.5)	Yield Hinge at Center Span, Collapse Mechanism	—	> 3.0	—

* Major capacities associated with probable structure collapse. The collapse values are shown to several significant values only to indicate the relative order of the capacities. The level of analysis does not justify this accuracy.

EDAC

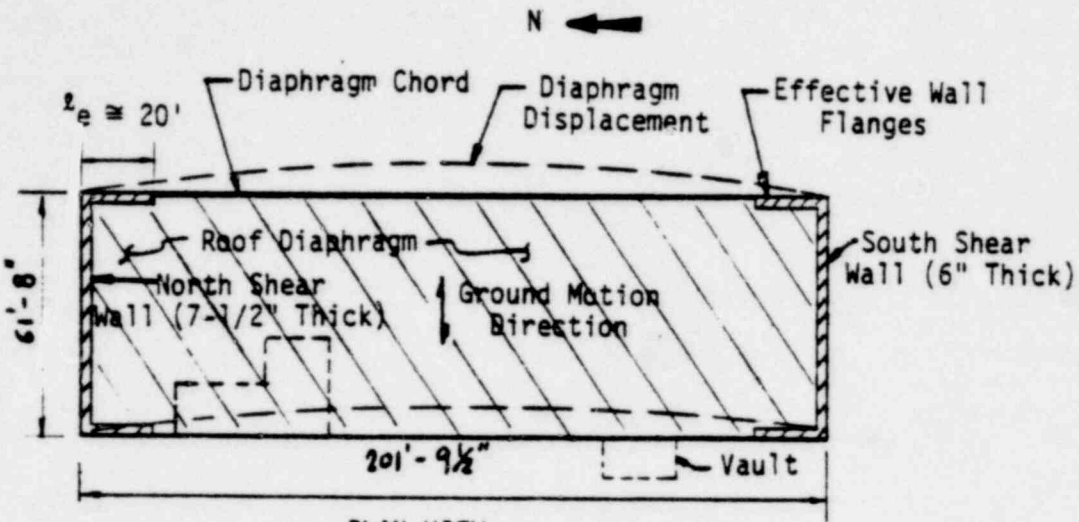

PLAN VIEW

GROUND MOTION IN EAST-WEST DIRECTION

PLAN VIEW

GROUND MOTION IN NORTH-SOUTH DIRECTION

FIGURE 3-1. LATERAL FORCE RESISTING SYSTEMS

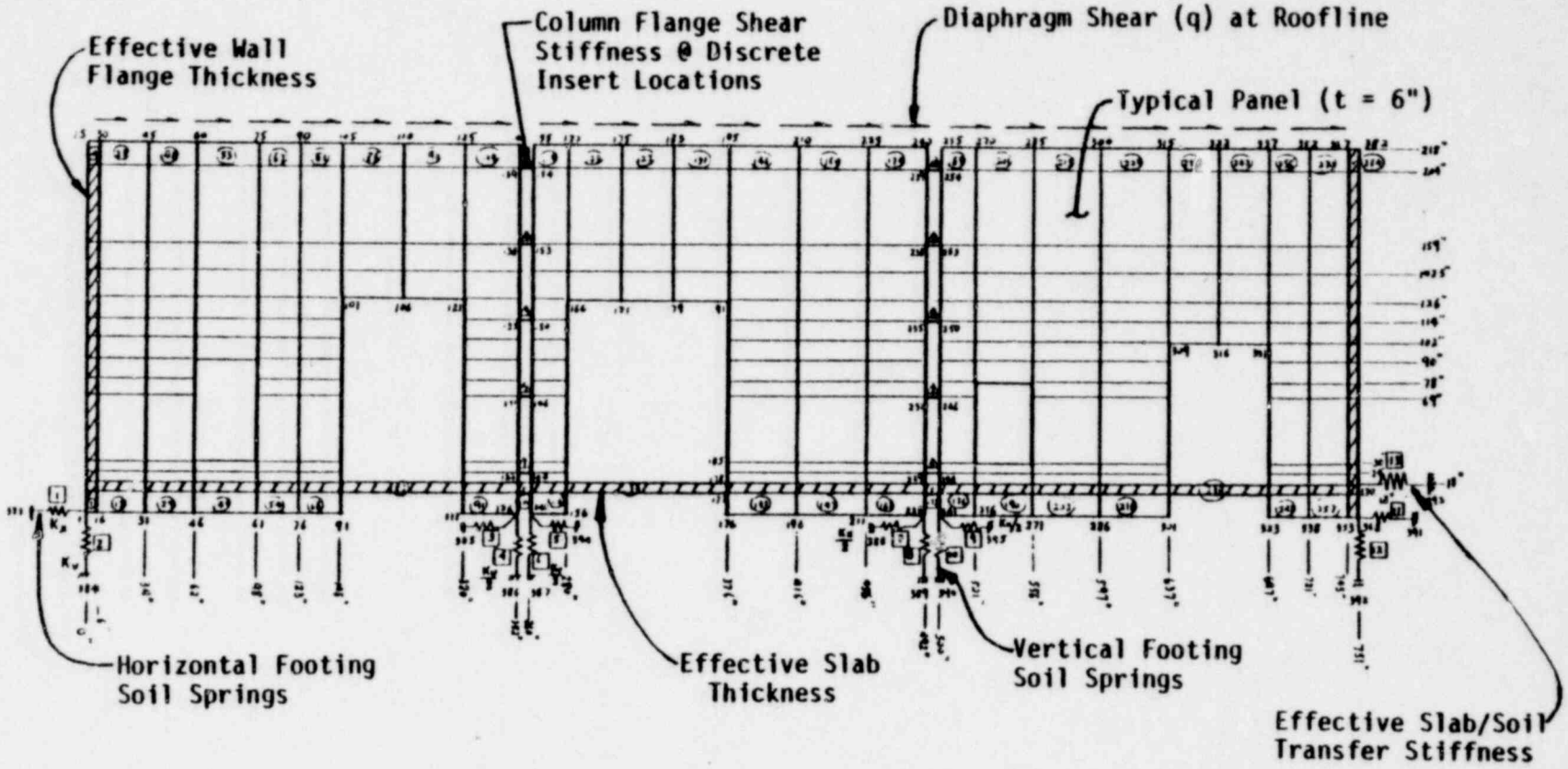

FIGURE 3-2. FINITE ELEMENT MODEL OF SOUTH WALL

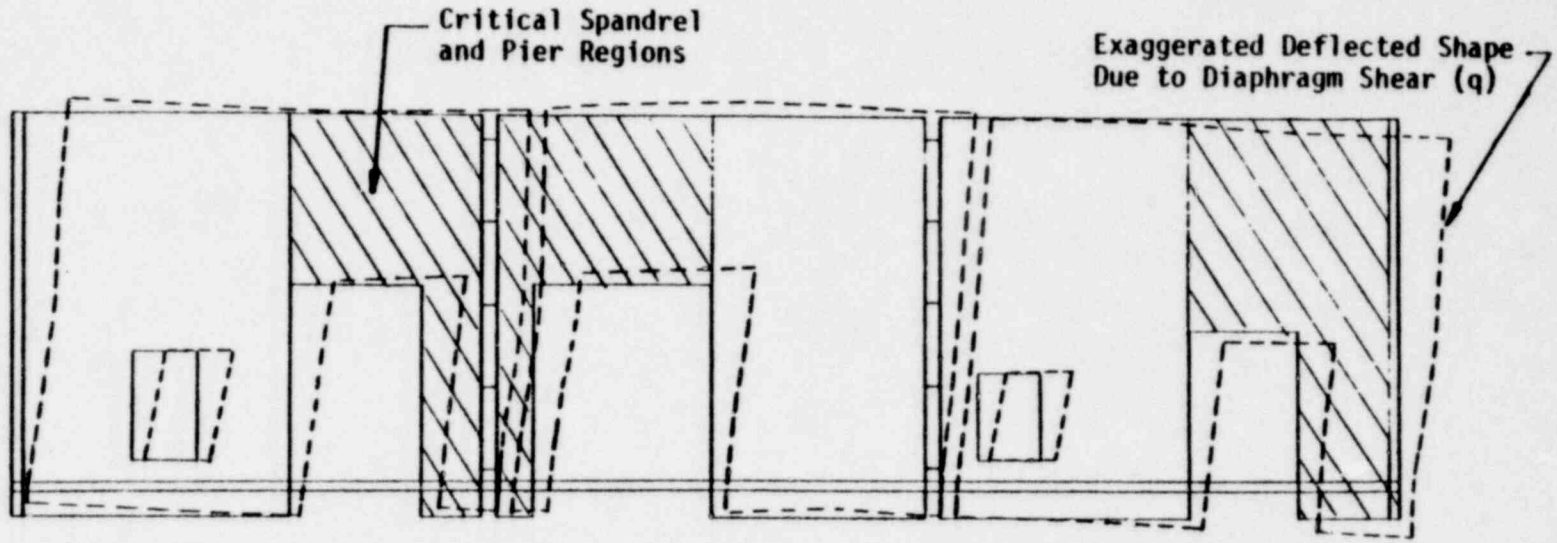

FIGURE 3-3. SOUTH WALL CRITICAL REGIONS AND DEFLECTED SHAPE

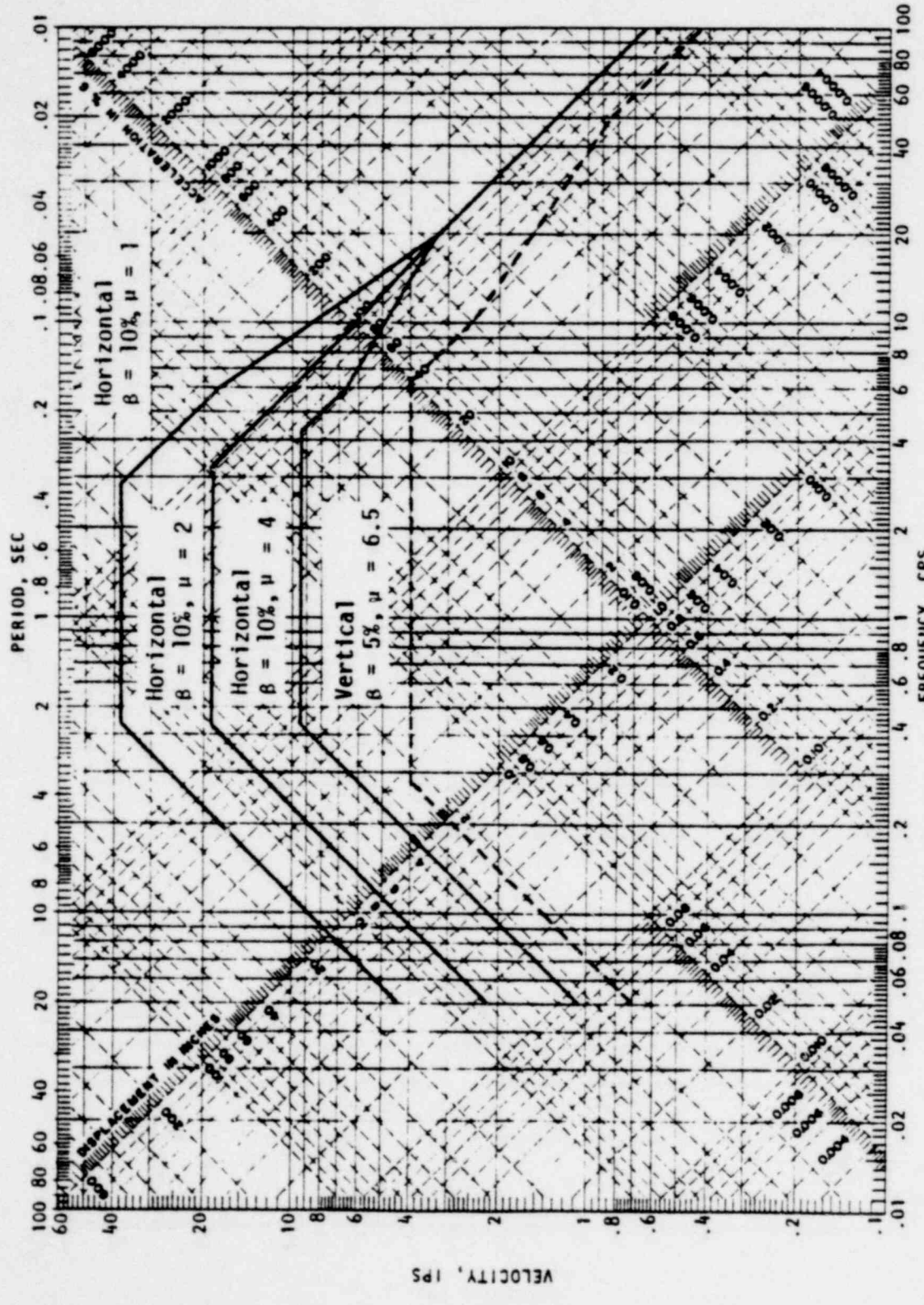

FIGURE 3-4. ANALYSIS RESPONSE SPECTRA
(Rock Site, Ref. 18 Base Spectra)

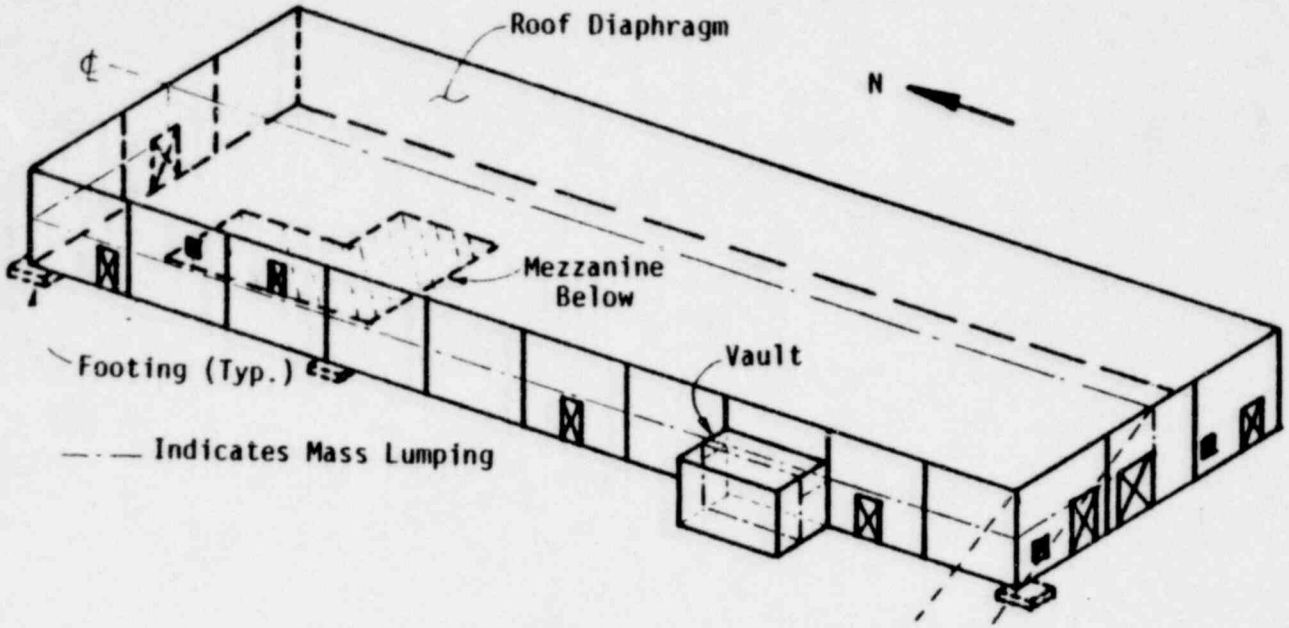

NMDF BUILDING OUTLINE

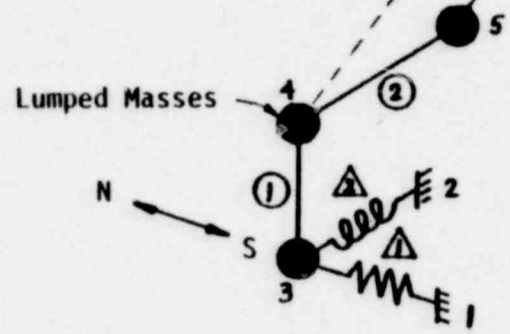

N-S DYNAMIC MODEL (one-half of structure)

① West wall cantilever shear/flexure beam

② Diaphragm (1/2) shear beam

△1 Translational soil spring

△2 Rotational soil spring

FIGURE 3-5. NORTH-SOUTH LATERAL FORCE RESISTING SYSTEM MODEL

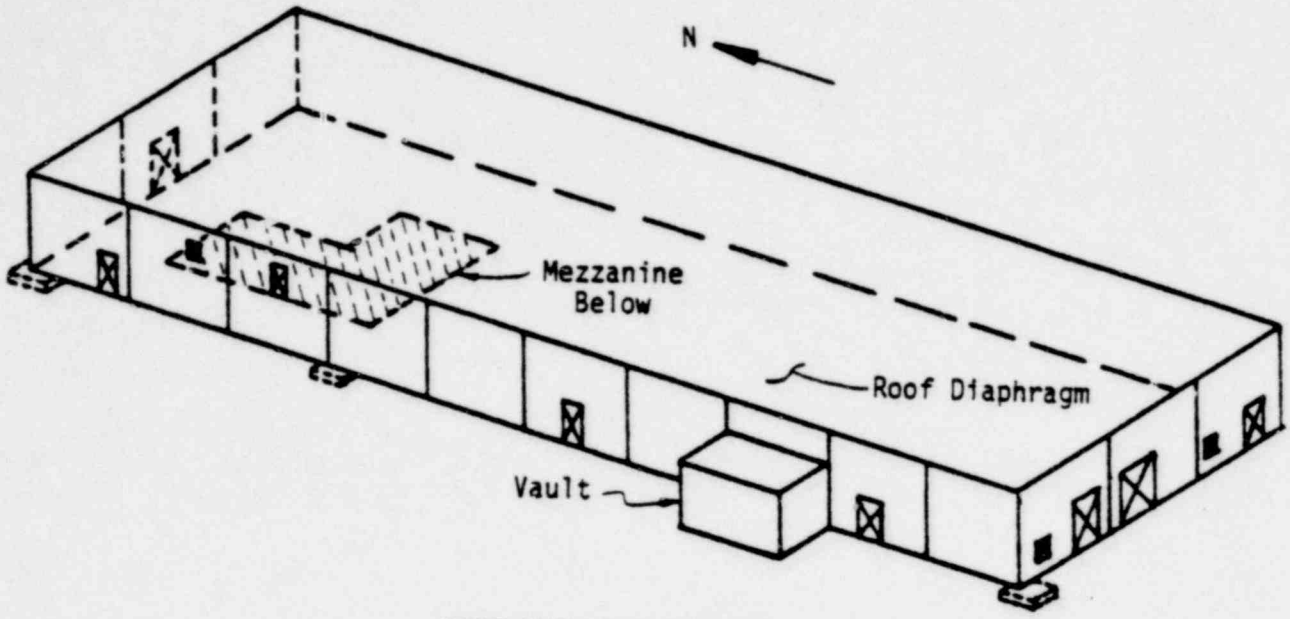

NMDF BUILDING OUTLINE

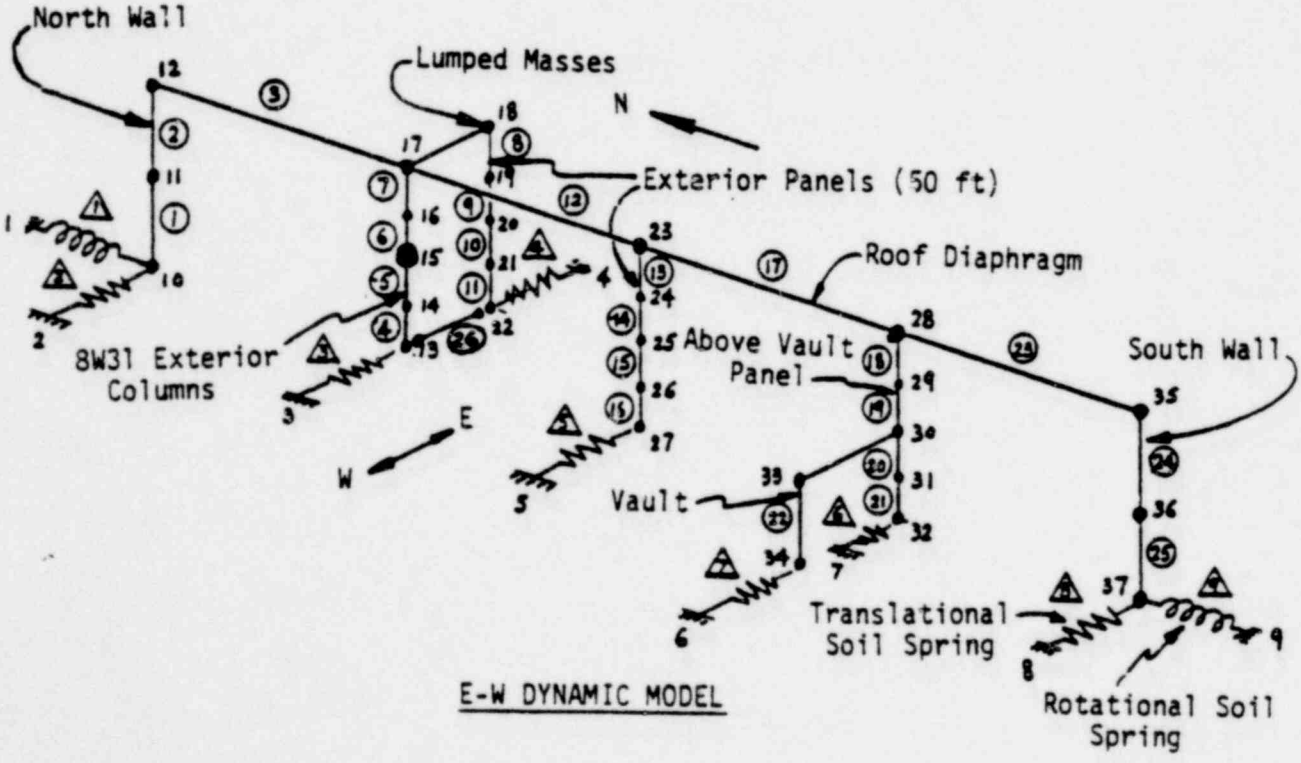

E-W DYNAMIC MODEL

FIGURE 3-6. EAST-WEST LATERAL FORCE RESISTING SYSTEM MODEL

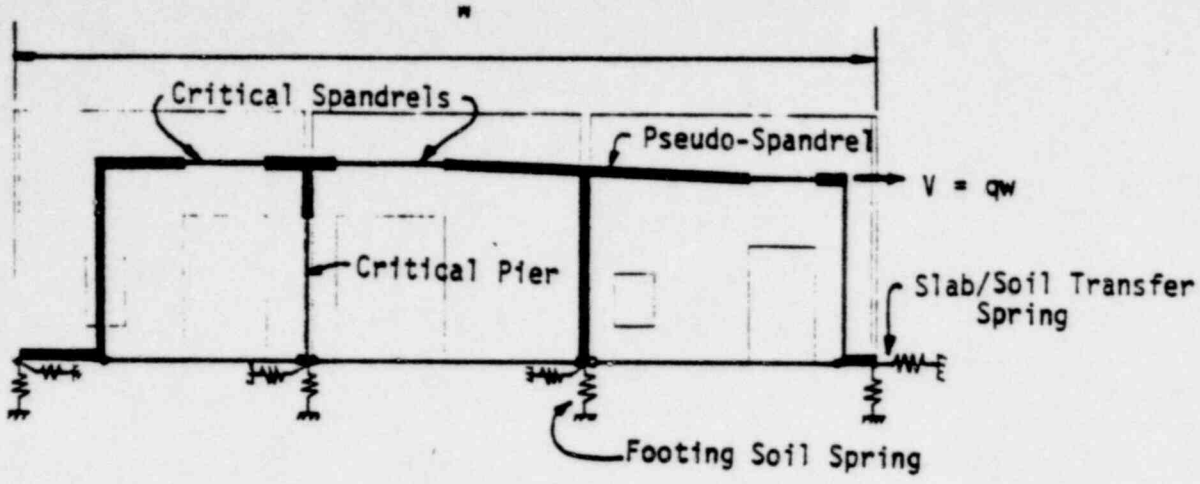

(a) Equivalent Frame

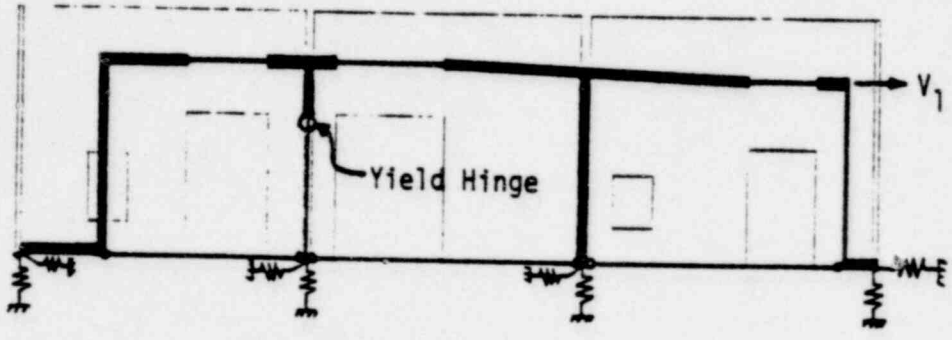

(b) First Hinge Formation

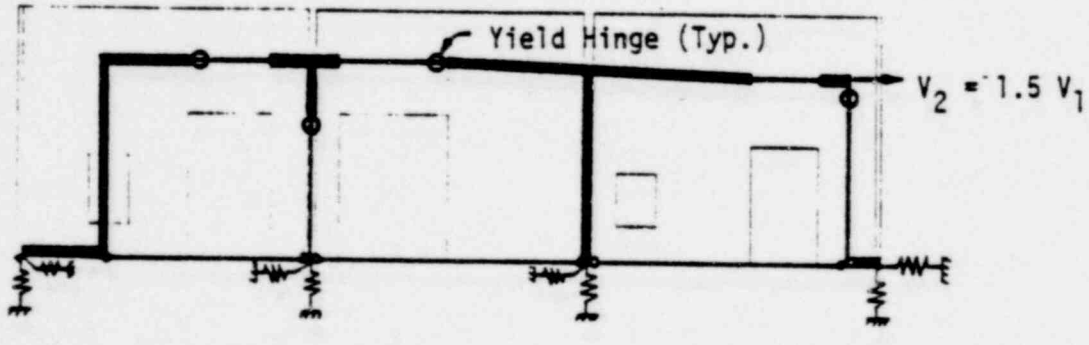

(c) Final Collapse Mechanism

1361 239

FIGURE 3-7. EQUIVALENT FRAME MODEL OF SOUTH WALL

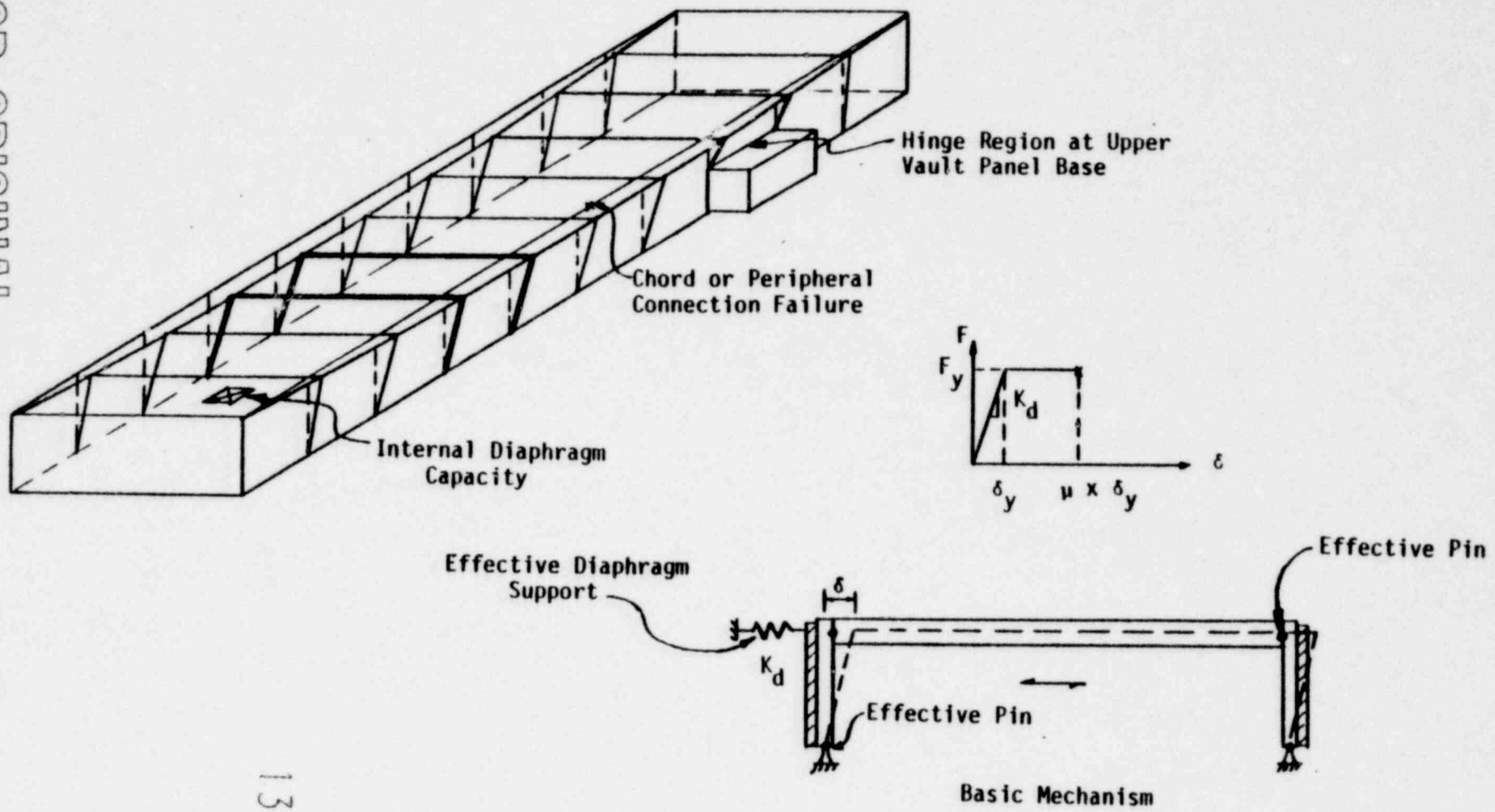

FIGURE 3-8. BASIC STRUCTURE COLLAPSE MODE

4. EVALUATION OF CRITICAL EQUIPMENT

This section of the report presents a discussion of the analysis of the critical equipment items including the analysis procedures used in the evaluation. The Task I Report (Reference 3) provides background information to which the interested reader is directed. For convenient reference, selected data and equipment details which are most pertinent to the critical equipment analyzed are abstracted from the Task I Report in Appendix E.

4.1 CRITICAL EQUIPMENT CONSIDERED

The critical areas of the NMDF building identified for study evaluation are the glove box room and the storage vault. The location of the critical process equipment within the glove box area is shown in Figure 4-1 by delineation of the two process lines. Each of these process lines consist of a sequence of glove boxes connected by transfer tubes. An elevation drawing of a typical process glove box is shown in Figure 4-2. Typical glove box construction is welded 12 ga. stainless steel (304) sheet with 3/8 inch acrylic plastic viewing windows. Each glove box is supported on a cross-braced, anchored steel tubular frame. In terms of potential release of hazardous chemicals in dispersible form, stations 3 and 5 are identified as the most critical items for study evaluation. Station 31 is also identified as critical due to the extreme fire hazard presented by sodium if exposed to air. The remaining glove boxes are of secondary concern.

Within the glove box room, all process piping, electric bus duct, instrumentation duct, glove box argon/air supply piping, and main exhaust piping are routed in a pipeway located directly overhead each process line as shown in Figure 4-3. This pipeway is horizontally and longitudinally braced from the roof at 20-foot intervals using the bracing details shown in Figure 4-4. The glove box argon/air supply and exhaust piping is 2.5 inch diameter welded steel pipe which are branch lines of the main 8-inch exhaust line.

Additional items considered for evaluation are the HEPA final exhaust filters and associated ductwork, 1A gas cylinders (within the glove box room), hydraulic fluid reservoirs, and the storage rack and containers located within the vault.

4.2 EQUIPMENT ANALYSIS PROCEDURES

The seismic capacity of the glove boxes and most other equipment is substantially higher than that of the building structure for the NMDF facility and, therefore, the approximate methods described below were used to establish the ground motion capacity since a higher degree of accuracy was not warranted.

4.2.1 STRUCTURE RESPONSE

The basic glove box structure was modeled as a planar rigid body supported on an equivalent lateral spring representing the support frame stiffness. A finite element idealization (EDAC/MSAP) of the braced support was utilized to assess the frame stiffness. The system response was determined directly from the response spectrum due to the simple single degree-of-freedom representation. Reference 18 indicates that for systems with 5% or greater damping, no response amplification occurs for system frequencies greater than 20 Hz. Since preliminary studies had established that the glove box frame system frequency was greater than 20 Hz and had assessed the system damping at 5% of critical, no ductility modified response spectra were considered.

4.2.2 OBJECT IMPACT

The evaluation of confinement breach caused by falling objects was based on an assumed critical loading caused by falling roof or wall segments. Prior evaluations conducted for other facilities in the Natural Hazards Study (Reference 50) outlined the general approach for impact evaluation of glove boxes and storage containers, considering energy relations for plastic impact of a falling object on the equipment.

The basic conclusion of these prior evaluations was that small missile impact or puncture of the glove boxes was not a significant hazard, due to the low velocity of objects falling from the ceiling (approximately 9 feet above the glove boxes). Thus, only with building collapse and subsequent impact of massive objects on the glove boxes, is significant release of hazardous chemicals from equipment possible.

4.2.3 RELATIVE DISPLACEMENT

Since the individual glove boxes and support stands exhibit a high degree of rigidity, the top of the glove boxes was considered to move with the ground while the horizontal piping runs were considered to move with the roof system. Thus, the glove box argon/air supply and exhaust piping (2.5 inch diameter) must accommodate the imposed relative displacement between the braced piping runs and the glove box attachment point. In addition, the piping located within the pipeway must accommodate the relative displacement between the horizontal support points within the plane of the roof.

The diaphragm displacement response (SRSS) of the east-west dynamic model (Figure 3-6) was utilized to evaluate the effects of relative displacement on the supported piping. Simple beam models of the piping were subjected to the displacement response of the support points to determine the capacity of these pipelines to sustain the imposed relative roof displacements prior to structure collapse.

4.3 EQUIPMENT ANALYSIS RESULTS

The Task II evaluation of the critical equipment items was concerned with damage resulting from both direct seismic induced loading of the eqiupment structure and damage caused by differential movement between duct and piping support points. The ground acceleration capacity of the glove box and exhaust pipe supports are tabulated in Table 4-1. Lower and upper bounds were determined using the procedure described in Appendix A. Comparison to Table 3-3 will indicate that none of the equipment capacities govern.

4.3.1 GLOVE BOXES

Using a single degree-of-freedom model, the fundamental frequency and the corresponding median spectral acceleration of a typical glove box and support frame were determined. The glove box frame and anchors were then analyzed for an equivalent lateral force which characterizes its response to horizontal ground motion. The connection of the glove box to the frame, the frame members, and the frame anchorage were evaluated for the transfer of the equivalent lateral (inertia) force. The lowest capacity was determined by the anchorage of the frame to the concrete slab. The effects of concurrent lateral and vertical ground motion were included in the evaluation. The capacity of the glove box assembly in terms of peak ground acceleration was then computed using equation 3-2 with F_c given by the equivalent lateral force which caused insert failure and with $F_{SRSS,1g}$ given by the glove box mass multiplied by the median spectral acceleration (Capacity = 1.7 g).

4.3.2 PIPING AND DUCTWORK

The effect of relative displacement between pipeway supports was evaluated by determining the internal bending moments and support reactions for the 8 inch main exhaust duct when subjected to the roof deformation response caused by east-west ground motion. The additional support reations and internal stress caused by the inertia response of the pipeway to the amplified roof motion were superimposed to determine the total element forces caused by the imposed roof response to a ground acceleration of 1.0g. The capacity of the pipeway was found to be governed by the shear capacity of the bolt connections for the pipeway bracing angles. Again, Equation 3-2 was utilized to determine the peak ground acceleration capacity (Capacity = 2.1 g).

The effect of relative roof displacement on the 2.5 inch glove box exhaust branch lines was assessed in an approximate manner to indicate the level of ground motion which would create a ductility demand on the glove box filter/pipe connection equivalent to the system ductility. Since the piping connections have a ductility capacity in excess of the structural

system ductility, the capacity for the branch line given in Table 4-1 should be viewed as a benchmark value indicating that this mode of behavior is not governing.

4.3.3 OTHER CRITICAL EQUIPMENT ITEMS

A hydraulic system which includes a reservoir and power unit is located in the glove box room. A floor mounted reservoir is connected to glove box 8 by means of high pressure hoses and glove box entry couplings. Upright type 1A gas cyclinders are mounted adjacent to glove box 18. While not directly associated with a potential mode of hazardous chemical release, the secondary effects of high flash point hydraulic fluid release as well as the potential missile capability of gas cylinders upon loss of a valve must be considered. Review of the hydraulic reservoir and gas cylinder mounting details indicated that damage due to direct seismic shaking is unlikely. The general conclusion is that these items will remain in place until impacted by collapsing structure (Capacity > 0.60 g).

The final building exhaust filters are located adjacent to the glove box room. In general, the filter assembly is held within welded frames and clamped within a sheet metal casing supported on anchored base channels. Review of the details of the filter and casing construction indicated that the assembly is flexible enough to accommodate several inches of displacement. The general conclusion is that the filter will remain intact until the casing (16 ga. steel) is subjected to external crushing loads caused by collapsing structure (Capacity > 0.60 g).

Hazardous chemicals are stored within the vault in 5-inch diameter, 12-inch long, 28 gauge sealed storage containers or "cans" fabricated from stainless steel tube. A storage rack of special design is anchored both to the vault floor and walls to support the storage containers in a precise configuration. The storage containers are placed in individual cans (#10) which are bolted to the rack shelves in a vertical position. The general construction of the storage rack is welded steel structural channel sections

with bolted diagonal bracing. The amount of material which can be stored at any given time is limited by the required configuration and clearances which must be maintained. Thus, the inertia loading on the rack is minimal. Review of the rack details and anchorage indicated that the rack and cans will remain in place until the vault walls are substantially damaged (Capacity > 2.4 g).

TABLE 4-1

SUMMARY OF SEISMIC CAPACITIES AFFECTING CRITICAL EQUIPMENT

Equipment Item	Expected Damage	Ground Acceleration Capacity, $A_g(g)$		
		Lower	Median	Upper
Glove Boxes	Concrete insert failure at frame anchorage	1.34	1.7	2.16
Pipeway Bracing	Shear of 3/8" diameter connection bolt	1.44	2.10	3.06
Exhaust Pipe Branch	Yield hinge ductility demand at filter of glove box equivalent to system ductility	1.19	1.71	2.45

1361 247

EDAC

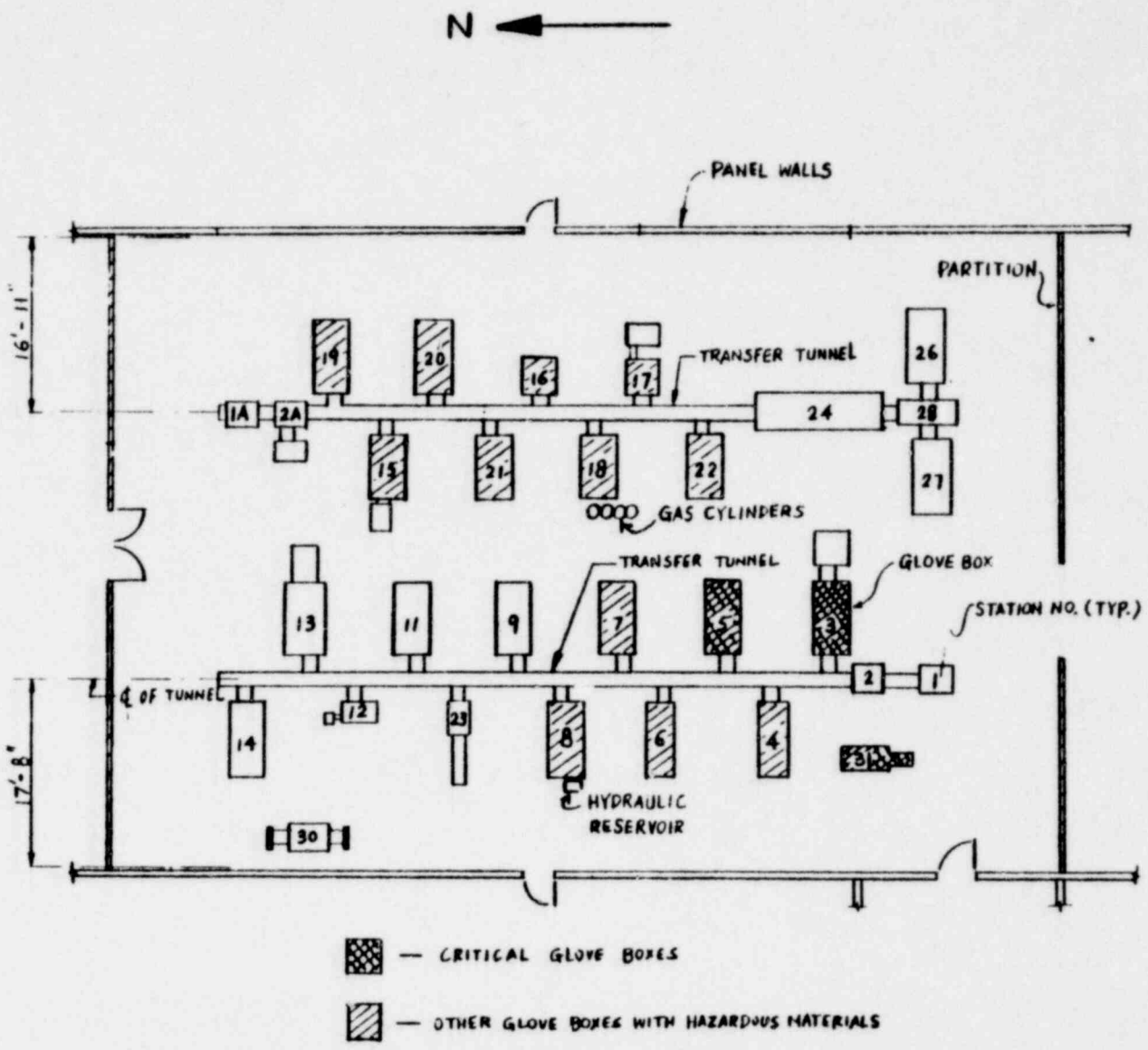

FIGURE 4-1. LOCATION OF CRITICAL GLOVE BOXES AND EQUIPMENT WITHIN GLOVE BOX ROOM

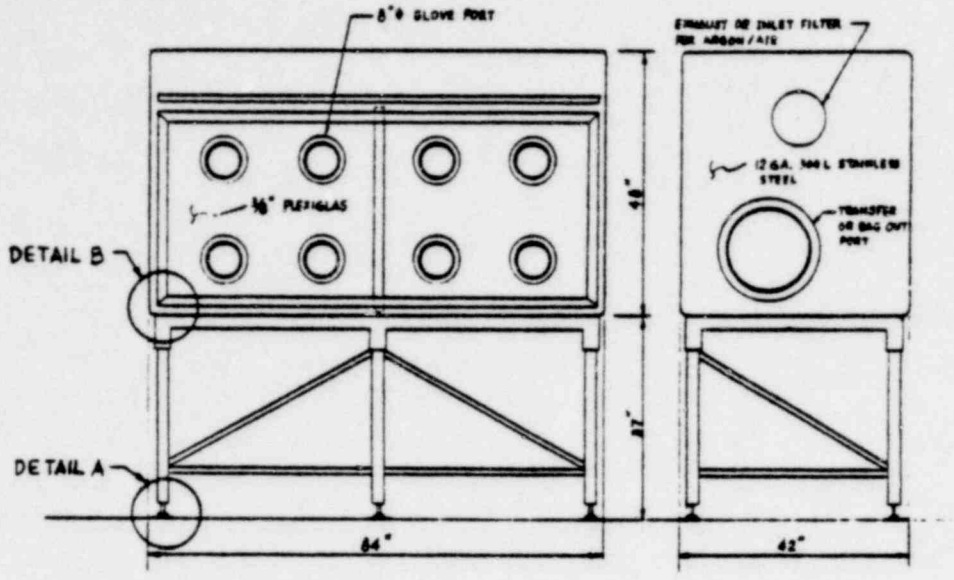

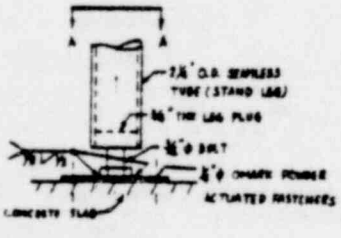

Detail A

Connection Between Frame and Floor

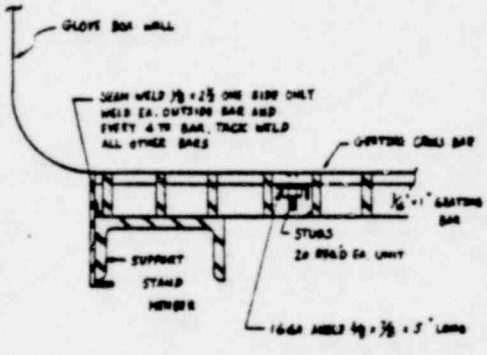

Detail B

Connection Between Glove Box and Frame

FIGURE 4-2. BASIC GLOVE BOX ASSEMBLY

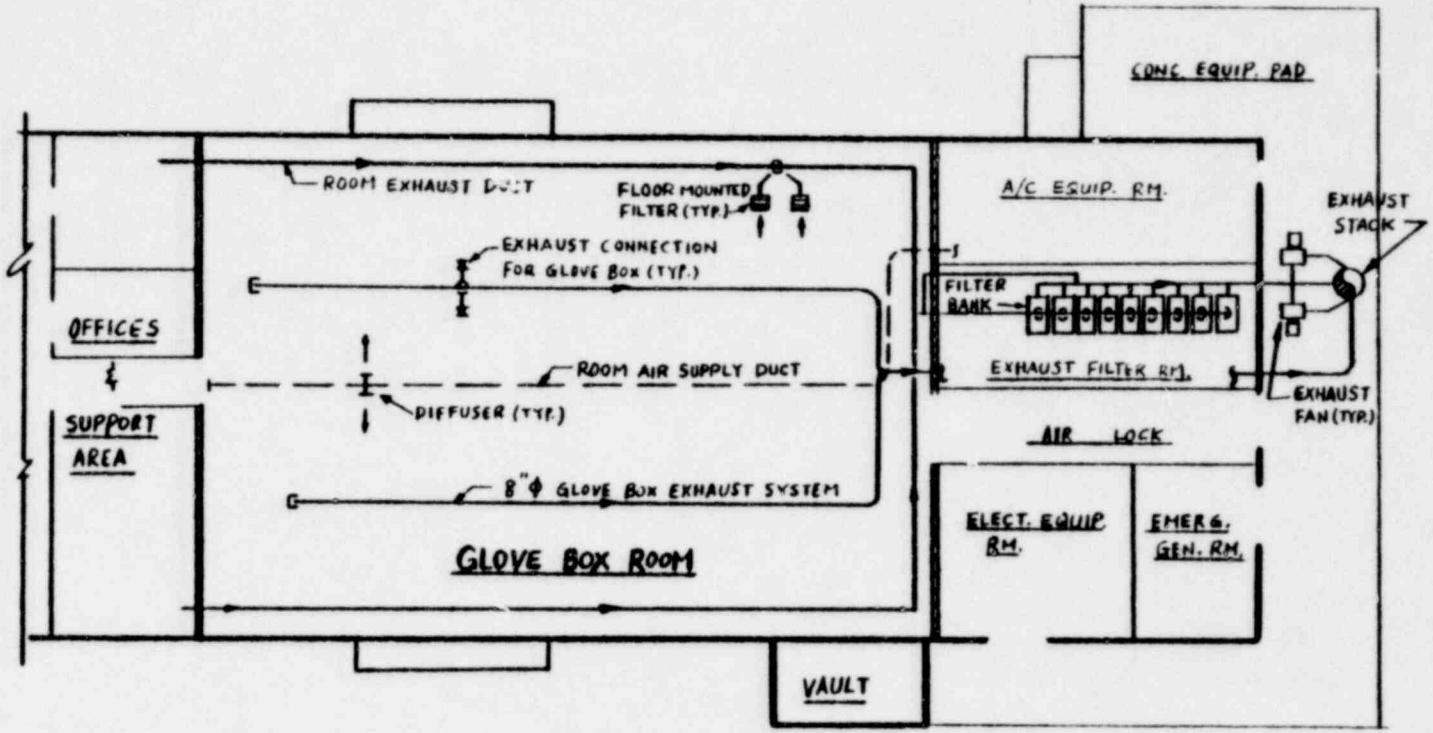

FIGURE 4-3. LOCATION OF DUCTWORK AND EXHAUST FILTERS

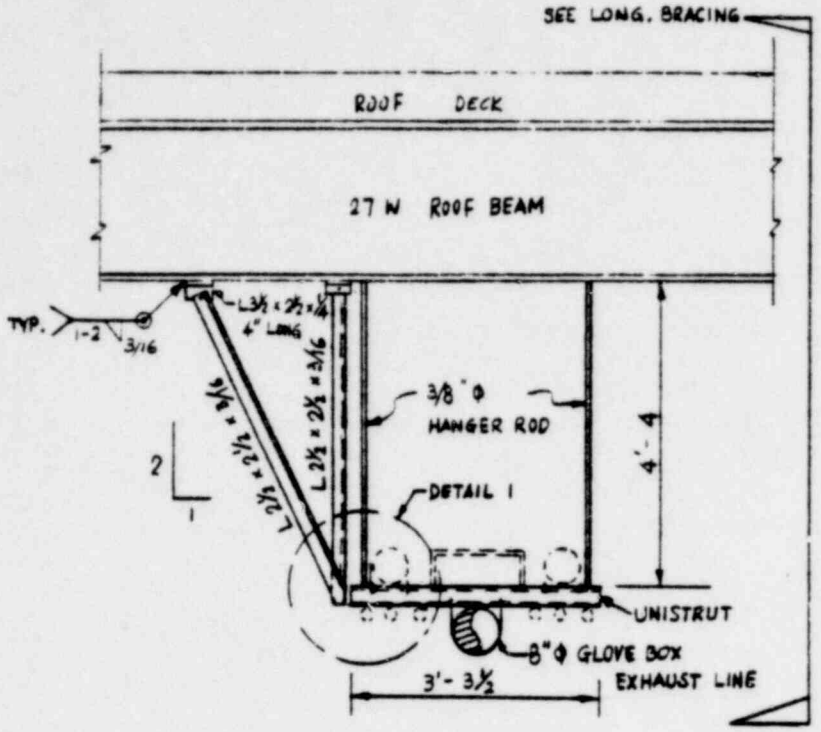

PIPEWAY - LATERAL BRACING (MAX. SPACING = 20'-0)

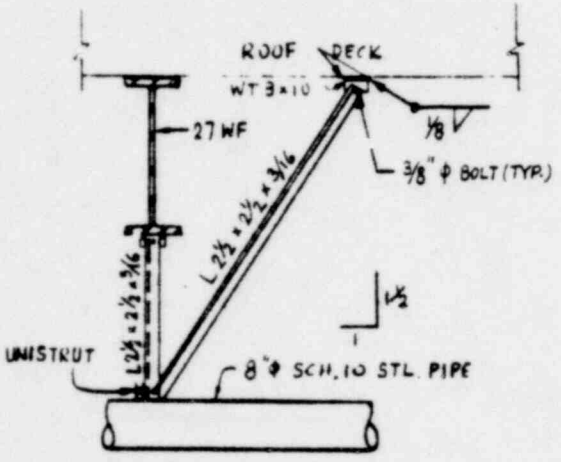

PIPEWAY - LONGITUDINAL BRACING (MAX. SPACING = 40'-0)

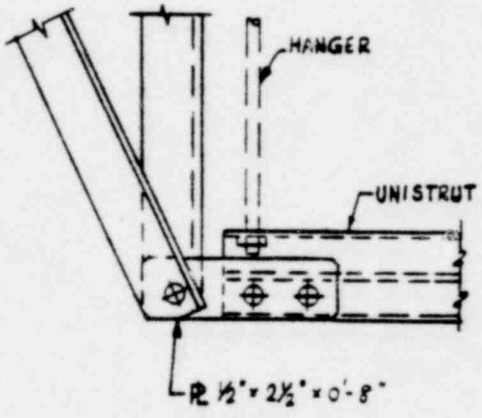

DETAIL 1

FIGURE 4-4. PIPEWAY SUPPORT AND BRACING

5. SUMMARY OF RESULTS AND STRUCTURAL DAMAGE SCENARIO

This section presents a summary tabulation of the results of the analyses described previously and presents the interpretation of these results in terms of a structural damage scenario, which describes the progression of expected damage to the NMDF facility with increasing intensity of earthquake ground motion.

Table 5-1 presents a tabulation of the critical seismic capacities of the structural systems evaluated during the Task II effort. These capacities are associated with structural collapse and as such establish the ground motion acceleration levels associated with probable release of hazardous material. Evaluation of the glove boxes and exhaust piping/ductwork indicates that these equipment systems have ground acceleration capacities in excess of the structural collapse capacities. The equipment systems cannot withstand the imposed falling weight of the collapsing structure. Thus, these ground motion acceleration capacities represent the level of seismic motion which causes complete loss of confinement for hazardous materials.

The analyses of structural capacity were conducted using median material strength properties and median estimates of dynamic response to ground shaking. Based upon the assumption that the important contributing variables are approximately lognormally distributed, the calculated upper and lower bound capacity values represent an estimated one standard deviation variation. The median capacity values represent the evaluation of the various systems as they currently exist in the NMDF facility. The values are shown to two significant figures to indicate the relative order of capacities. It should not be implied that the level of the analysis justifies collapse values to this accuracy.

The transverse or east-west structural system of the NMDF exhibits a lower seismic capacity than the longitudinal or north-south structural system. Collapse of the structure due to east-west ground motion will occur at a median ground acceleration level of 0.60g. This collapse mode is associated with the loss of roof diaphragm support for the east and west walls. For north-south ground motion, collapse will occur due to diaphragm failure at an acceleration level of 0.83g. It should be noted that both of these collapse estimates include the effect of concurrent ground motion orthogonal to the principal direction of shaking considered. Extensive structural modification is necessary to prevent these modes of collapse.

The following scenarios present a description of the behavior of the structure resulting from increasing ground motion acceleration. The scenarios are based upon the median predicted capacities of the NMDF structural systems. The return periods associated with the scenario for each level of ground shaking are taken from the "best estimate" data presented in Reference 5 relating peak ground acceleration in g's to return period in years. The three scenarios correspond to ranges of 0.20g to 0.35g, 0.35g to 0.55g and 0.55g greater ground motion acceleration.

Ground Shaking of 0.20 to 0.35g (T = 100 years for 0.35g)

At a ground acceleration below 0.20g, there is no significant effect of the occurrence of an earthquake. Above 0.20g minor structural damage in the form of concrete cracking in the vicinity of panel inserts and minor yielding of diaphragm connections is initiated.

Ground Shaking of 0.35 to 0.55g (T = 550 years for 0.55g)

Progressive concrete cracking damage and yielding of steel connections continues beyond .35g. Pier No. 2 of the south wall forms a yield hinge at the pier-spandrel junction at 0.41g. Also at an acceleration of 0.41g, the concrete panel inserts connected to the exterior mezzanine columns fail in shear preventing further composite panel/column behavior in resisting the mezzanine floor inertia. Further resistance

is provided by the columns acting alone. The portion of the panel wall above the vault forms a yield hinge at an acceleration level of 0.47g, but the vault box structure is not affected. For ground motion in excess of 0.50g, the diaphragm is highly overstressed with significant yielding of both perimeter and interior connections.

Ground Shaking of 0.55g and Greater (T = 750 years for 0.60g)

Beyond 0.55g the diaphragm is being severely damaged. At an acceleration of 0.60g, the diaphragm chord along the west and east walls will fail in tension at the splice plates. The internal diaphragm seam welds will fail at 0.62g, therefore, complete loss of diaphragm strength must be associated with 0.60g. After a few cycles of motion at this level of shaking, the pin-jointed roof girder-column connection will allow wall collapse to initiate for the glove box room area. The progression of collapse beyond this level of acceleration is uncertain, but the crushing of critical glove boxes by falling roof girders must be assumed to occur at 0.60g. The exact number of glove boxes likely to be crushed in this event is unknown. However, since the glove boxes are connected by common transfer tubes and air and exhaust piping, loss of one glove box or section of transfer tube will lead to loss of confinement for the hazardous material in essentially the complete transfer line. Thus, this establishes the ground motion level associated with loss of confinement. The hinging of the above vault panel will allow partial roof collapse in this area of the glove box room, but the vault will remain intact at levels in excess of 2.0g.

TABLE 5-1. SUMMARY OF CRITICAL SEISMIC CAPACITIES

STRUCTURAL DAMAGE	GROUND ACCELERATION CAPACITY (g)		
	LOWER	MEDIAN	UPPER
Diaphragm Chord Failure (E-W Motion)	0.41	0.60	0.88
Diaphragm Internal Connection Failure (E-W Motion)	0.42	0.62	0.91
Diaphragm Internal Connection Failure (N-S Motion)	0.56	0.83	1.22
Diaphragm Perimeter Connection Failure (N-S Motion)	0.59	0.87	1.28

REFERENCES

1. Ayer, J. A., and W. Burkhardt, "Analysis of the Effects of Abnormal Natural Phenomena on Existing Plutonium Fabrication Plants", United States Nuclear Regulatory Commission, Washington, D.C., 1976.

2. Letter, transmitting "Evaluation of Possible Flooding at Atomic International Nuclear Development Field Laboratory", R. W. Starostecki of USNRC to M. E. Remley of AI, dated January 27, 1978.

3. "Structural Condition Documentation and Structural Capacity Evaluation of the Atomics International Nuclear Material Development Facility, at Santa Susana, California for Earthquake and Flood, Task I - Structural Condition", Engineering Decision Analysis Company, Inc. (EDAC), EDAC 175-070.1R for Lawrence Livermore Laboratory, Livermore, California, March, 1978.

4. Mishima, J., "Identification of Features Within Plutonium Fabrication Facilities Whose Failure May Have A Significant Effect On The Source Terms", Working Paper on Increment of Analysis for Atomics International, Nuclear Material Development Facility, Part of USNRC Study of Analysis of the Effect of Natural Phenomena Upon Existing Plutonium Fabrication Facilities, Battelle, Pacific Northwest Laboratory, Richland, Washington, May, 1978.

5. "Seismic Risk Analysis for the Atomics International Facility, Santa Susana, California", TERA Corporation, for Lawrence Livermore Laboratory, Livermore, California, July, 1978.

6. Hadjian, A. H. and T. S. Atalik, "Discrete Modeling of Symmetric Box-Type Structures", Proceedings, International Symposium on Earthquake Structural Engineering, St. Louis, Missouri, August, 1976, pp. 1151-1164.

7. S. B. Barnes and Associates, "Report on Use of H. H. Robertson Steel Roof and Floor Decks as Horizontal Diaphragms", Los Angeles, California, July, 1963.

8. H. H. Robertson Company, "Shear Values and Flexibility Factors", Technical Report Q-135-70, Pittsburgh, Pa.

9. Departments of the Army, the Navy, and the Air Force, "Seismic Design Design for Buildings", TM 5-809-10, NAV FAC P-355, AFM 88-3, Chap. 13, April 1973.

10. Paulay, T., "Earthquake Resistant Structural Walls", Presented at the NSF Workshop on Earthquake Resistant Concrete Building Construction, University of California, Berkeley, July 11-16, 1977.

11. Portland Cement Association, Analysis of Small Reinforced Concrete Buildings for Earthquake Forces, Chicago, Illinois, 1955 & 1974.

12. Benjamin, J. R. Statically Indeterminent Structures, McGraw-Hill Book Company, Inc., 1959.

13. Peterson, H. B., Popov E. P., and Bertero, V. V., "Practical Design of R/C Structural Walls Using Finite Elements", IASS World Congress on Space Enclosures (WCOSE-76), Building Research Centre, Concordia University, Montreal, Canada, July 5-8, 1976.

14. Bathe, K.J., Wilson, E. L., and F. E. Peterson, "Sap IV - A Structural Analysis Program for Static and Dynamic Response of Linear Systems", Report No. EERC 73-11, University of California, Berkeley, June 1973.

15. Richart, F. E., Hall, J. R., and R. D. Woods, Vibration of Soils and Foundations, Prentice-Hall, Inc., New Jersey, 1970.

16. Novak, M., "Effect of Soil on Structural Response to Wind and Earthquake", Earthquake Engineering and Structural Dynamics, Vol. 3, 1974, pp. 79-96.

17. Novak, M., "Vibrations of Embedded Footings and Structures", Meeting Preprint 2029, presented at the ASCE National Structural Engineering Meeting, April 9-13, 1973, San Francisco, California.

18. "A Study of Vertical and Horizontal Earthquake Spectra", WASH--1255, Nathan M. Newmark Consulting Engineering Services for Directorate of Lincensing, United States Atomic Energy Commission, April 1973.

19. Hall, W. J., B. Mohraz, and N. M. Newmark, "Statistical Analysis of Earthquake Response Spectra", Transactions Third International Conference on Structural Mechanics in Reactor Technology, (London), Paper K1/6, 1975.

20. Blume, J. A., Newmark, N. M., and L. H. Corning, Design of Multistory Reinforced Concrete Buildings for Earthquake Motion, Portland Cement Association, 1961.

1361 257

21. Newmark, N. M., and E. Rosenblueth, Fundamentals of Earthquake Engineering, Prentice Hall, Inc., 1971, Chapter 11.

22. Newmark, N. M., "Earthquake Response Analysis of Reactor Structures", Nuclear Engineering and Design, Volume 20, 1972, pp. 303-322.

23. Newmark, N. M., and W. J. Hall, "Procedures and Criteria for Earthquake Resistant Design", Building Practices for Disaster Mitigation, National Bureau of Standards (Washington, D.C.) Building Science Series 46, Vol. 1, February 1975, pp. 209-236.

24. Applied Technology Council, An Evaluation of a Response Spectrum Approach to Seismic Design of Buildings, ATC-2, U.S. Department of Commerce, National Bureau of Standards, 1974.

25. Newmark, N. M., "A Response Spectrum Approach for Inelastic Seismic Design of Nuclear Reactor Facilities", Transactions Third International Conference on Structural Mechanics in Reactor Technology (London), Paper K5/1, Vol. 4, Part K, 1975.

26. Newmark, N. M., "Inelastic Design of Nuclear Reactor Structures and Its Implication on Design of Critical Equipment", Transactions Fourth International Conference on Structural Mechanics in Reactor Technology (San Francisco), Paper K4/1, Vol. K(a), 1977.

27. Freudenthal, A. M., Garrelts, J. M., and Shinozuka, M., "The Analysis of Structural Safety", Journal of the Structural Division, ASCE, STI, February, 1966, pp. 267-325.

28. Kennedy, R. P., "A Statistical Analysis of the Shear Strength of Reinforced Concrete Beams", Technical Report No. 78, Department of Civil Engineering, Stanford University, Stanford, California, April, 1967.

29. Kennedy, R.P., and C. V. Chelapati, "Conditional Probability of a Local Flexural Wall Failure for a Reactor Building as a Result of Aircraft Impact", Holmes & Narver, Inc. for General Electric Company, San Jose, California, June 1970.

30. Benjamin, J.R., and C. A. Cornell, Probability, Statistics, and Decision for Civil Engineers, McGraw-Hill Book Company, New York, 1970.

1361 258

31. Building Code Requirements for Reinforced Concrete (ACI 318-71), American Concrete Institute, 1971.

32. PCI Design Handbook, Prestressed Concrete Institute, 1971.

33. Ollgaard, J. G., Slutter, R. G., and J. W. Fisher, "Shear Strength of Stud Connectors in Lightweight and Normal-Weight Concrete" AISC Engineering Journal", April, 1971, pp. 55-64.

34. McMackin, P. J., Slutter, R. G., and J. W. Fisher, "Headed Steel Anchors under Combined Loading", AISC Engineering Journal, Second Quarter, 1973, pp. 43-52.

35. Davies, C., "Small-scale Push-out Tests on Welded Stud Shear Connectors", Concrete, September, 1967, pp. 311-316.

36. Becker, J. M. and C. Llorente, "Seismic Design of Precast Concrete Panel Buildings", presented at the NSF Workshop on Earthquake Resistant Concrete Building Construction, University of California, Berkeley, July 11-16, 1977.

37. Hawkins, N. M., "Analytical and Experimental Studies of Prestressed and Precast Concrete Elements", presented at the NSF Workshop on Earthquake Resistant Concrete Building Construction, University of California, Berkeley, July 11-16, 1977.

38. Perry, E. S. and J. Nabil, "Pullout Bond Stress Distribution Under Static and Dynamic Repeated Loadings", ACI Journal, May, 1969, pp. 377-380.

39. Mast, R. F., "Auxiliary Reinforcement in Concrete Connections", Journal of the Structural Division, ASCE, ST6, June, 1968, pp. 1485-1504.

40. Birkeland, P. W. and H. W. Birkeland, "Connections in Precast Concrete Construction", ACI Journal, March, 1966, pp. 345-367.

41. Walker, H. C., et al., "Summary of Basic Information on Precast Concrete Connections", PCI Journal, December, 1969, pp. 14-58.

42. Mattock, A. H., L. Johal and H. C. Chow, "Shear Transfer in Reinforced Concrete and Moment or Tension Acting Across the Shear Plane", PCI Journal, July-August, 1975, pp. 76-93 (see also following discussion by H. W. Birkeland).

43. Mattock, A. H., and N. M. Hawkins, "Shear Transfer in Reinforced Concrete-Recent Research", PCI Journal, March-April, 1972, pp. 55-75.

1361 259

44. Hofbeck, J. A., Ibrahim, I. O., and A. H. Mattock, "Shear Transfer in Reinforced Concrete", ACI Journal, February, 1969, pp. 119-128.

45. Park, R. and T. Paulay, Reinforced Concrete Structures, John Wiley and Sons, New York, 1975.

46. Manual of Steel Construction, Seventh Edition, American Institute of Steel Construction, 1970.

47. Bresler, B., T. Y. Lin, and J. B. Scalzi, Design of Steel Structures, John Wiley and Sons, New York, 1968.

48. Nilson, A. H., "Shear Diaphragms of Light Gage Steel", Journal of the Structural Division, ASCE, ST11, November, 1960, pp. 111-139.

49. Freeman, S. A. "Racking Tests of High-Rise Building Partitions" Journal of the Structural Division, ASCE, ST8, August 1977, pp. 1673-1685.

50. "Structural Condition Documentation and Structural Capacity Evaulation of the Westinghouse Laboratory Facility at Cheswick, Pennsylvania for Earthquake and Flood, Task II - Structural Capacity Evaluation: Seismic Evaluation", Engineering Decision Analysis Company, Inc. (EDAC), EDAC 175-040.2R, for Lawrence Livermore Laboratory, Livermore, California, July, 1978.

1361 260

APPENDIX A

UNCERTAINTY BOUND ANALYSIS PROCEDURE

APPENDIX A

Uncertainty Bound Analysis Procedure

The basic statistical procedure used in the uncertainty bound analysis was based upon the general statistical properties of a lognormal distribution. The procedure involved the identification of each major random variable which can be considered as a potential source of substantial uncertainty in computing the median capacity values and the appropriate combination of the uncertainty potential from each variable to obtain the total uncertainty. Lognormal distributions were selected for use in estimating uncertainty bounds in the overall Task II evaluation results since the statistical variation of many material properties and seismic input functions may be represented by the distribution. It is generally acknowledged (References 27, 28) that the mechanical strength properties (e.g., yield and tensile strength) of structural materials may be characterized by a lognormal distribution. In addition, studies (Reference 19) have indicated that the statistical variation of response to seismic ground motion, as characterized by response spectra (Reference 18), may be represented by a lognormal distribution. Thus, while a lognormal distribution might not be the optimum choice of distribution for structural element capacities or element forces due to dynamic response, it provides a sufficient approximation and is computationally convenient since the assumption of a lognormal distribution leads to a simplified combination of product random variables.

For a lognormal distribution, the mean value does not have a phyiscal interpretation, thus the median value is used as the characteristic parameter (i.e., 50% of the values are above the median value and 50% are below the median value). The upper and lower bound values of the important

contributing variables were estimated to represent a variation of one standard deviation and are based upon engineering judgement concerning the variation of the contributing variable values rather than on detailed statistical studies. Thus, the lower bound and upper bound represent the estimated 16% and 84% percentile values, respectively, with 68% of all samples falling between the upper and lower bounds. The estimated lower and upper bound material parameter values were presented in the Task I Report along with estimated upper and lower bounds for damping and ductility to be utilized in the response analysis. The median and upper bound values of response were taken from the median and one sigma response spectra given in Reference 18.

A.1 BASIC RELATIONS

Before discussing the detailed method for estimating the uncertainty factors and bounds, some general relations for lognormally distributed variables will be presented which are used more specifically in the subsequent development. Background and futher information on these relationships are given in References 29 and 30.

Stated mathematically, a random variable x is said to be lognormally distributed if its natural logarithm $\tilde{x}$ given by

$$\tilde{x} = \ln(x)$$

is normally distributed. If a, b, and c are independent lognormally distributed random variables, and if

$$d = \frac{a^r \cdot b^s}{c^t} \qquad \text{(A-1)}$$

where r, s, and t are given exponents, then d is also a lognormally distributed random variable. Further, the median value of d, denoted by D, and the logrithmic variance σ_d^2, which is the square of the lognormal standard deviation of d, are given by

$$D = \frac{A^r \cdot B^s}{C^t} \qquad \text{(A-2)}$$

and

$$\sigma_d^2 = r^2\sigma_a^2 + s^2\sigma_b^2 + t^2\sigma_c^2 \qquad \text{(A-3)}$$

where A, B, and C are the median values, and σ_a^2, σ_b^2, and σ_c^2 are the logrithmic variance of a, b, and c, respectively. The logrithmic standard deviation for each independent variable may be estimated as shown below for the variable a, from the estimated lower bound, median, and upper bound values given by a_ℓ, a_m, and a_u respectively.

$$\sigma_a \cong \frac{1}{2}\left[\ln\left(\frac{a_m}{a_\ell}\right) + \ln\left(\frac{a_u}{a_m}\right)\right] \qquad \text{(A-4)}$$

Note that if a is exactly lognormal,

$$\sigma_a = \ln\left(\frac{a_m}{a_\ell}\right) = \ln\left(\frac{a_u}{a_m}\right) \qquad \text{(A-5)}$$

Given the estimated logrithmic standard deviation for each variable, it follows that the estimated one standard deviation upper and lower bound values of d, given by d_u and d_ℓ, may be computed as

$$d_u = D\ \exp(\sigma_d) \qquad \text{(A-6)}$$

$$d_\ell = D\ \exp(-\sigma_d) \qquad \text{(A-7)}$$

The coefficient of variation of d, V_d, is given by the relation (Reference 30)

$$V_d = \sqrt{\exp(\sigma_d^2)-1} \qquad \text{(A-8)}$$

A.2 APPLICATION TO CAPACITY EVALUATION

The application of the statistical procedure described above to the evaluation of the structural system is demonstrated in the following discussion. From equation 3-2, the median ground acceleration capacity, $(A_g)_m$, of a structural element may be computed as follows:

$$(A_g)_m = F_C / F_{SRSS,1g} \qquad \text{(A-9)}$$

where

F_C = Median element force capacity

$F_{SRSS,1g}$ = Median element force response determined by square-root-sum-of-square (SRSS) combination of modal response components obtained from a modal spectral analysis of building models using median 1.0 g ground acceleration non-linear (reduced) response spectrum with median damping, β, and median ductility factor, μ.

The estimate of median element force response, may be expressed (Equation 3-1) as

$$F_{SRSS,1g} = \sqrt{\sum_n \left(F_{n,1g}\right)^2} \qquad \text{(A-10)}$$

where $F_{n,1g}$ represent the modal components of element force response. Given that the modal component corresponding to the fundamental frequency (or period) of the structural system is 2 or 3 times the other modal response components, the fundamental component (n = 1) will account for 85-95% of the SRSS estimate given by Equation A-9. Thus, due to the dominance of the first mode, the median element force response may be considered to be approximately proportional to the spectral acceleration, SA_{1g}, given by the ordinate of the median response spectrum (normalized to 1.0g) associated with the fundamental frequency of the structural system. It should be noted that this approximation is also valid for element response governed by a mode other than the fundamental as long as the dominant modal component exceeds the remaining modal components by a factor of 2 or greater.

The variation in element force capacity, F_C, is considered to be independently a function of the variation in material strength and construction quality. The variation in element force response, F_{SRSS}, is considered to be independently a function of the structural idealization represented by the dynamic model and the spectral acceleration associated with the dominant modal frequency. The variability associated with the capability of the dynamic model to duplicate actual structural response due to earthquake ground motion is assessed by a subjective judgement factor. For simplicity, the variability of the spectral acceleration is considered to be independently a function of the variation in the spectral response ordinate, SA, due to the variation of input ground motion, the variation in system damping, β, and the variation in the value of spectral acceleration reduction factor, R, as influenced by the variation in system ductility factor, μ. The factor R is taken as unity for the ground acceleration portion of the response spectrum, $1/\sqrt{2\mu - 1}$ for the amplified acceleration spectral region and $1/\mu$ for the spectral velocity and spectral displacement regions. Thus, the ground acceleration capacity may be expressed as a function of the following variables centered on median values of unity:

$$A_q = \left(A_g\right)_m E_c W_c J / S_a C_\beta D_\mu \qquad \text{(A-11)}$$

where

E_c = Factor expressing the variation of element capacity as a function of the ratio of material strength to the median material strength governing the element failure mode (median value for $E_c = 1.0$).

W_c = Subjective factor expressing the variation of element capacity as a function of construction quality and workmanship (median value for $W_c = 1.0$).

S_a = Factor expressing the variation of spectral acceleration response due to the variance in ground motion input (given median system damping β, and median system ductility, μ) as a function of the ratio of response spectrum ordinate to the median response spectrum ordinate at the system frequency at the dominant mode. (Median value for $S_a = 1.0$).

C_β = Factor expressing the variation of spectral acceleration response due to the variance in system damping (given median response spectra and median system ductility) as a function of the ratio of response spectrum ordinate to the median response spectrum ordinate at the dominant system frequency. (Median value for $C_\beta = 1.0$).

D_μ = Factor expressing the variation of spectral acceleration response due to the variance in system ductility, characterized by the spectral reduction factor, as a function of the ratio of response spectrum ordinate to the median response spectrum ordinate at the dominant system frequency. (Median value for $D_\mu = 1.0$).

J = Subjective judgement factor expressing the variation of ground acceleration capacity as a function of the overall assessment of the procedure accuracy, element force capacity conservatism, and capability of the building dynamic model to duplicate actual structural response due to earthquake ground motion. (Median value for J = 1.0).

The logarithmic variance in ground acceleration capacity may then be defined in terms of the logarithmic variance of each of the independent contributing random variables

$$\beta_{A_g}^2 = \beta_{E_c}^2 + \beta_{W_c}^2 + \beta_{S_a}^2 + \beta_{C_B}^2 + \beta_{D_\mu}^2 + \beta_J^2 \qquad \text{(A-12)}$$

Thus, the upper and lower bound values for the seismic acceleration capacity may be computed as

$$\left(A_g\right)_u = \left(A_g\right)_m \exp(\beta_{A_g})$$

$$\left(A_g\right)_\ell = \left(A_g\right)_m \exp(-\beta_{A_g}) \qquad \text{(A-13)}$$

A.3 SAMPLE CALCULATION

This section provides a description of the use of the uncertainty bound procedure in establishing the estimated upper and lower bound seismic capacity values for the NMDF facility. The sample calculation included in this appendix pertains to the major failure capacity identified for the lateral force resisting structural systems.

As discussed above, the variables which contribute to the ground acceleration capacity uncertainty may be characterized by a strength capacity factor, a workmanship assessment factor, spectral response factors considering the independent effects of input, damping, and ductility variation, and an analysis judgement factor. The effect of the variation in ground motion (variable S_a) and the effect of the variation in system damping (variable C_β) were assessed from the criteria spectra data presented in WASH 1255 (Reference 18). Table A-1, which was abstracted from the WASH 1255 document, presents the median (50 percentile) and the one standard deviation (84.1 percentile values of spectral amplification for various levels of damping and for the three major spectral frequency regions. The results of the determination of the variation in spectral acceleration response due to the independent variation of input motion, damping, and ductility are tabulated in Table A-2 for the fundamental frequency of the structure in the east-west direction (f_1 = 5 Hz). The variation of material strengths for each element failure mode which governs each major capacity estimate for the NMDF yielding is tabulated in Table A-3. The resulting normalized contributing factors, as defined for Equation A-11, are tabulated in Table A-4. The upper and lower bound assigned to the subjective construction quality and workmanship factor, W_c, and the analysis judgement factor are also given in the tabulation.

A.3.1 Example Calculation: Diaphragm Capacity

The failure of the diaphragm chord is controlled by the fundamental mode of response (5 Hz) for east-west shaking. Referring to Table A-4, we obtain the estimates of the logarithmic standard deviation for each contributing factor.

Diaphragm shear response

$\sigma_{S_a} = 0.199$, $\sigma_{C_\beta} = 0.137$, $\sigma_{D_\mu} = 0.191$

Diaphragm capacity

$\sigma_{E_c} = 0.168$, $\sigma_{W_c} = 0.0$

Analysis assessment

$\sigma_J = 0.164$

Now, utilizing Equation A-12 we obtain

$$\sigma_{A_g}^2 = (0.168)^2 + (0.0)^2 + (0.199)^2 + (0.137)^2 + (0.191)^2 + (0.164)^2 = 0.150$$

$$\sigma_{A_g} = 0.387$$

and from Equation A-13, the ground acceleration capacity is, given $(A_g)_m = 0.60$,

$$A_g = 0.60 \exp(\pm 0.387) \qquad A_{g_u} = 0.88$$

$$A_{g_\ell} = 0.41$$

Using Equation A-8, we obtain the coefficient of variation for the ground acceleration capacity,

$$V_{A_g} = \sqrt{\exp(0.150) - 1} = 0.402$$

1361 270

EDAC

TABLE A-1. HORIZONTAL DESIGN SPECTRA AMPLIFICATIONS AND BOUNDS

(Reference 18)

Percentile	Damping percent	Amplification D	Amplification V	Amplification A	Faring frequency hertz	Spectrum bounds (alluvium) D in	Spectrum bounds (alluvium) V in/sec	Spectrum bounds (alluvium) A g	Spectrum bounds (rock) D in	Spectrum bounds (rock) V in/sec	Spectrum bounds (rock) A g
50	0.5	1.97	2.58	3.67	40	71	124	3.67	24	72	3.67
	2.0	1.68	2.06	2.76	30	60	99	2.76	20	58	2.76
	5.0	1.40	1.66	2.11	20	50	80	2.11	17	46	2.11
	10.0	1.15	1.34	1.65	20	41	64	1.65	14	38	1.65
75	0.5	2.66	3.41	4.65	40	96	164	4.65	32	95	4.65
	2.0	2.24	2.68	3.36	30	81	129	3.36	27	75	3.36
	5.0	1.83	2.10	2.48	20	66	101	2.48	22	59	2.48
	10.0	1.47	1.66	1.89	20	53	80	1.89	18	46	1.89
84.1 (1 σ)	0.5	2.99	3.81	5.12	40	108	183	5.12	36	107	5.12
	2.0	2.51	2.98	3.65	30	90	143	3.65	30	83	3.65
	5.0	2.04	2.32	2.67	20	73	111	2.67	25	65	2.67
	10.0	1.62	1.81	2.01	20	58	87	2.01	19	51	2.01
90	0.5	3.28	4.16	5.53	40	118	200	5.53	39	116	5.53
	2.0	2.74	3.23	3.90	30	99	155	3.90	33	90	3.90
	5.0	2.21	2.51	2.82	20	80	120	2.82	27	70	2.82
	10.0	1.75	1.94	2.11	20	63	93	2.11	21	54	2.11
95	0.5	3.65	4.60	6.05	40	131	220	6.05	44	129	6.05
	2.0	3.04	3.57	4.22	30	109	171	4.22	36	100	4.22
	5.0	2.44	2.75	3.03	20	88	132	3.03	29	77	3.03
	10.0	1.91	2.11	2.24	20	69	101	2.24	23	59	2.24
97.7 (2 σ)	0.5	4.01	5.04	6.57	40	144	242	6.57	48	141	6.57
	2.0	3.34	3.89	4.54	30	120	187	4.54	[illegible]	109	4.54
	5.0	2.67	2.98	3.23	20	96	143	3.23	32	83	3.23
	10.0	2.08	2.28	2.37	20	75	109	2.37	25	64	2.37

Ground motions	a, g	v, in/sec	d, in
alluvium	1.0	48	36
rock	1.0	28	12

1361 271

EDAC

TABLE A-2. SPECTRAL ACCELERATION RESPONSE VARIATION

Contributing Variable	Contributing Variable Values		
	Lower	Median	Upper
Spectral Response Input Variation (f_1 = 5Hz, β = 10%, μ = 2)	-	0.95g	1.16g
System Damping (β, percent of critical)	7%(2)	10%	14%(2)
Spectral Response Damping Variation (f_1 = 5Hz, Median spectra, μ = 2	0.82(1)	0.95g	1.07G(1)
System Ductility (μ)	1.5(2)	2.0	2.6(2)
Spectral Reduction Factor (Amplified Acceleration Region, $R = 1/\sqrt{2\mu-1}$)	0.488	0.577	0.707
Spectral Response Ductility Variation (F_1 = 5Hz, Median spectra, β = 10%	0.80g	0.95g	1.17g

(1) Extrapolation based on Reference 19

(2) Reference 3 data base

1361 272

TABLE A-3. ELEMENT MATERIAL STRENGTH VARIATION
(Reference 3 data base)

Contributing Variable	Contributing Variable Values		
	Lower	Median	Upper
Diaphragm Capacity (E70 welding ultimate shear)	40 ksi	47 ksi	56 ksi
Concrete Flexure Capacity (Grade 40 Yield Strength)	44 ksi	48 ksi	53 ksi
Interface Shear Transfer (Grade 40 Yield Strength)			
Steel Column Flexure (A36 Yield Strength)	40 ksi	44 ksi	48.5 ksi
Concrete Shear Ultimate Capacity $v_u = 2\sqrt{f'_c}$)	117 psi	126 psi	137 psi
Concrete Insert Shear Capacity (A307 Ultimate Tension)	64 ksi	68 ksi	73 ksi

1361 273

TABLE A-4. UNCERTAINTY BOUND STATISTICAL PARAMETERS

Contributing Factor		Contributing Factor Values			Estimated Standard Deviation
		Lower	Median	Upper	
Spectral Response Input	Sa	-	1.0	1.22	0.199
Spectral Response Damping	C_β	0.86	1.0	1.13	0.137
Spectral Response Ductility	D_μ	0.84	1.0	1.23	0.191
Element Capacity	E_c (Diaphragm)	0.85	1.0	1.19	0.168
	E_c (Wall/flexure)	0.92	1.0	1.10	0.089
	E_c (Slab Joint)				
	E_c (Mezzanine Column)	0.91	1.0	1.10	0.095
	E_c (Wall Shear)	0.93	1.0	1.09	0.079
	E_c (Insert (Shear)	0.94	1.0	1.07	0.065
Construction Quality and Workmanship	W_c(Steel)	1.0	1.0	1.0	0.0
	W_c(Concrete)	0.90	1.0	1.11	0.100
Analysis Judgement	J	0.85	1.0	1.18	0.164

EDAC

APPENDIX B

MEDIAN ELEMENT CAPACITIES

SUMMARY OF COMPUTED ELEMENT CAPACITIES

1. Diaphragm chord, splice plate Tension capacity

   - - - - - - - - - - - - - = 51.38×10^3 lbs.

2. Diaphragm internal seam weld shear capacity

   - - - - - - - - - - - - - = 3.12×10^3 lb/ft

3. Diaphragm perimeter (east and west walls) puddle

   weld shear capacity - - - - - - - - - - = 2.31×10^3 lb/ft

4. Roof girder (27 W 114), moment capacity

   - - - - - - - - - = 15.09×10^6 in-lb

5. Pier No. 2, South wall

   Moment capacity - - - - - - = 2.07×10^6 in-lb

   Shear capacity - - - - - - - = 45.36×10^3 lbs.

6. Concrete inserts capacity

   Pull-out capacity - - - - - - - - = 25.2×10^3 lbs.

   Shear capacity - - - - - - - = 24.6×10^3 lbs

SUMMARY OF COMPUTED ELEMENT CAPACITIES (CONT'D)

7. Exterior mezzanine column (8 W 31)

   moment capacity ------- = 1.34×10^6 in-lb

8. Upper vault wall panel, moment capacity

   (50 ft. wide) ---------- = 1.43×10^6 in-lb

9. Vault wall shear capacity (2 walls)

   --------- = 243.81×10^3 lbs.

10. Precast panels (east and west walls)

    Transverse moment capacity (per foot strip)-- = 3.20×10^4 in-lb

11. Floor slab construction joint (south wall)

    Shear friction capacity ------ = 235.5×10^3 lbs.

12. Corner columns' anchor bolts (3/4" ϕ)

    Shear capacity per bolt---- = 21.1×10^3 lbs

    Tensile capacity per bolt--- = 22.8×10^3 lbs

13. Gypsum board / steel stud partition wall

    maximum imposed top deflection ---- = 0.96 in.

APPENDIX C

BUILDING DYNAMIC MODELS AND RESPONSE ANALYSIS

APPENDIX C

BUILDING DYNAMIC MODELS AND RESPONSE ANALYSIS

As discussed in Section 3.1 of this report, the east-west and north-south structural systems were analyzed as independent lateral force systems. Dynamic models of each independent system were formulated employing the EDAC/MSAP computer code which is a version of the general structural analysis computer program SAP IV (Reference 14). The three-dimensional elastic beam element and boundary spring elements were utilized to construct the finite element mathematical idealization of the diaphragm, shear walls, and foundation compliance. Sufficient detail was provided in each model to represent the general behavior of all key structural components which comprise the lateral force transfer system. Within each model, the necessary kinematic constraints were provided to achieve the element stiffnesses desired. The input data for the element properties, idealized lumped mass, and model constraints are tabulated for each model herein. The format utilized for the presentation is the input data (echo) print-out generated by the MSAP program. The format and nomenclature is identical to that utilized in Reference 14. Units are inches, pounds, and seconds.

C.1 NORTH-SOUTH LATERAL FORCE RESISTING SYSTEM

The finite element model used to evaluate the north-south direction is shown in Figure C-1 along with the SRSS element forces obtained from a modal spectral analysis using the input spectra given in Figure 3-4 ($\mu = 2.0$). The modal point spatial definition along with the element properties and lumped mass values are tabulated in Figure C-2. The diaphragm element is constrained to provide only shear displacement between nodes (i.e., a shear spring). The wall elements are constrained to act as a shear-flexure cantilever.

C.2 EAST-WEST LATERAL FORCE RESISTING SYSTEM

The dynamic model used to evaluate the response of the NMDF building for east-west ground motion is shown in Figure C-3. The nodal point spatial definition along with the element properties and lumped mass values are tabulated in Figure C-4. The diaphragm element is constrained to act as a shear spring between nodes. The wall elements are constrained to act as equivalent shear-flexure cantilevers. The effective stiffness assigned to the south wall element was based upon the results of the static wall study discussed in Appendix D. The effective transverse walls were included in the model to account for the additional mass provided by the mezzanine area and the interaction provided by the vault. Note that the effective transverse walls are modeled as pin-pin beam elements which transfer only the forces required for lateral support by the diaphragm and the footing/slab foundation. The dominant principal mode shapes obtained from a modal analysis of the model are shown in Figures C-5 and C-6. The SRSS element forces obtained from a modal spectral analysis, using the input spectra given in Figure 3-4 (μ = 2.0), are shown in Figure C-7.

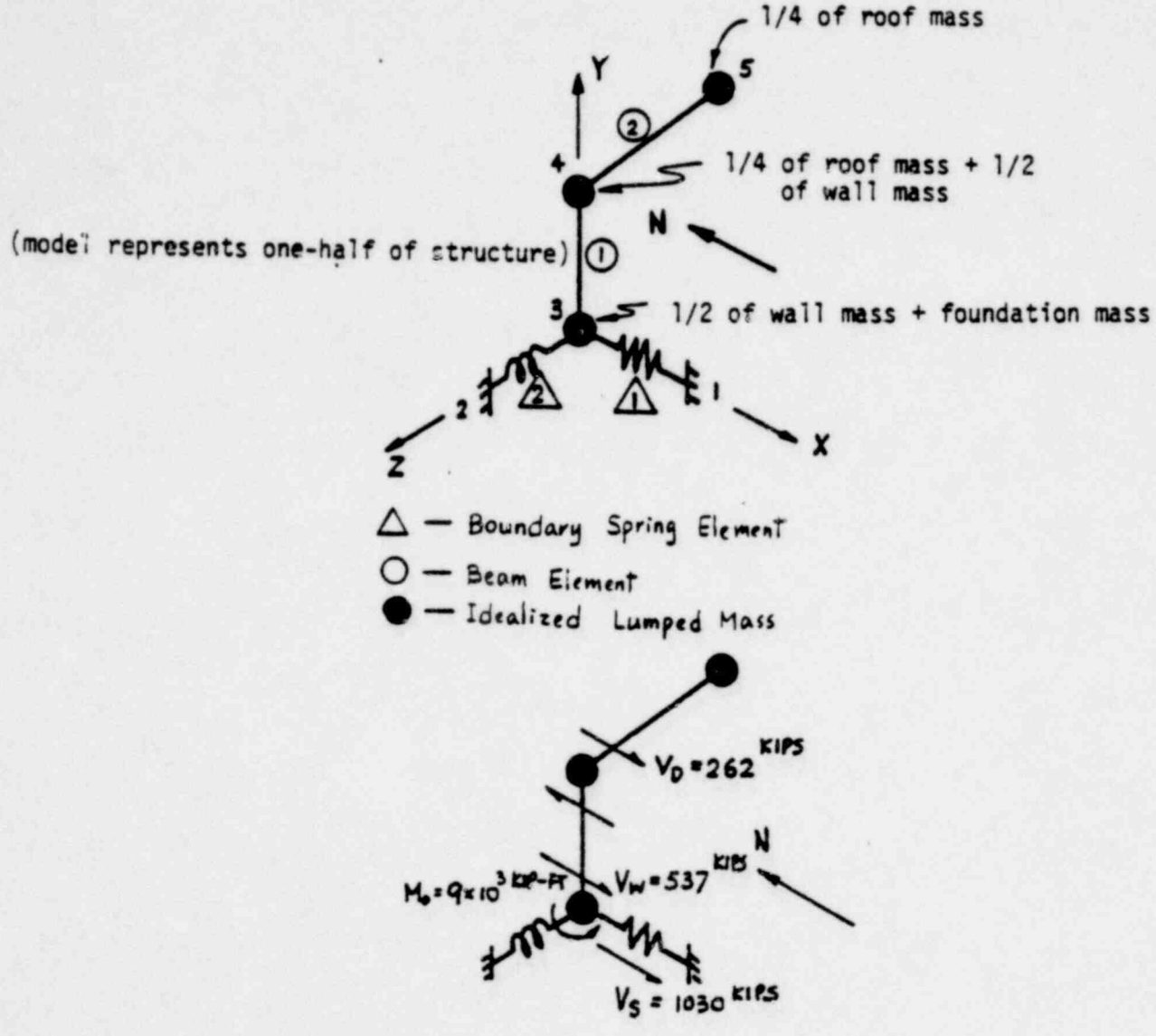

FIGURE C-1. N-S DYNAMIC NMDF MODEL AND MODAL ANALYSIS RESULTS (SRSS, μ = 2.0)

GENERATED NODAL DATA

NODE NUMBER	BOUNDARY CONDITION CODES x	y	z	xx	yy	zz	NODAL POINT COORDINATES x	y	z	T
1	1	-1	-1	-1	-1	1	100.000	0.000	0.000	0.000
2	1	-1	-1	-1	-1	1	0.000	0.000	100.000	0.000
3	0	-1	-1	-1	-1	0	0.000	0.000	0.000	0.000
4	0	-1	-1	-1	-1	0	0.000	204.000	0.000	0.000
5	0	-1	-1	-1	-1	1	0.000	204.000	-309.500	0.000

S/D BEAM ELEMENTS

NUMBER OF BEAMS	=	2
NUMBER OF GEOMETRIC PROPERTY SETS	=	2
NUMBER OF PIPED END FORCE SETS	=	0
NUMBER OF MATERIALS	=	2

MATERIAL PROPERTIES

MATERIAL NUMBER	YOUNGS MODULUS	POISSONS RATIO	MASS DENSITY	WEIGHT DENSITY	DMP
1	.3000E+07	.2000	0.	0.	0.
2	.2900E+08	.3000	0.	0.	0.

BEAM GEOMETRIC PROPERTIES

SECTION NUMBER	AXIAL AREA A(1)	SHEAR AREA A(2)	SHEAR AREA A(3)	TORSION J(1)	INERTIA I(2)	INERTIA I(3)
1	.1053E+05	.1211E+05	.1211E+05	.1000E+01	.7100E+10	.7100E+10
2	.1000E+01	0.	0.	.1000E+01	.7540E+06	.7540E+06

S/D BEAM ELEMENT DATA

BEAM NUMBER	NODE -I	NODE -J	NODE -K	MATERIAL NUMBER	SECTION NUMBER	ELEMENT LOAD CODES A	B	C	D	END CODES -I	-J
1	3	4	1	1	1	0	0	0	0	0	0
2	0	5	2	2	2	0	0	0	0	0	100

1361 282

FIGURE C-2. N-S DYNAMIC MODEL INPUT DATA (SAP IV FORMAT)

SUBMERGED ELEMENTS

ELEMENT TYPE = 7
NUMBER OF ELEMENTS = 2

ELEMENT LOAD CASE MULTIPLIERS

CASE(A)	CASE(B)	CASE(C)	CASE(D)
0.0000	0.0000	0.0000	0.0000

ELEMENT NUMBER	NODE (N)	NODES DEFINING (NI)	(NJ)	CONSTRAINT DIRECTION (NK)	(NL)	CODE AD	CODE AM	GENERATION CODE (AS)	SPECIFIED DISPLACEMENT	SPECIFIED ROTATION	SPRING RATE	DAMPING
1	1	1	0	0	0	1	0	0	0.	0.	.3700E+08	0.0000
2	1	2	0	0	0	0	1	0	0.	0.	.1950E+10	0.0000

NODAL LOADS (STATIC) OR PASSES (DYNAMIC)

NODE NUMBER	LOAD CASE	X-AXIS FORCE	Y-AXIS FORCE	Z-AXIS FORCE	X-AXIS MOMENT	Y-AXIS MOMENT	Z-AXIS MOMENT
3	0	.1912DE+04	0.	0.	0.	0.	0.
4	0	.9570E+03	0.	0.	0.	0.	0.
5	0	.3190DE+03	0.	0.	0.	0.	0.

FIGURE C-2. N-S DYNAMIC MODEL INPUT DATA (Cont.)

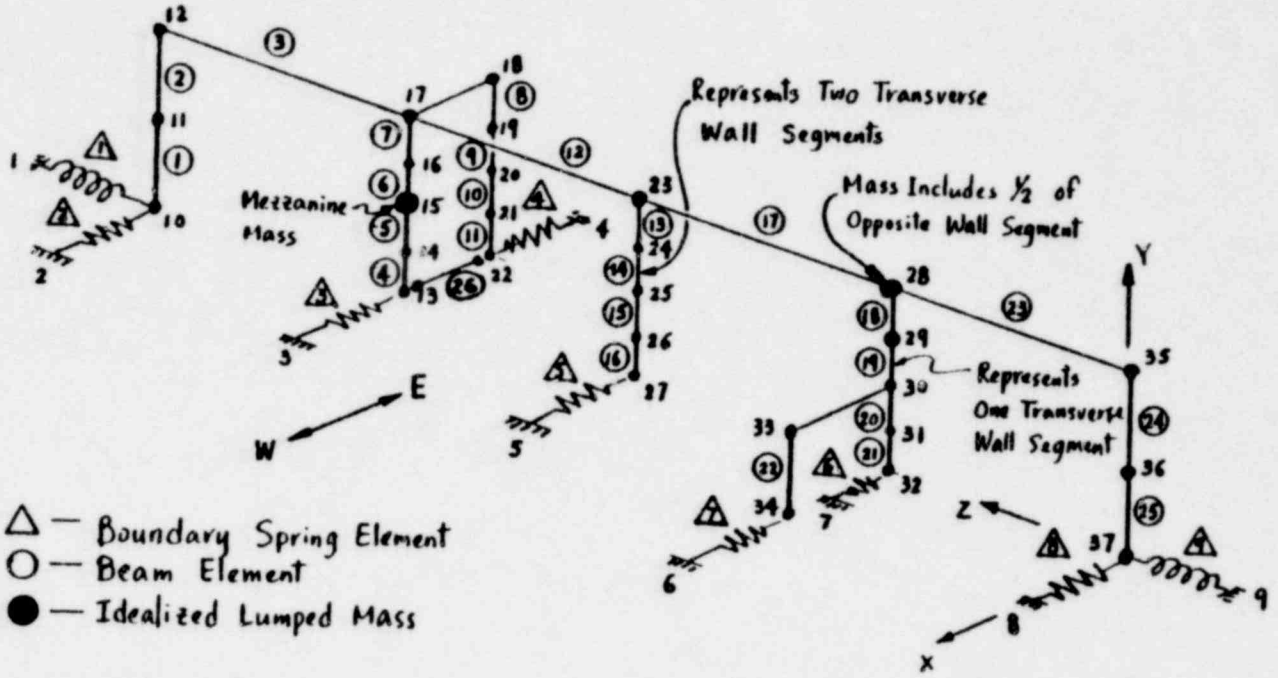

FIGURE C-3. E-W DYNAMIC MODEL OF NMDF

GENERATED NODAL DATA

NODE NUMBER	BOUNDARY CONDITION CODES						NODAL POINT COORDINATES			
	X	Y	Z	XX	YY	ZZ	X	Y	Z	T
1	-1	-1	-1	-1	-1	-1	0.000	0.000	2521.500	0.000
2	-1	-1	-1	-1	-1	-1	100.000	0.000	2421.500	0.000
3	-1	-1	-1	-1	-1	-1	100.000	0.000	1816.100	0.000
4	-1	-1	-1	-1	-1	-1	-200.000	0.000	1816.100	0.000
5	-1	-1	-1	-1	-1	-1	100.000	0.000	1210.800	0.000
6	-1	-1	-1	-1	-1	-1	200.000	0.000	605.400	0.000
7	-1	-1	-1	-1	-1	-1	50.000	0.000	605.400	0.000
8	-1	-1	-1	-1	-1	-1	100.000	0.000	0.000	0.000
9	1	-1	-1	-1	-1	1	0.000	0.000	-100.000	0.000
10	0	-1	-1	-1	-1	0	0.000	0.000	2421.500	0.000
11	0	-1	-1	-1	-1	0	0.000	101.000	2421.500	0.000
12	0	-1	-1	-1	-1	0	0.000	202.000	2421.500	0.000
13	0	-1	-1	-1	-1	0	0.000	0.000	1816.100	0.000
14	0	-1	-1	-1	-1	0	0.000	50.500	1816.100	0.000
15	0	-1	-1	-1	-1	0	0.000	101.000	1816.100	0.000
16	0	-1	-1	-1	-1	0	0.000	151.500	1816.100	0.000
17	0	-1	-1	-1	-1	1	0.000	202.000	1816.100	0.000
18	17	-1	-1	-1	-1	0	-100.000	202.000	1816.100	0.000
19	0	-1	-1	-1	-1	0	-100.000	151.500	1816.100	0.000
20	0	-1	-1	-1	-1	0	-100.000	101.000	1816.100	0.000
21	0	-1	-1	-1	-1	0	-100.000	50.500	1816.100	0.000
22	0	-1	-1	-1	-1	0	-100.000	0.000	1816.100	0.000
23	0	-1	-1	-1	-1	1	0.000	202.000	1210.800	0.000
24	0	-1	-1	-1	-1	0	0.000	151.500	1210.800	0.000
25	0	-1	-1	-1	-1	0	0.000	101.000	1210.800	0.000
26	0	-1	-1	-1	-1	0	0.000	50.500	1210.800	0.000
27	0	-1	-1	-1	-1	0	0.000	0.000	1210.800	0.000
28	0	-1	-1	-1	-1	1	0.000	202.000	605.400	0.000
29	0	-1	-1	-1	-1	0	0.000	151.500	605.400	0.000
30	0	-1	-1	-1	-1	0	0.000	121.000	605.400	0.000
31	0	-1	-1	-1	-1	0	0.000	60.500	605.400	0.000
32	0	-1	-1	-1	-1	0	0.000	0.000	605.400	0.000
33	30	-1	-1	-1	-1	0	100.000	101.000	605.400	0.000
34	0	-1	-1	-1	-1	1	100.000	0.000	605.400	0.000
35	0	-1	-1	-1	-1	0	0.000	202.000	0.000	0.000
36	0	-1	-1	-1	-1	0	0.000	101.000	0.000	0.000
37	0	-1	-1	-1	-1	0	0.000	0.000	0.000	0.000

FIGURE C-4. E-W DYNAMIC MODEL INPUT DATA (SAP IV FORMAT)

S / R BEAM ELEMENTS

NUMBER OF BEAMS	= 26
NUMBER OF GEOMETRIC PROPERTY SETS	= 8
NUMBER OF FIXED END FORCE SETS	= 0
NUMBER OF MATERIALS	= 2

MATERIAL PROPERTIES

MATERIAL NUMBER	YOUNG'S MODULUS	POISSON'S RATIO	MASS DENSITY	WEIGHT DENSITY	DMP
1	.3400E+07	.2000	0.	0.	0.
2	.2900E+08	.3000	0.	0.	0.

BEAM GEOMETRIC PROPERTIES

SECTION NUMBER	AXIAL AREA A(1)	SHEAR AREA A(2)	SHEAR AREA A(3)	TORSION J(1)	INERTIA I(2)	INERTIA I(3)
1	.8150E+04	.3405E+04	.3465E+04	.1000E+01	.189UE+09	.1890E+09
2	.1000E+01	0.	0.	.1000E+01	.6250E+06	.6250E+06
3	.1770E+04	.1475E+04	.1475E+04	.1000E+01	.4800E+09	.4800E+09
4	.7265E+04	.6054E+04	.6054E+04	.1000E+01	.2231E+05	.2230E+05
5	.2322E+04	.1935E+04	.1935E+04	.1000E+01	.3200E+07	.3200E+07
6	.3632E+04	.3027E+04	.3027E+04	.1000E+01	.1090E+05	.1090E+05
7	.1A29E+02	0.	0.	.1000E+01	.220UE+03	.2200E+03
8	.1000E+05	0.	0.	.1000E+01	.100UE+07	.1000E+07

FIGURE C-4. E-W DYNAMIC MODEL INPUT DATA (Cont.)

3/D BEAM ELEMENT DATA

BEAM NUMBER	NODE -I	NODE -J	NODE -K	MATERIAL NUMBER	SECTION NUMBER	ELEMENT LOADS A	B	END LOADS C	D	END CODES -I	-J
1	10	11	1	1	1	0	0	0	0	0	0
2	11	12	1	1	1	0	0	0	0	0	0
3	12	17	1	2	2	0	0	0	0	0	100
4	13	14	1	2	7	0	0	0	0	0	0
5	14	15	1	2	7	0	0	0	0	0	0
6	15	16	1	2	7	0	0	0	0	0	0
7	16	17	1	2	7	0	0	0	0	0	100
8	18	19	1	1	4	0	0	0	0	0	0
9	19	20	1	1	4	0	0	0	0	0	0
10	20	21	1	1	4	0	0	0	0	0	0
11	21	22	1	1	4	0	0	0	0	0	0
12	17	23	1	2	2	0	0	0	0	0	100
13	23	24	1	1	4	0	0	0	0	10	0
14	24	25	1	1	4	0	0	0	0	0	0
15	25	26	1	1	4	0	0	0	0	0	0
16	26	27	1	1	4	0	0	0	0	0	0
17	23	28	1	2	2	0	0	0	0	0	100
18	28	29	1	1	6	0	0	0	0	10	0
19	29	30	1	1	6	0	0	0	0	0	0
20	30	31	1	1	6	0	0	0	0	0	0
21	31	32	1	1	6	0	0	0	0	0	0
22	33	34	32	1	5	0	0	0	0	0	0
23	28	35	1	2	2	0	0	0	0	0	100
24	35	36	1	1	3	0	0	0	0	0	0
25	36	37	1	1	3	0	0	0	0	0	0
26	13	22	1	1	8	0	0	0	0	10	10

FIGURE C-4. E-W DYNAMIC MODEL INPUT DATA (Cont.)

BOUNDARY ELEMENTS

ELEMENT TYPE = 7
NUMBER OF ELEMENTS = 9

ELEMENT LOAD CASE MULTIPLIERS

CASE(A)	CASE(B)	CASE(C)	CASE(D)
0.0000	0.0000	0.0000	0.0000

ELEMENT NUMBER	NODE (N)	NODES DEFINING (NI)	(NJ)	CONSTRAINT DIRECTION (NK)	(NL)	CODE AD	CODE AR	GENERATION CODE (NN)	SPECIFIED DISPLACEMENT	SPECIFIED ROTATION	SPRING RATE	DAMPING
1	10	1	0	0	0	0	1	0	0.	0.	.1160E+13	0.00000
2	10	2	0	0	0	1	0	0	0.	0.	.2150E+08	0.00000
3	13	3	0	0	0	1	0	0	0.	0.	.9050E+07	0.00000
4	22	4	0	0	0	1	0	0	0.	0.	.9050E+07	0.00000
5	27	5	0	0	0	1	0	0	0.	0.	.2140E+08	0.00000
6	32	7	0	0	0	1	0	0	0.	0.	.1810E+08	0.00000
7	34	6	0	0	0	1	0	0	0.	0.	.3100E+07	0.00000
8	37	8	0	0	0	1	0	0	0.	0.	.2150E+08	0.00000
9	37	9	0	0	0	0	1	0	0.	0.	.1160E+13	0.00000

FIGURE C-4. E-W DYNAMIC MODEL INPUT DATA (Cont.)

NODAL LOADS (STATIC) ON MASSES (DYNAMIC)

NODE NUMBER	LOAD CASE	X-AXIS FORCE	Y-AXIS FORCE	Z-AXIS FORCE	X-AXIS MOMENT	Y-AXIS MOMENT	Z-AXIS MOMENT
10	0	.50100E+03	0.	0.	0.	0.	0.
11	0	.20800E+03	0.	0.	0.	0.	0.
12	0	.26300E+03	0.	0.	0.	0.	0.
13	0	.35500E+03	0.	0.	0.	0.	0.
14	0	0.	0.	0.	0.	0.	0.
15	0	.15300E+03	0.	0.	0.	0.	0.
16	0	0.	0.	0.	0.	0.	0.
17	0	.36000E+03	0.	0.	0.	0.	0.
18	0	.82000E+02	0.	0.	0.	0.	0.
19	0	.82000E+02	0.	0.	0.	0.	0.
20	0	.82000E+02	0.	0.	0.	0.	0.
21	0	.82050E+02	0.	0.	0.	0.	0.
22	0	.35500E+03	0.	0.	0.	0.	0.
23	0	.36000E+03	0.	0.	0.	0.	0.
24	0	.82000E+02	0.	0.	0.	0.	0.
25	0	.82000E+02	0.	0.	0.	0.	0.
26	0	.82000E+02	0.	0.	0.	0.	0.
27	0	.71000E+03	0.	0.	0.	0.	0.
28	0	.42200E+03	0.	0.	0.	0.	0.
29	0	.41000E+02	0.	0.	0.	0.	0.
30	0	.41000E+02	0.	0.	0.	0.	0.
31	0	.49000E+02	0.	0.	0.	0.	0.
32	0	.75600E+03	0.	0.	0.	0.	0.
33	0	.12800E+03	0.	0.	0.	0.	0.
34	0	.12800E+03	0.	0.	0.	0.	0.
35	0	.25100E+03	0.	0.	0.	0.	0.
36	0	.18300E+03	0.	0.	0.	0.	0.
37	0	.44800E+03	0.	0.	0.	0.	0.

FIGURE C-4. E-W DYNAMIC MODEL INPUT DATA (Cont.)

FIGURE C-5. MODE SHAPES OF E-W DYNAMIC MODEL
(MEZZANINE AND DIAPHRAGM MODES)

FIGURE C-6. MODE SHAPES OF E-W DYNAMIC MODEL
(WALL MODES)

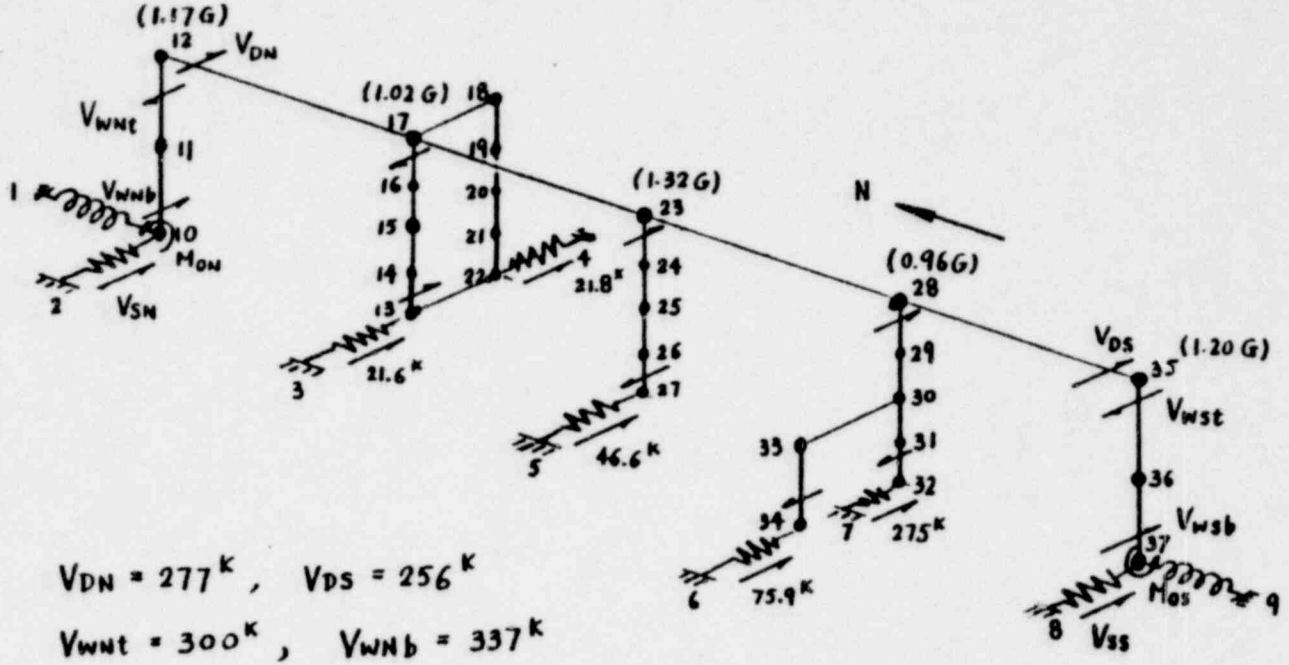

$V_{DN} = 277^K$, $V_{DS} = 256^K$

$V_{WNt} = 300^K$, $V_{WNb} = 337^K$

$V_{Wst} = 281^K$, $V_{Wsb} = 312^K$

$V_{CV} = 15^K$

$V_{SN} = 424^K$, $V_{SS} = 375^K$

$M_{ON} = 0.64 \times 10^5$ in-kips

$M_{OS} = 0.60 \times 10^5$ in-kips

FIGURE C-7. SUMMARY OF MODAL ANALYSIS OF E-W MODEL (SRSS, $\mu = 2.0$)

APPENDIX D

SOUTH WALL FINITE ELEMENT DETAILED ANALYSIS

APPENDIX D

SOUTH WALL FINITE ELEMENT DETAILED ANALYSIS

A detailed analysis of the south wall was undertaken to insure that the capacity estimate was not biased by conservative design approximations. As noted in Section 3.2.1, the behavior of long, one-story walls with numerous openings is a problem which has not been adequately addressed in the literature. A static analysis of the finite element model shown in Figure D-1 was conducted to determine the distribution of stress within the south wall when subjected to a uniform diaphragm load applied at the roof line. The EDAC/MSAP computer code, which is a version of the general structural analyses computer program SAP IV (Reference 14), was employed to formulate a general representation of the wall construction. Membrane elements were utilized for the wall, the portion of the transverse wall acting as an equivalent flange, and to simulate the base floor slab attachment. Boundary spring elements were utilized to represent the compliance of the individual footings and the equivalent shear stiffness of the floor slab/soil. Beam elements were utilized to represent the column flange attachment at the panel insert locations. The beam elements were constrained to act as effective shear springs to simulate the column flange acting as a shear transfer element. Thus, the model allowed the critical regions of wall shear and flexure to be identified, allowed the determination of insert reaction forces and also provided the distribution of base shear resisted by each footing and the wall shear transferred to the floor slab/soil. The general deflected shape (exaggerated) for the south wall under the imposed seismic roof loading is shown in Figure D-2. As can be noted, the wall stiffness in shear is governed by the flexure of the shaded critical spandrel and pier regions. The load/deflection behavior of the overall wall was used to assess the equivalent wall stiffness utilized in the dynamic model of the E-W system described in Appendix C. The distribution of average shear stress within each element is shown in Figure D-3. An

indication of the axial stress and horizontal stress distribution within critical areas of the wall is shown in Figures D-4 and D-5. The distribution of principal stresses around each major opening is shown in Figure D-6 and an indication of the shear stress intensity within selected groups of elements is shown in Figure D-7. As can be noted the behavior of the wall cannot be represented by the usual design analysis (References 9 and 11) methods utilized for low-rise concrete shear wall structures. The insert reactions for the applied roof loading are shown in Figure D-8.

After evaluation of the wall stress distribution, an equivalent frame model of the wall, as shown in Figure D-9 was proposed to allow the collapse behavior of the wall to be evaluated. To achieve approximate correspondence between the detailed model of Figure D-1 and the equivalent frame model shown in Figure D-9, the pseudo-spandrel transition stiffnesses of each pier were adjusted until the overall displacement and distribution of wall shear within each pier and critical spandrel were in approximate agreement with the detailed finite element model. Again the EDAC/MSAP code using beam and boundary spring elements was utilized for the frame model. The purpose of the frame model was to allow the evaluation of the flexural and shear behavior of the critical spandrel and pier regions. The input data (SAP IV, Reference 14 format) for the element properties utilized for the equivalent frame model are tabulated in Figure D-10. The final collapse mechanism for the wall was identical using the three separate analysis cases for the equivalent frame shown in Figure D-11. After initial yield hinge formation at the top of pier No. 2, the wall can carry approximately 50% more shear (static) until hinges form at the ends of the idealized spandrels, which frame into pier No. 2, and an additional hinge forms at the top of pier No. 4.

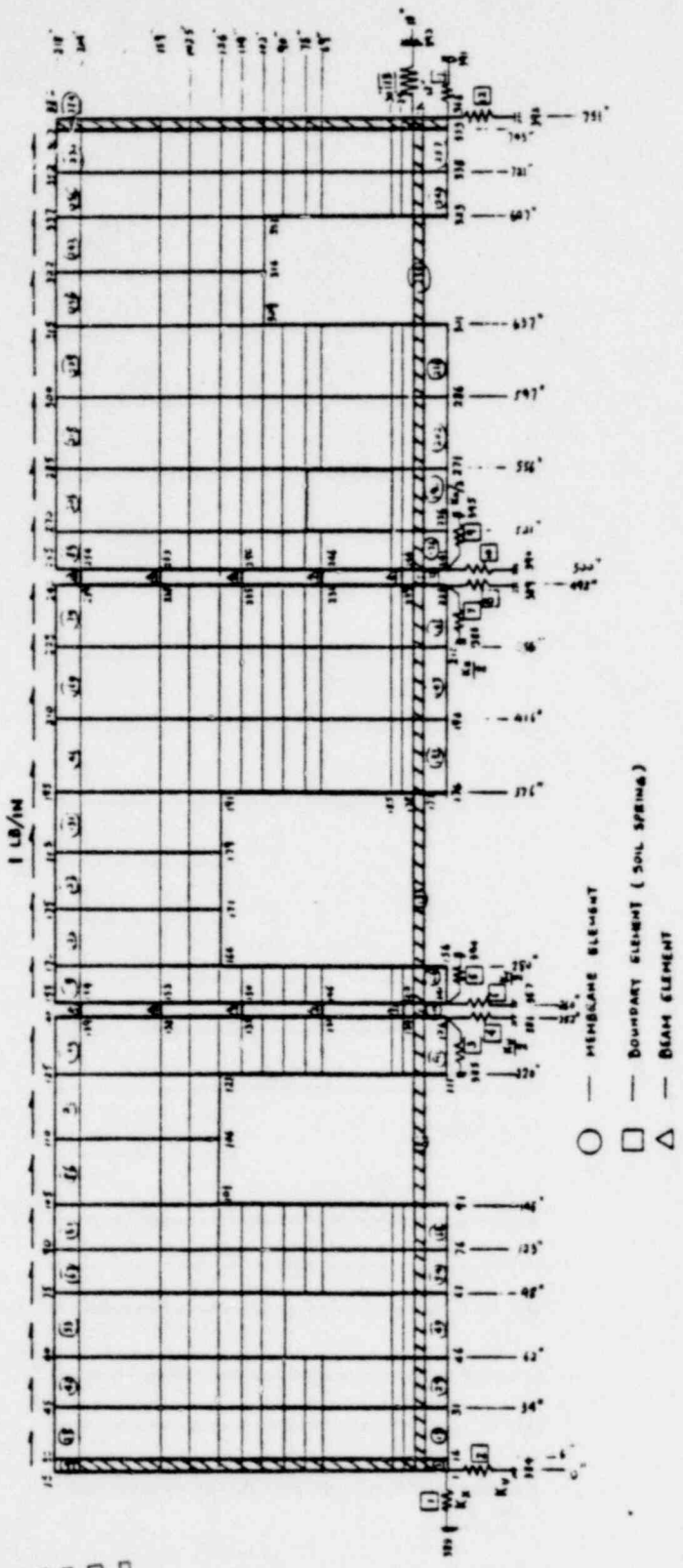

FIGURE D-1. FINITE ELEMENT MODEL OF SOUTH WALL

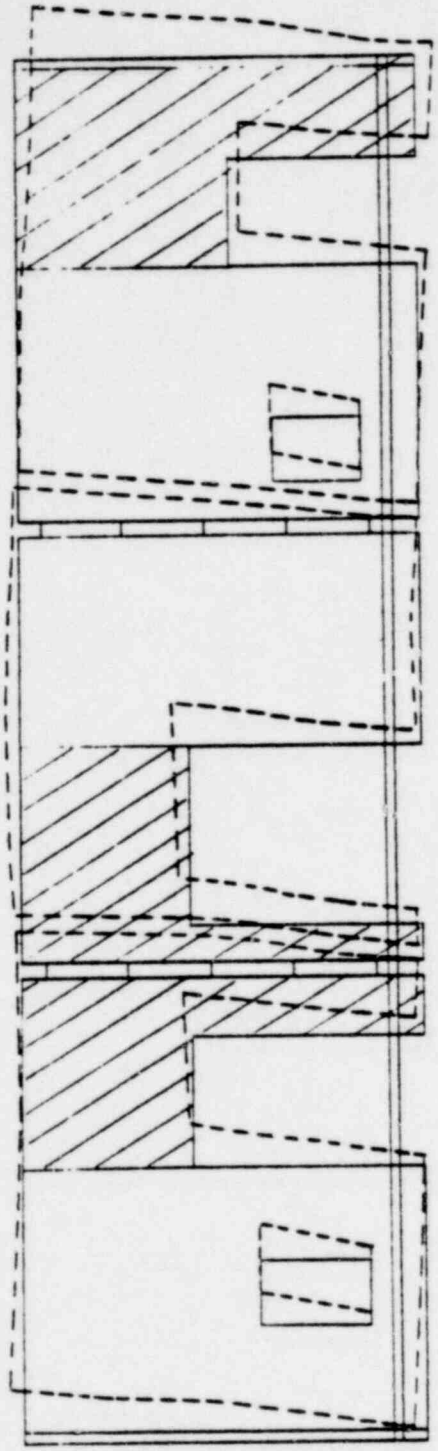

FIGURE D-2. DEFLECTED SHAPE OF SOUTH WALL

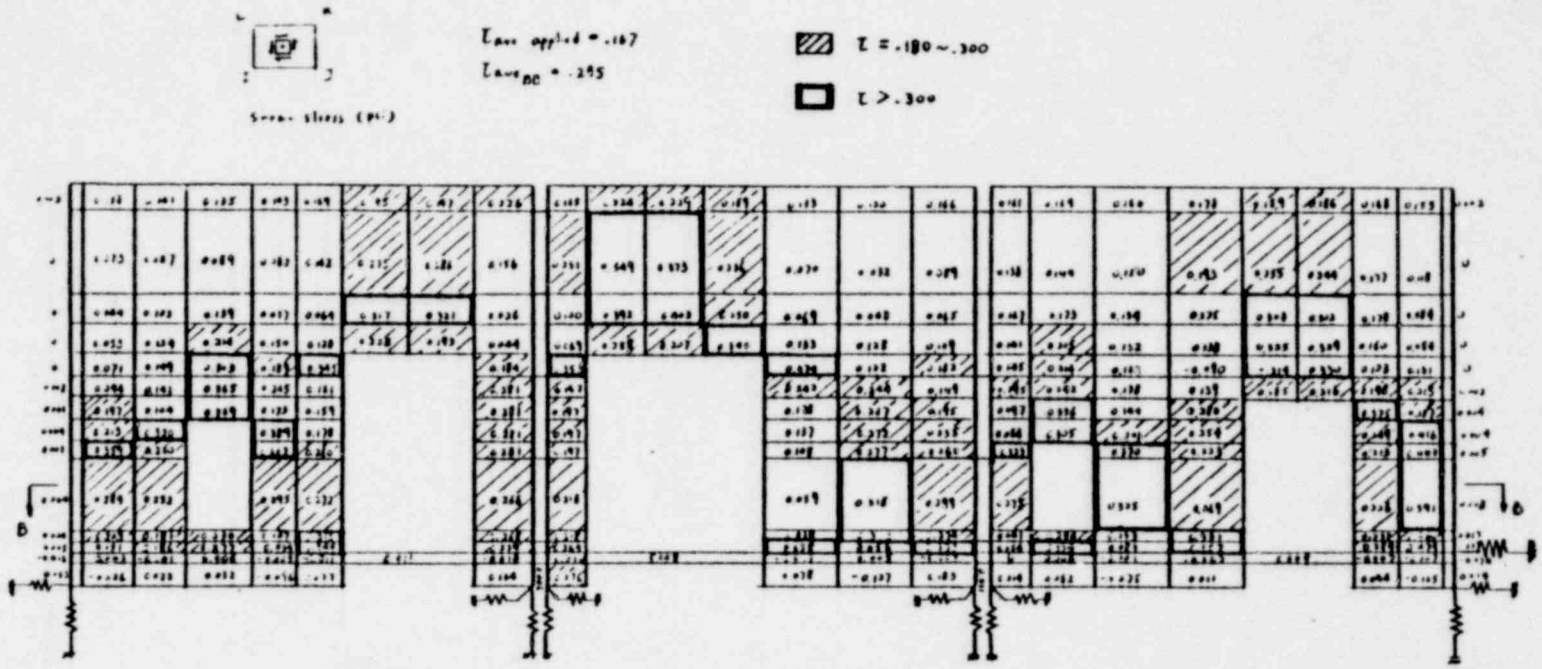

FIGURE D-3. SHEAR STRESS DISTRIBUTION OF SOUTH WALL

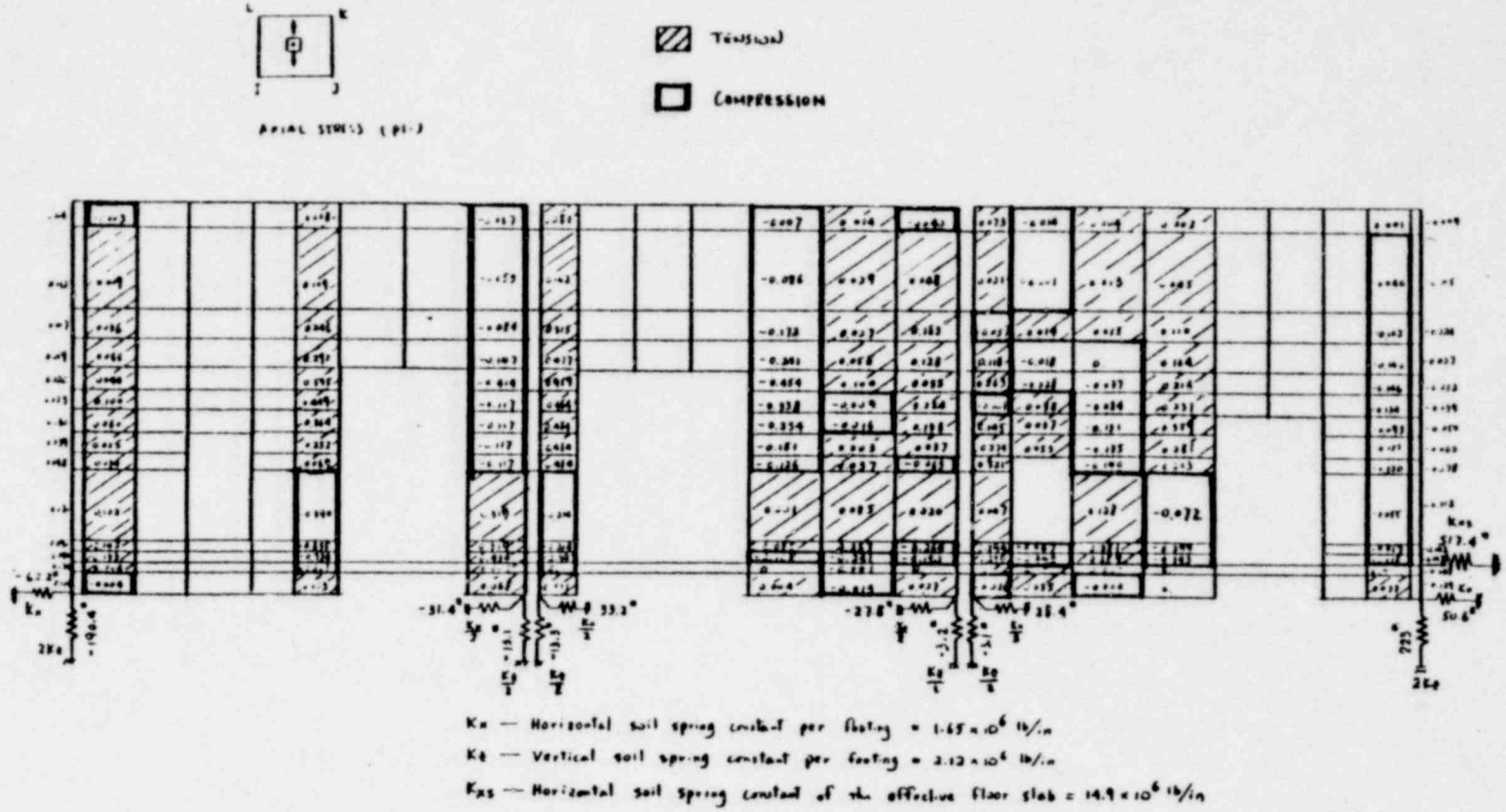

FIGURE D-4. AXIAL STRESS DISTRIBUTION OF SOUTH WALL

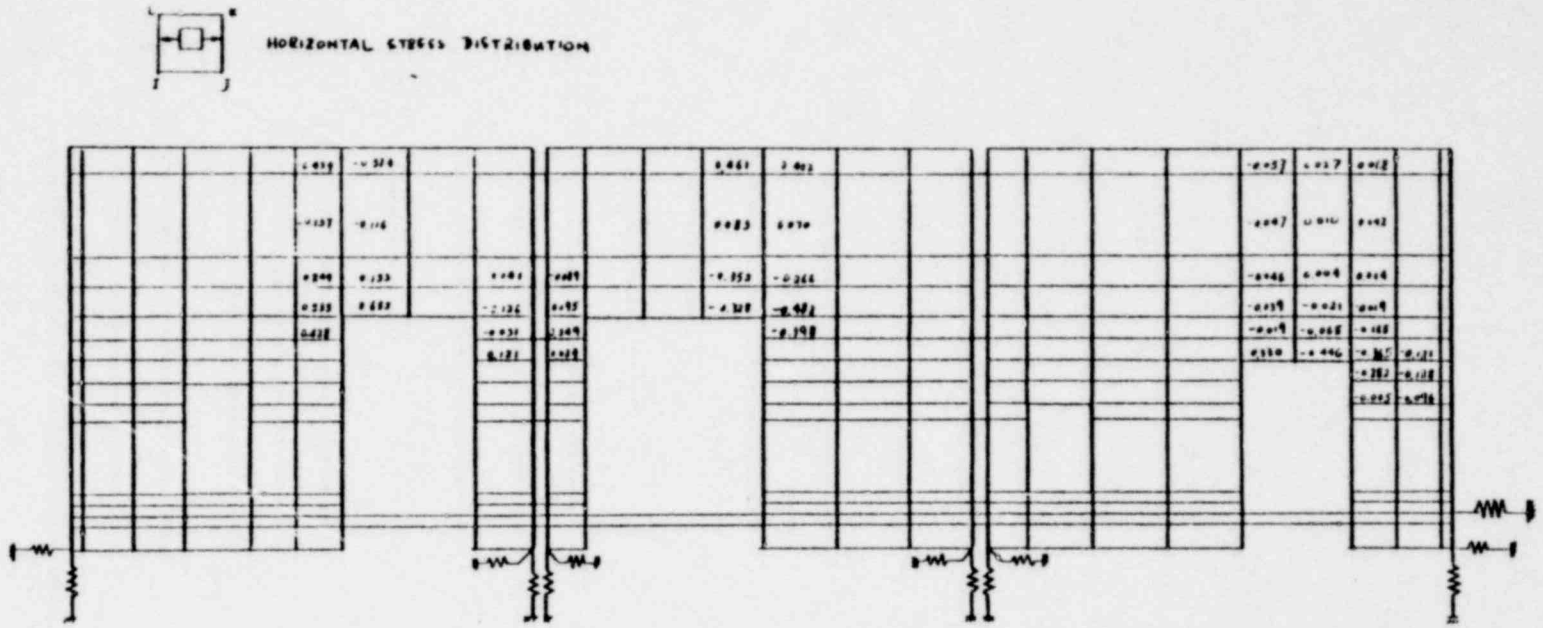

FIGURE D-5. HORIZONTAL STRESS DISTRIBUTION OF SOUTH WALL

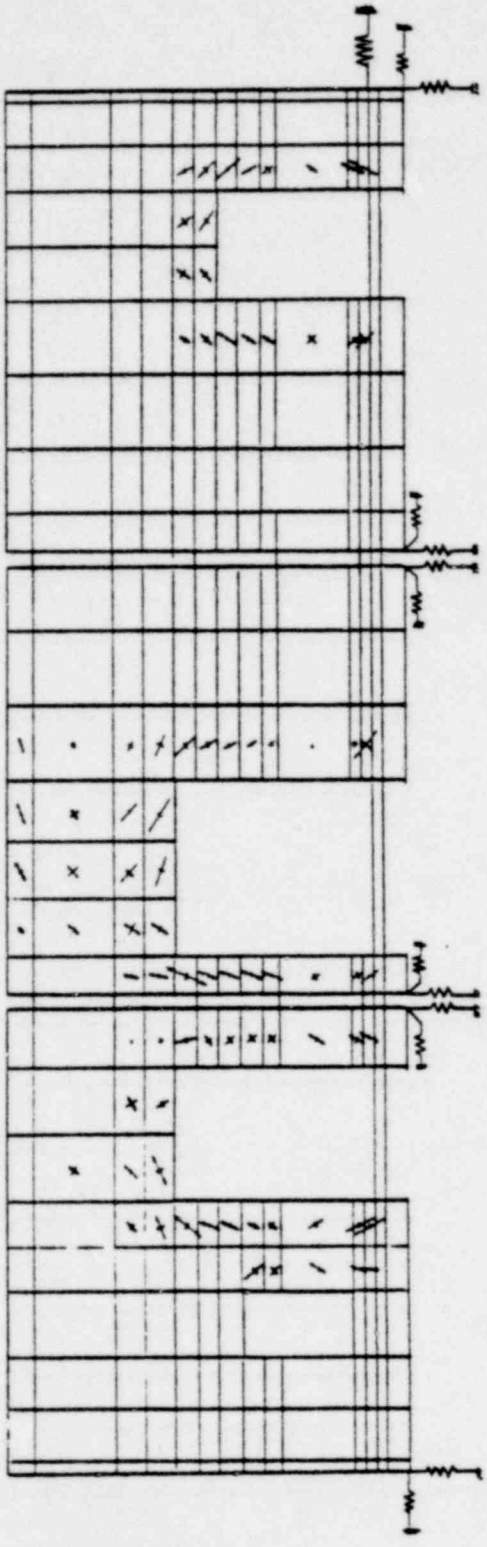

FIGURE D-6. DISTRIBUTION OF PRINCIPAL STRESSES IN SOUTH WALL

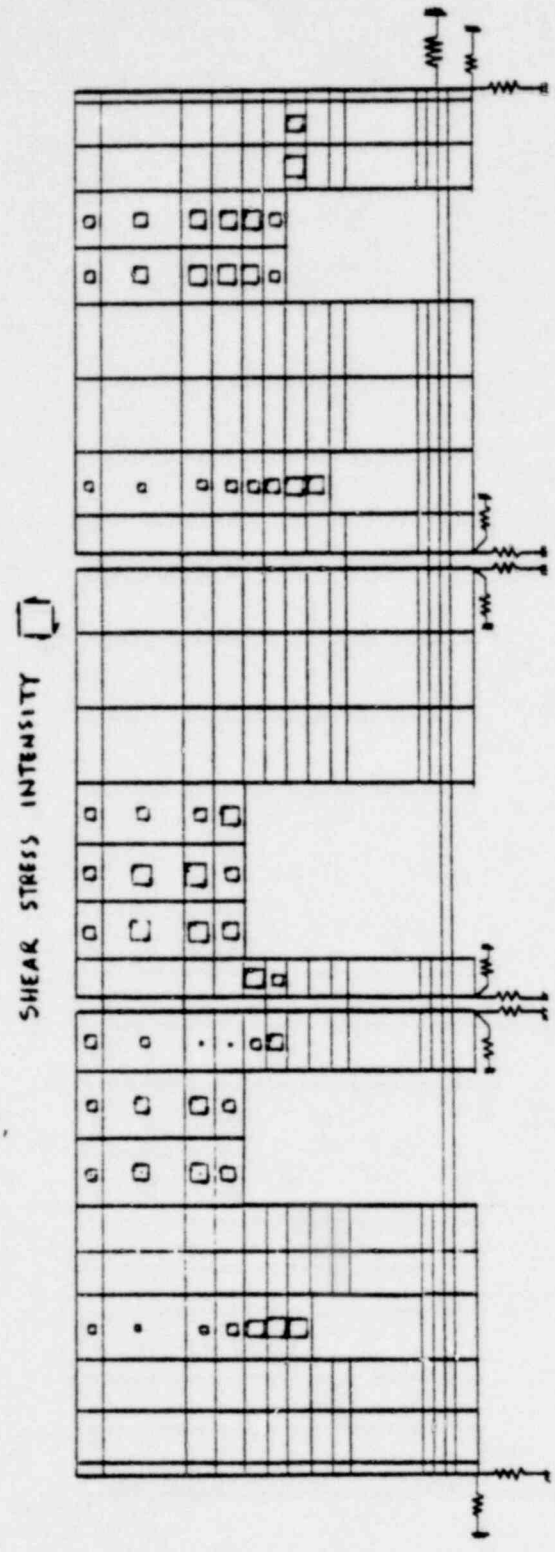

FIGURE D-7. DISTRIBUTION OF SHEAR STRESSES IN SOUTH WALL

BEAM NO.	1	2	3	4	5	6	7	8	9	10
AXIAL FORCE (LBS)	5.5 (-)	2.6 (-)	18.7 (-)	13.8 (-)	24.6 (-)	3.4 (-)	6.0 (-)	9.3 (-)	10.7 (-)	8.9 (-)
SHEAR FORCE (LBS)	21.9	55.7	57.0	28.3	97.1	10.8	59.8	87.3	34.6	30.4

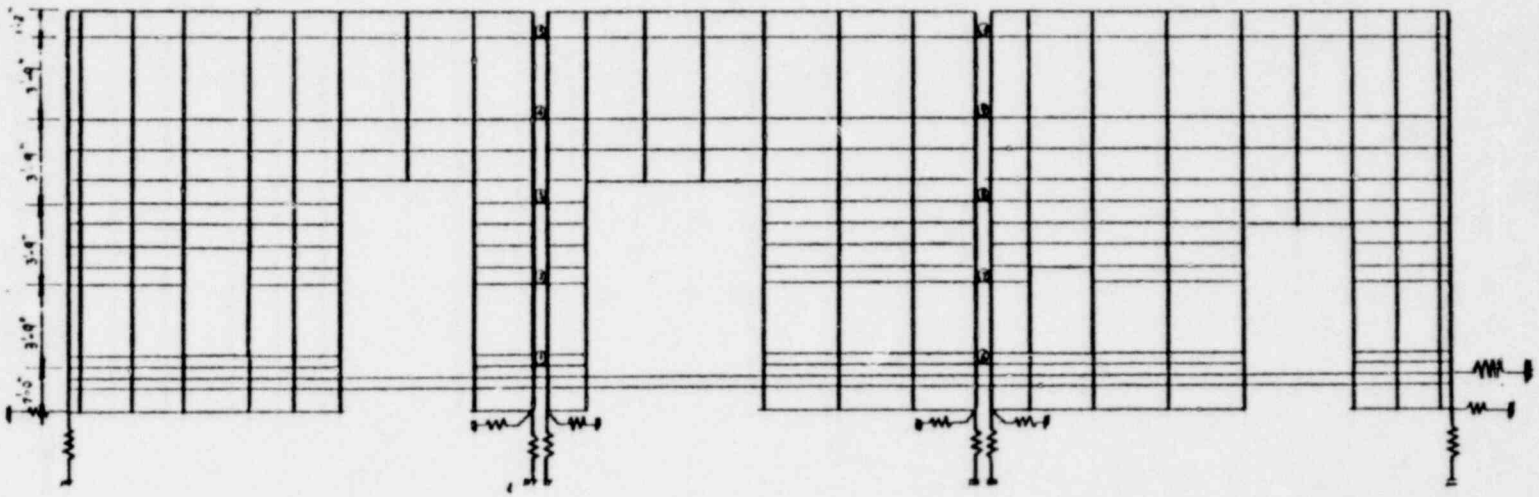

FIGURE D-8. FORCES IN WALL PANEL CONNECTING LINKS (BEAM FLANGES)

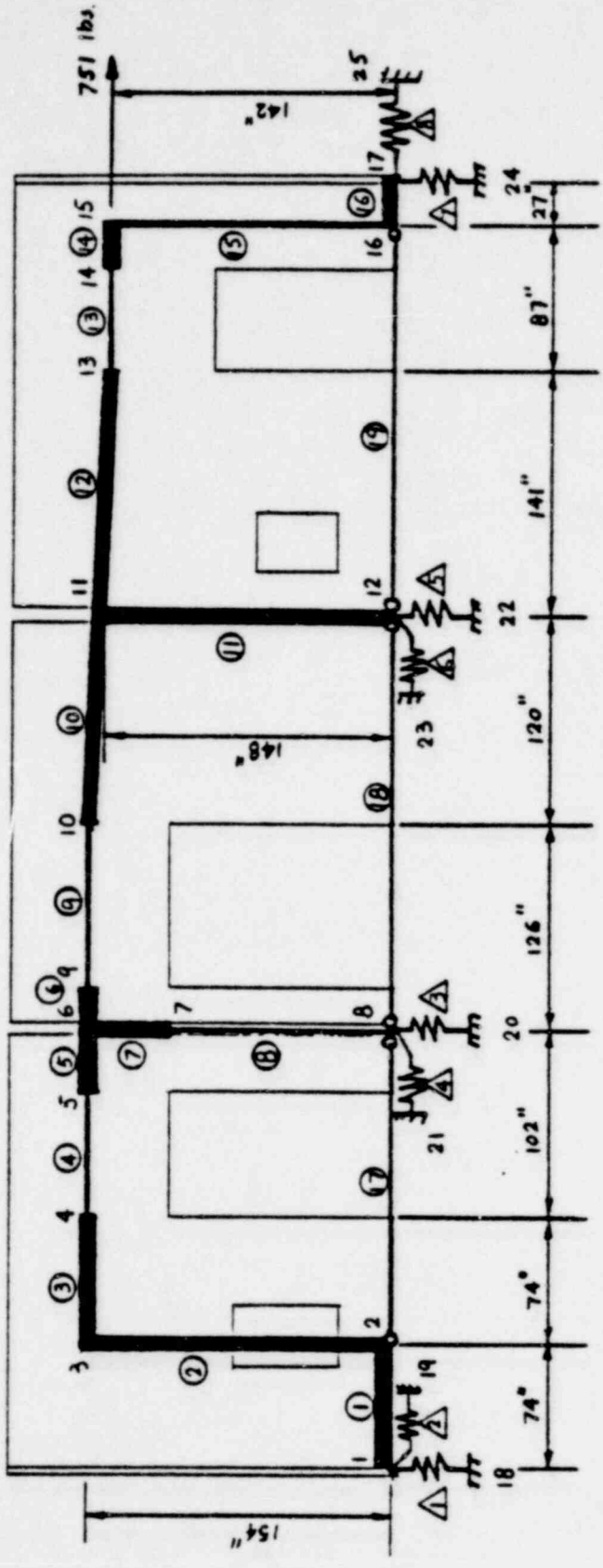

FIGURE D-9. MATHEMATICAL MODEL OF NMDF SOUTH WALL EQUIVALENT FRAME

GENERATED NODAL DATA

NODE NUMBER	BOUNDARY CONDITION CODES X	Y	Z	XX	YY	ZZ	NODAL POINT COORDINATES X	Y	Z	T
1	0	0	-1	-1	-1	0	0.000	0.000	0.000	0.000
2	0	0	-1	-1	-1	0	74.000	0.000	0.000	0.000
3	0	0	-1	-1	-1	0	74.000	154.000	0.000	0.000
4	0	0	-1	-1	-1	0	148.000	154.000	0.000	0.000
5	0	0	-1	-1	-1	0	220.000	154.000	0.000	0.000.
6	0	0	-1	-1	-1	0	250.000	154.000	0.000	0.000
7	0	0	-1	-1	-1	0	250.000	108.000	0.000	0.000
8	0	0	-1	-1	-1	0	250.000	0.000	0.000	0.000
9	0	0	-1	-1	-1	0	280.000	154.000	0.000	0.000
10	0	0	-1	-1	-1	0	376.000	154.000	0.000	0.000
11	0	0	-1	-1	-1	0	496.000	148.000	0.000	0.000
12	0	0	-1	-1	-1	0	496.000	0.000	0.000	0.000
13	0	0	-1	-1	-1	0	637.000	142.000	0.000	0.000
14	0	0	-1	-1	-1	0	697.000	142.000	0.000	0.000
15	0	0	-1	-1	-1	0	726.000	142.000	0.000	0.000
16	0	0	-1	-1	-1	0	726.000	0.000	0.000	0.000
17	0	0	-1	-1	-1	0	751.000	0.000	0.000	0.000
18	-1	-1	-1	-1	-1	-1	0.000	-50.000	0.000	0.000
19	-1	-1	-1	-1	-1	-1	50.000	0.000	0.000	0.000
20	-1	-1	-1	-1	-1	-1	250.000	-50.000	0.000	0.000
21	-1	-1	-1	-1	-1	-1	300.000	0.000	0.000	0.000
22	-1	-1	-1	-1	-1	-1	496.000	-50.000	0.000	0.000
23	-1	-1	-1	-1	-1	-1	546.000	0.000	0.000	0.000
24	-1	-1	-1	-1	-1	-1	751.000	-50.000	0.000	0.000
25	-1	-1	-1	-1	-1	-1	801.000	0.000	0.000	0.000

B / M BEAM ELEMENTS

NUMBER OF BEAMS	=	19
NUMBER OF GEOMETRIC PROPERTY SETS	=	14
NUMBER OF FIXED END FORCE SETS	=	0
NUMBER OF MATERIALS	=	1

MATERIAL PROPERTIES

MATERIAL NUMBER	YOUNG'S MODULUS	POISSON'S RATIO	MASS DENSITY	WEIGHT DENSITY	DMP
1	.3A00E+07	.2000	0.	0.	0.

BEAM GEOMETRIC PROPERTIES

SECTION NUMBER	AXIAL AREA A(1)	SHEAR AREA A(2)	SHEAR AREA A(3)	TORSION J(1)	INERTIA I(2)	INERTIA I(3)
1	.3A00E+04	.1200E+04	.1200E+04	.1000E+01	.1620E+06	.1620E+06
2	.8880E+03	.8880E+03	.8880E+03	.1000E+01	.1620E+07	.1620E+07
3	.1200E+04	.1200E+04	.1200E+04	.1000E+01	.1000E+07	.1000E+07
4	.5520E+03	.5520E+03	.5520E+03	.1000E+01	.3890E+06	.3890E+06
5	.3A00E+03	.3000E+03	.3600E+03	.1000E+01	.1080E+06	.1080E+06
6	.1200E+04	.1200E+04	.1200E+04	.1000E+01	.1000E+07	.1000E+07
7	.1200E+04	.1200E+04	.1200E+04	.1000E+01	.7800E+07	.7800E+07
8	.1560E+04	.1560E+04	.1560E+04	.1000E+01	.8490E+07	.8490E+07
9	.6840E+03	.6840E+03	.6840E+03	.1000E+01	.7800E+06	.7800E+06
10	.1200E+04	.1200E+04	.1200E+04	.1000E+01	.7800E+07	.7800E+07
11	.5280E+03	.5280E+03	.5280E+03	.1000E+01	.1400E+06	.1400E+06
12	.3A00E+04	.1200E+04	.1200E+04	.1000E+01	.1400E+07	.1400E+07
13	.1380E+04	.1380E+04	.1380E+04	.1000E+01	.1500E+07	.1500E+07
14	.3A00E+04	.3600E+04	.3600E+04	.1000E+01	.1000E+01	.1000E+01

1361 305

FIGURE D-10. INPUT DATA OF EQUIVALENT FRAME MODEL (SAP IV FORMAT)

BOUNDARY ELEMENTS

ELEMENT TYPE = 7
NUMBER OF ELEMENTS = 8

ELEMENT LOAD CASE MULTIPLIERS

CASE(A)	CASE(B)	CASE(C)	CASE(D)
0.0000	0.0000	0.0000	0.0000

ELEMENT NUMBER	NODE (N)	NODES DEFINING (NI)	(NJ)	CONSTRAINT DIRECTION (NK)	(NL)	CODE KD	CODE KR	GENERATION CODE (KN)	SPECIFIED DISPLACEMENT	SPECIFIED ROTATION	SPRING RATE	DAMPING
1	1	18	0	0	0	1	0	0	0.	0.	.4240E+07	0.00000
2	1	19	0	0	0	1	0	0	0.	0.	.1650E+07	0.00000
3	5	20	0	0	0	1	0	0	0.	0.	.2120E+07	0.00000
4	8	21	0	0	0	1	0	0	0.	0.	.1650E+07	0.00000
5	12	22	0	0	0	1	0	0	0.	0.	.2120E+07	0.00000
6	12	23	0	0	0	1	0	0	0.	0.	.1650E+07	0.00000
7	17	24	0	0	0	1	0	0	0.	0.	.4240E+07	0.00000
8	17	25	0	0	0	1	0	0	0.	0.	.1655E+08	0.00000

NODAL LOADS (STATIC) OR MASSES (DYNAMIC)

NODE NUMBER	LOAD CASE	X-AXIS FORCE	Y-AXIS FORCE	Z-AXIS FORCE	X-AXIS MOMENT	Y-AXIS MOMENT	Z-AXIS MOMENT
15	1	.7510OE+03	0.	0.	0.	0.	0.

FIGURE D-10. INPUT DATA OF EQUIVALENT FRAME MODEL (Cont.)

S/O BEAM ELEMENT DATA

BEAM NUMBER	NODE -I	NODE -J	NODE -K	MATERIAL NUMBER	SECTION NUMBER	ELEMENT END LOADS A	B	C	D	END CODES -I	-J
1	1	2	3	1	1	0	0	0	0	1	0
2	2	3	1	1	2	0	0	0	0	0	0
3	3	4	1	1	3	0	0	0	0	0	0
4	4	5	1	1	4	0	0	0	0	0	0
5	5	6	1	1	4	0	0	0	0	0	0
6	6	9	1	1	4	0	0	0	0	0	0
7	6	7	1	1	13	0	0	0	0	0	0
8	7	8	1	1	5	0	0	0	0	0	1
9	9	10	1	1	4	0	0	0	0	0	0
10	10	11	1	1	6	0	0	0	0	0	0
11	11	12	1	1	8	0	0	0	0	0	0
12	11	13	1	1	7	0	0	0	0	0	1
13	13	14	1	1	9	0	0	0	0	0	0
14	14	15	1	1	10	0	0	0	0	0	0
15	15	16	1	1	11	0	0	0	0	0	0
16	16	17	15	1	12	0	0	0	0	0	1
17	2	8	3	1	14	0	0	0	0	1	1
18	8	12	3	1	14	0	0	0	0	1	1
19	12	16	3	1	14	0	0	0	0	1	1

FIGURE D-10. INPUT DATA OF EQUIVALENT FRAME MODEL (Cont.)

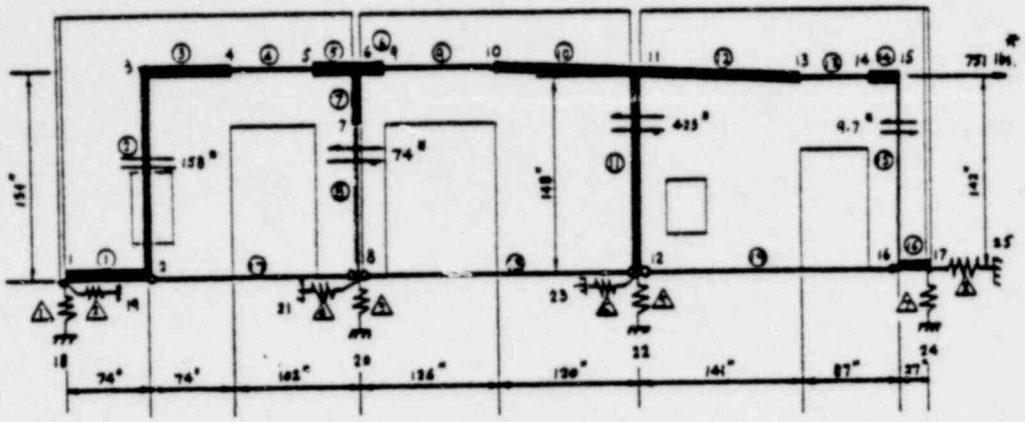

Before first hinging of Pier # 2

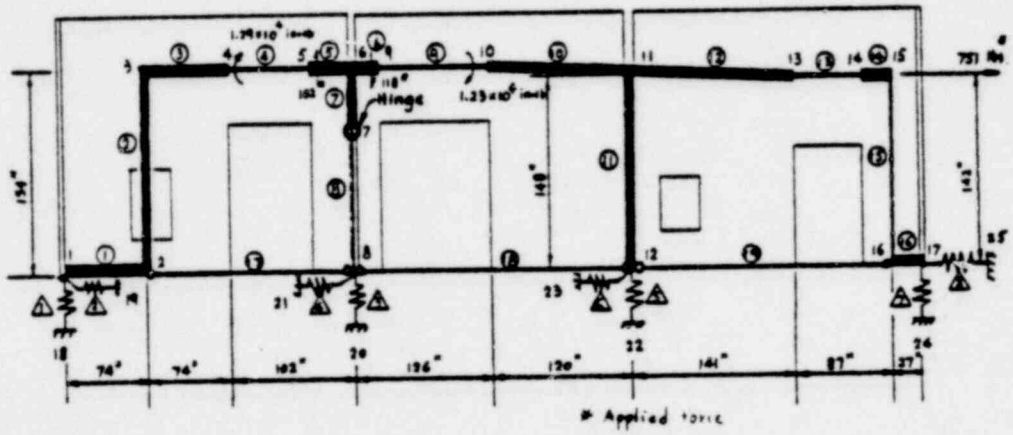

* Applied force

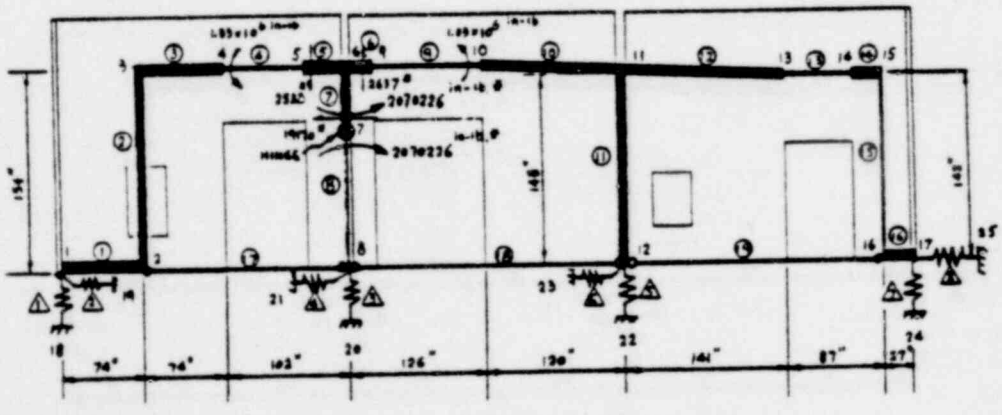

Moment capacity of Pier # 2 (Applied moment)

After hinge forms at Pier # 2

FIGURE D-11. STATIC ANALYSIS RESULTS OF THE EQUIVALENT FRAME

APPENDIX E

SELECTED STRUCTURAL DATA AND DETAILS FROM TASK I REPORT

EDAC

Table 4-2a - Steel Members

Structural Component	Member Designation	Depth (in.)	Area ($in.^2$)	Moment of Inertia	
				Major Axis, Ixx ($in.^4$)	Minor Axis, Iyy ($in.^4$)
Roof Framing - Girder	27 W 114	27.28	33.6	4090	159
Main Framing - Column	8 W 31	8.00	9.12	110	37
Roof Framing - Beam	10 W 21	9.90	6.20	107	10.8
Roof Diaphragm - Chord	8 C 13.75	8.00	4.04	36.1	1.53
Roof Diaphragm & Mezzanine Deck	Robertson FK I 16-16	4.50	—	7.57 (per 12 in.)	—
Mezzanine Framing - Floor Beam	12S40.8 , 7C9.8	12.366	14.87	343.3	34.9
Mezzanine Framing - Floor Beam	10 W 54	10.12	15.9	306	104
Mezzanine Framing - Floor Beam	10 W 45	10.12	13.2	249	53.2
Mezzanine Framing - Column	3" Extra Strong Pipe	—	2.23	3.02	1.72
Lateral Bracing for Exhaust Stack	2L4 x 3 x 3/8	—	4.97	3.84	1.73

Table 4-2b - Concrete Shear Walls

Wall	Thickness (in.)	Wall Shear Area (in^2)*	(10^6 $in.^4$)* Wall Moment of Inertia ($in.^4$)*
North Wall	7.5	5002	252
South Wall	6.0	2635	126
East Wall	6.0	13840	6789
West Wall	6.0	13244	6274

* Based on Net Wall Section

1361 310

EDAC

TABLE 4-3. STRUCTURAL MATERIAL PROPERTIES

Structural Element	Material Identification	Yield Strength				Ultimate Strength				Modulus of Elasticity	Comments
		Min. Spec. (ksi)	Lower Bound (ksi)	Median (ksi)	Upper Bound (ksi)	Min. Spec. (ksi)	Lower Bound (ksi)	Median (ksi)	Upper Bound (ksi)	E, psi x 10^6 (Median)	
Plate, Rolled Shapes and Miscellaneous Structural Steel	ASTM A36	36	40	44	48.5	58	64	68	73	29.0	Max. Spec. = 80 ksi
Steel Roof Deck	ASTM A245	—	33	38	45	—	—	—	54	29.0	
Reinforcing Steel	ASTM A15 Intermediate (ASTM A615) Grade	40	44[a]	48[a]	52[a]	70	76	80	85	29.0	Reference 14 Data
Structural Bolting, Connections, and Anchor Bolts	ASTM A307	36	40	44	49	60	64 (42)	68 (48)	73 (56)	29.0	Tension (shear)
Concrete Walls and Footings	Structural Concrete @ 28 days	—	—	—	—	3	3.4 (2.9)	4.0 (3.4)	4.7 (4.0)	3.6	Compression (Bolt Bearing)
Concrete Inserts		—	—	—	—	—	8.5*	10.1*	12.2*	—	Bolt Pullout
Welding	E 70	—	—	—	—	—	40	47	56	—	Shear
Pipe Column	ASTM A53 Grade B	35	39.5	43	47	60	65	69	74	29.0	

NOTE: All values are tensile unless otherwise noted

* In kips

TABLE 4-1 COLUMN AND FOOTING DATA

Location By Column Line*	Column	Footing	
		Size	Reinforcing
All on Lines A & L	8W 31	4'-2" x 4'-2" x 1'-2"	4-#5 Ea. Way
B-1 thru K-1, F-4, G-4, K-4	8W 31	6'-4" x 6'-4" x 1'-2"	9-#6 Ea. Way
B-4, E-4	8W 31	6'-6" x 6'-6" x 1'-2"	10-#6 Ea. Way
H-4, J-4	8W 31	6'-8" x 6'-8" x 1'-2"	11-#6 Ea. Way
C-4, D-4	8W 31	7'-0" x 7'-0" x 1'-2"	13-#6 Ea. Way
C_1-2A, D_1-2A, B_1-3A	3" Extra Strong Pipe	2'-6" x 2'-6" x 1'-2"	3-#5 Ea Way
D_1-3A	3" Extra Strong Pipe	3'-0" x 3'-0" x 1'-2"	3-#5 Ea. Way
C_1-3A	3" Extra Strong Pipe	4'-0" x 4'-0" x 1'-2"	4-#5 Ea. Way

* See Figure 4-1 Foundation Plan

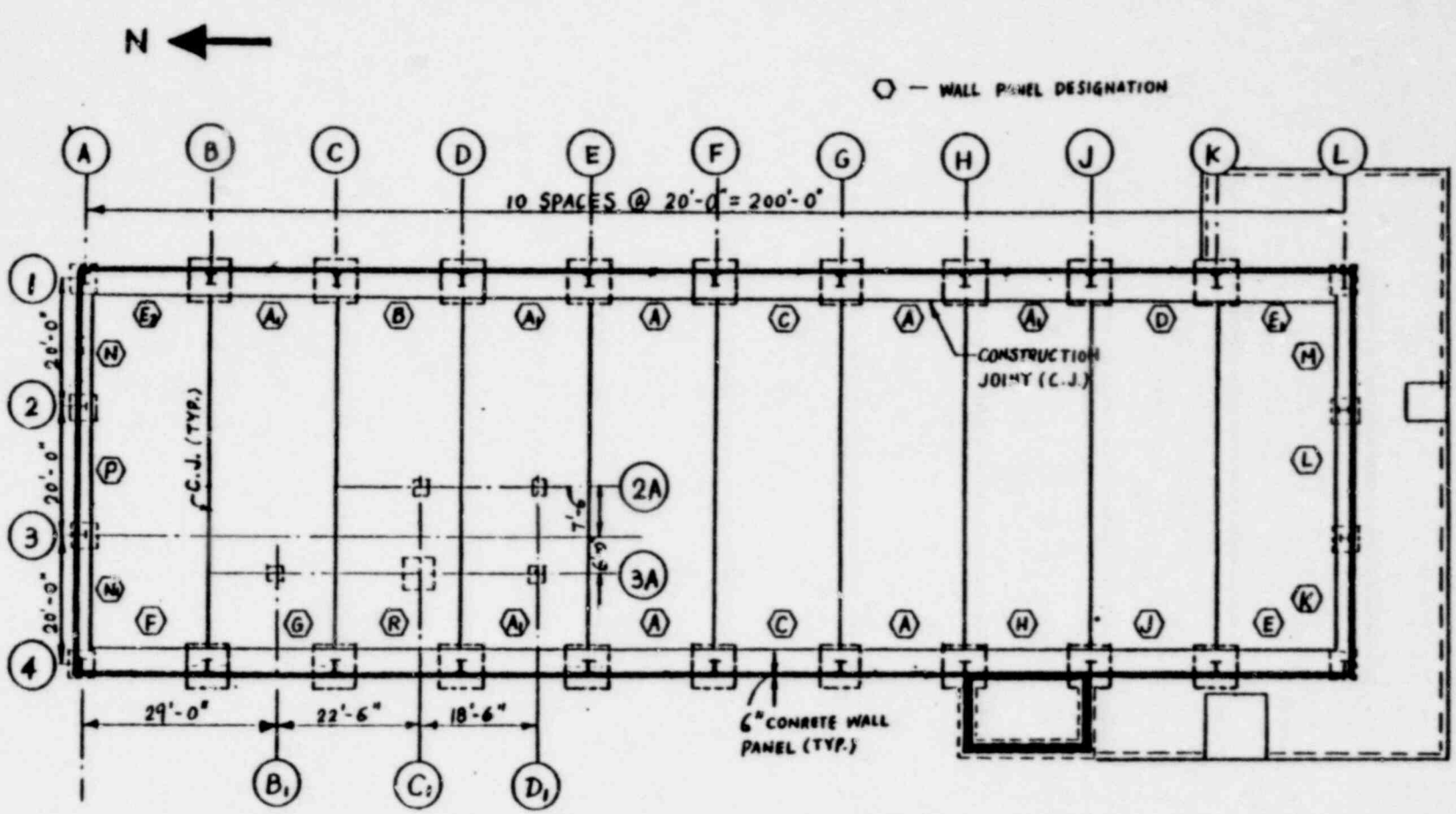

FIGURE 4-1. FOUNDATION PLAN

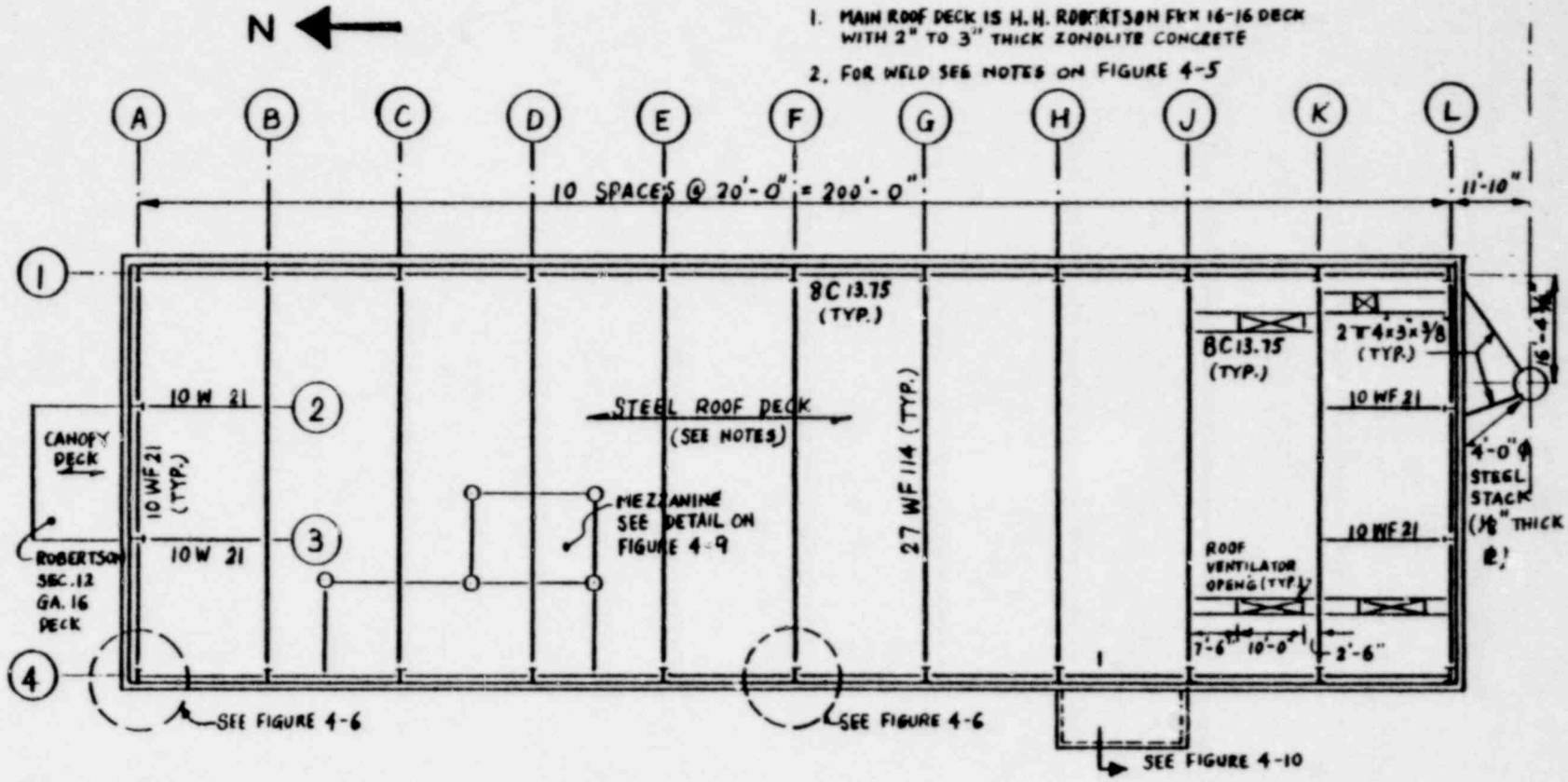

FIGURE 4-2. ROOF FRAMING PLAN

NOTES : ALL WELDS ARE ½"ϕ EFFECTIVE SPACED AS FOLLOWS :
1. 5 WELDS PER PANEL AT EACH SUPPORT (ROOF BEAM)
2. AT PERIMETER AND OPENINGS PARALLEL TO SEAM AT 4'-0" O.C.
ROOF DECK SEAM WELD :
1½" LONG WELD AT TOP OF SEAM AT 20" O.C.

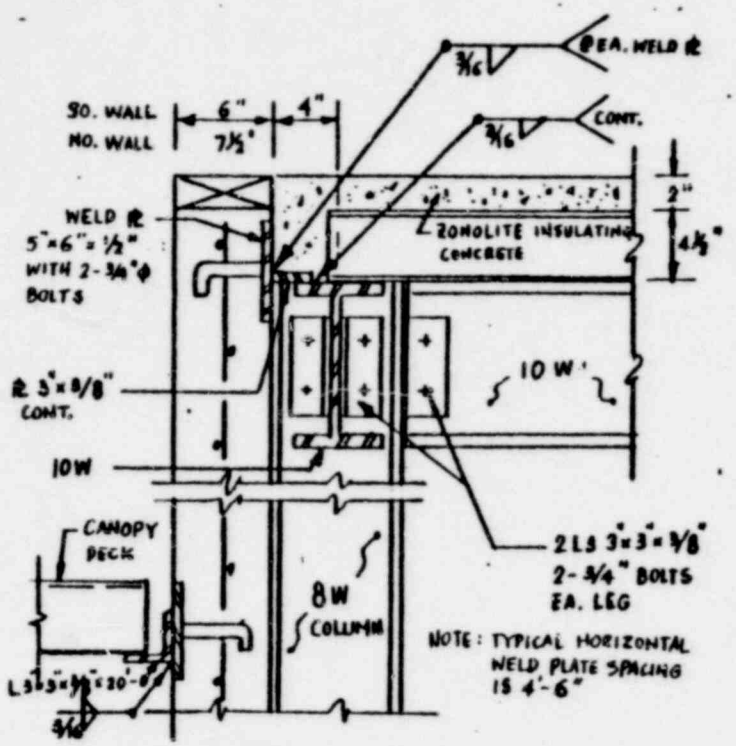

DIAPHRAGM CONNECTION AT NORTH AND SOUTH WALLS

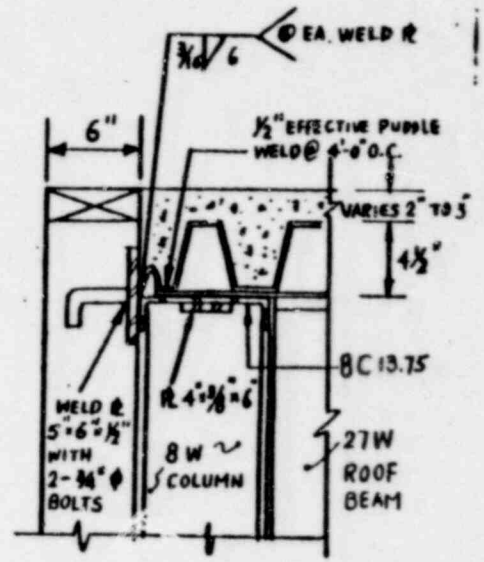

NOTE : ANCHOR BOLTS -- FULL PENETRATION WELD TO WELD PLATES, TYPICAL

DIAPHRAGM CONNECTION AT EAST AND WEST WALLS

FIGURE 4-5. TYPICAL ROOF DIAPHRAGM CONNECTION AT WALLS

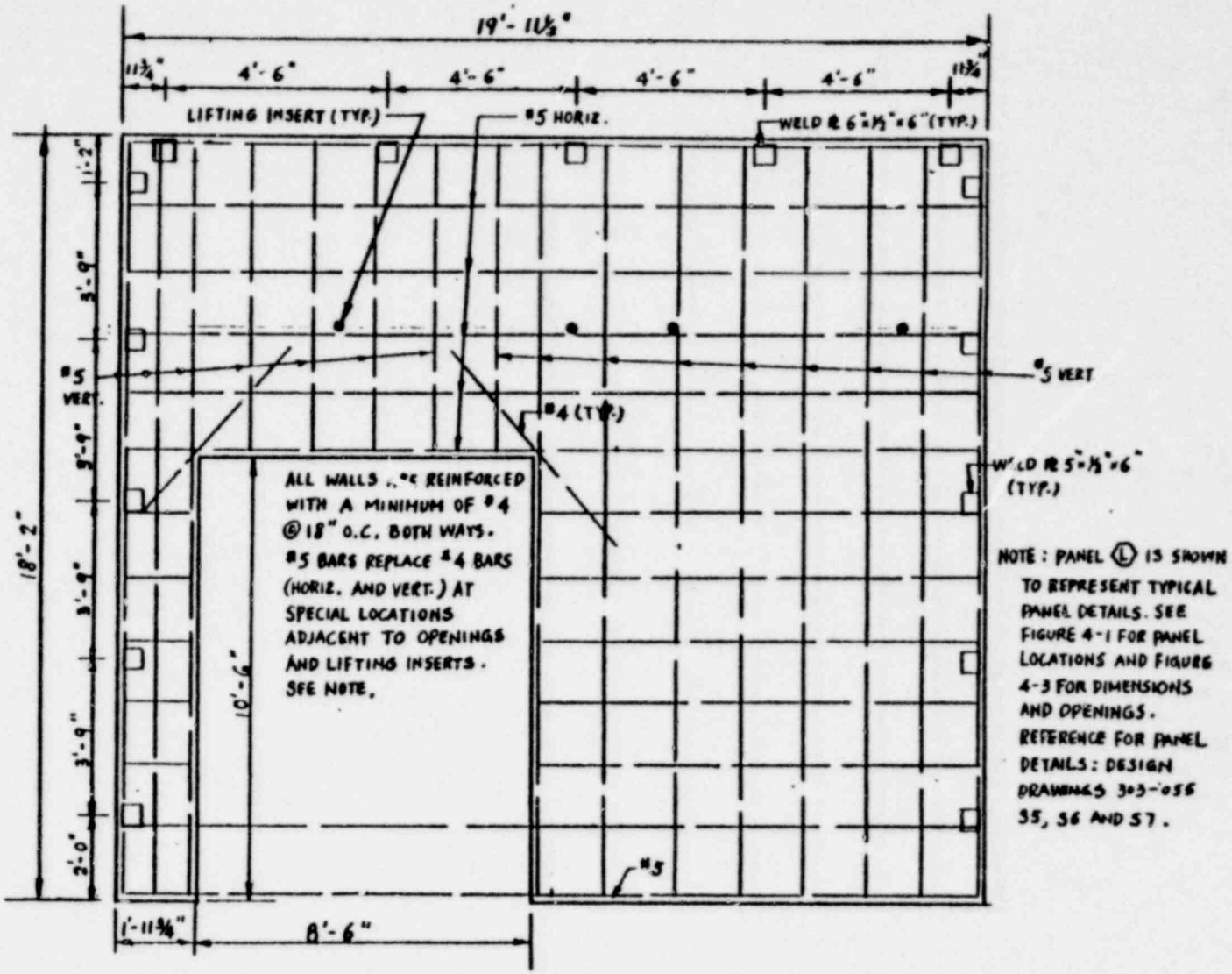

FIGURE 4-7. WALL PANEL DETAILS

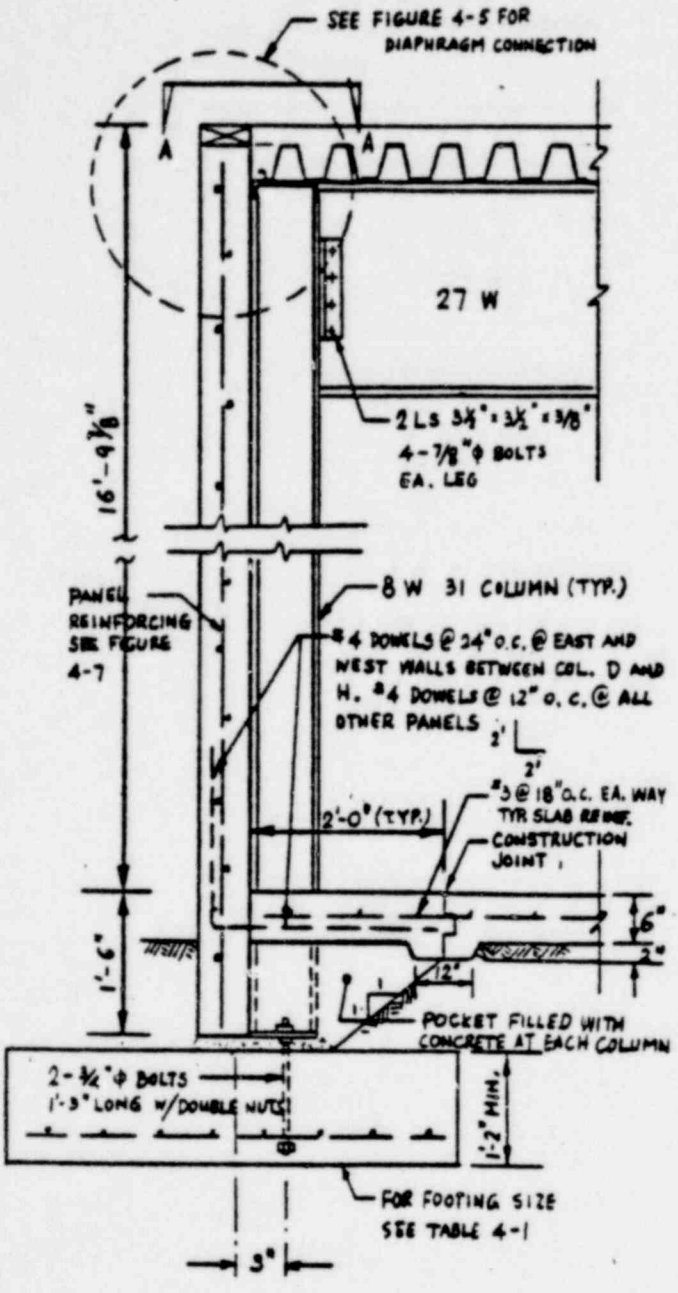

WALL SECTION

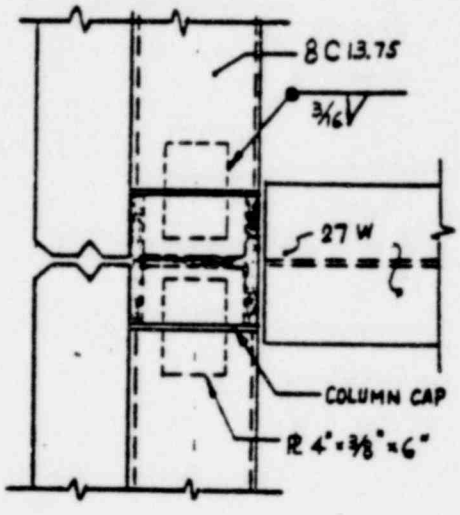

DETAIL A-A

1361 317

FIGURE 4-8. TYPICAL SECTION — EAST AND WEST WALLS
(NORTH AND SOUTH WALLS SIMILAR)

EDAC

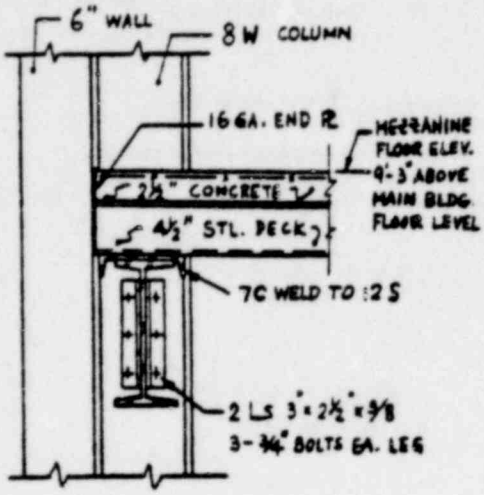

SIDE WALL SECTION AT MEZZANINE

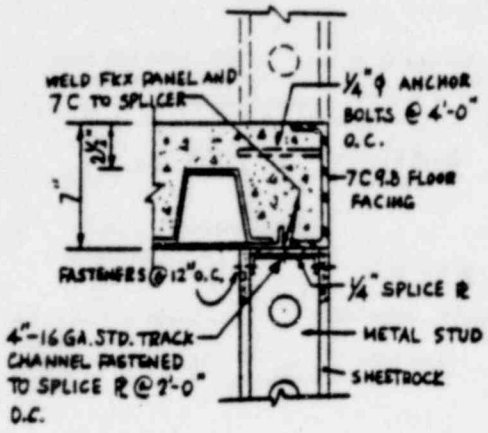

DETAIL OF STUD WALL TO MEZZANINE FLOOR CONNECTION

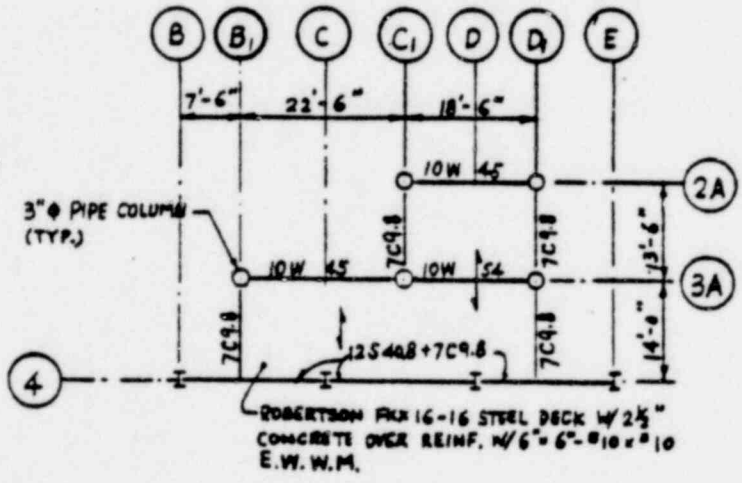

MEZZANINE FRAMING PLAN

FIGURE 4-9. MEZZANINE DETAILS

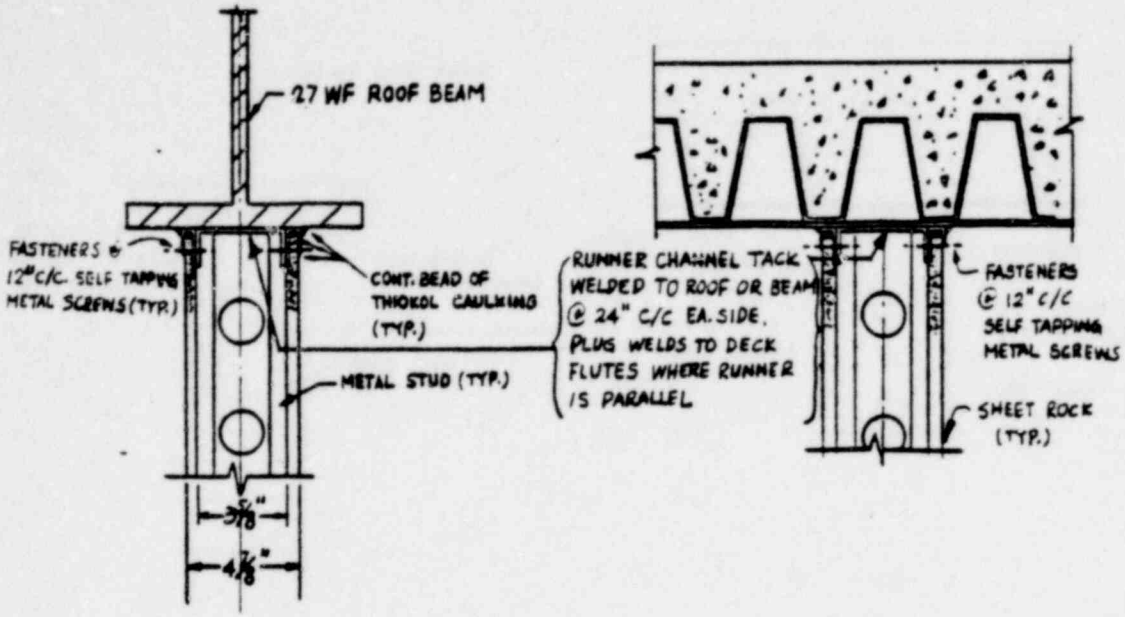

TYPICAL STUD WALL TO BEAM CONNECTION

TYPICAL STUD WALL TO METAL PAN CONNECTION

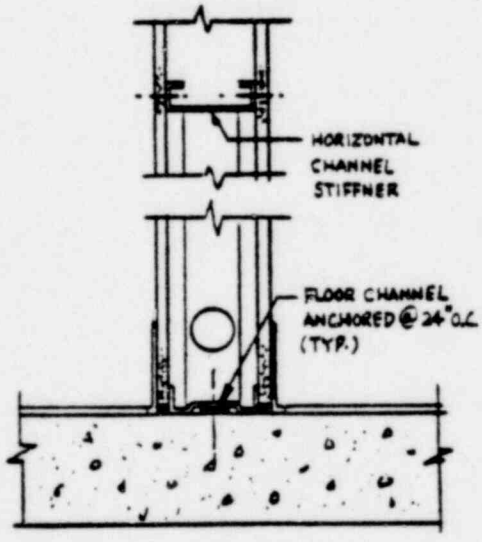

TYPICAL STUD WALL TO CONCRETE FLOOR CONNECTION

FIGURE 4-11. INTERIOR PARTITION DETAILS

1361 319

EDAC

TABLE 5-1. SUMMARY OF DATA FOR GLOVE BOXES

Glove Box Name Glove Box Name	Station No.	Box No.	Box Size (in.xin.xin.)	Box Weight (lbs.)	Support Stand Weight (lbs.)	Comment
Air Entrance	1	K-1	36x30/23x33	350	150	Trapezoid Side
Air Entrance	1A	K-1A	36x30/23x33	350	150	23" - upper dimension
Inert Gas Entrance	2	K-2	36x30/23x33	350	150	30" - lower dimension
Inert Gas Entrance	2A	K-2A	36x30/23x33	350	150	
Blend Box	3 *	K-3	84x42x42	1200	400	
Weigh Box	3A	K-3A	42x42x48	700	—	
Unload Box - Sinter Furnace	4 **	B-1	84x30x42	900	300	
Dry & Mill Box	5 *	K-11	84x42x42	1200	400	
Load Box - Sinter Furnace	6 **	B-2	84x30x42	900	300	
Press Box	7 **	K-7	84x42x48	1800	400	2" thick steel plate installed in the box
O.D. Grind Box	8 **	K-8	84x42x48	1800	400	2" thick steel plate installed in the box
Granulator & Screening Box	9	K-6	84x42x42	1200	400	
Transfer Box	10	B-3	42x24x42	500	280	
Inspection Box	11	B-8	84x42x48	1200	400	
Weigh Box	12	K-12A	42x24x42	500	—	
Pin Loading Box	13	K-12	84x42x42	1200	400	
Waste Packaging Box	14	K-14	84x42x42	1200	400	
Dissolution & Sample Preparation	15 **	K-15	84x42x42	1200	400	
Balance Box	15A	K-15A	42x24x42	500	—	
X-ray Fluoresence Box	16 **	K-16	42x42x42	700	280	
Emission Spectrograph Half Box	17 **	K-17	42x42x42	700	280	
Arc Spark Box	17A	K-17A	42x24x42	700	—	
Inert Gas Fusion Box	18 **	K-18	84x42x42	1200	400	
Metallography Preparation	19 **	K-19	84x42x42	1200	400	
Metallography Observation	20 **	K-20	84x42x42	1200	400	
Wet Chemistry Box	21 **	K-21	84x42x42	1200	400	
TGA Equipment Box	22 **	K-5	84x42x42	1200	400	
	23					Deleted, Move B-3 to Sta. 10
Power Processing Box	24	K-13	142x45x48	2400	800	
	25					Stub Outs Only for Future Box
Sintering Furnace Box	26	K-4	84x42x48	1200	400	
Pellet Pressing & Granulator	27	K-9	84x42x42	1200	400	
Transfer Box	28	B-4	69x24x42	800	400	Estimated Box Size
Arc Casting Box	29	B-5	72x42x42	1000	400	Estimated Box Size
Fuel Pin Weld Box	30	B-7	48x32x33	500	280	
Glove Box (AEC)	31 *		84x42x42	1200	400	

* Boxes of Most Concern

** Boxes of Secondary Concern

TABLE 5-2. EQUIPMENT STRUCTURAL MEMBER PROPERTIES

Equipment Item	Component Designation	Depth (in.)	Thickness (in.)	Area ($in.^2$)	Unit Weight	Moment of Inertia, I ($in.^4$)	Section Modulus S ($in.^3$)
Glove Box	Stainless Steel Sheet Metal (8 ga.)	—	0.105	—	4.3 lb/ft^2	1.16×10^{-3} (per 12 in.)	2.21×10^{-2} (per 12 in.)
	Stainless Steel Sheet Metal (12 ga. at Top & Ends)	—	0.164	—	6.7 lb/ft^2	4.41×10^{-3} (per 12 in.)	5.38×10^{-2} (per 12 in.)
	Window Frame Angle 12 ga. 1-1/2" x 7/8"	—	0.105	0.24	0.8 lb/ft	$5.6 \times 10^{-2}/1.7 \times 10^{-2}$	$5.7 \times 10^{-2}/2.5 \times 10^{-2}$
Glove Box Support Stand	Grating Bars 3/16" x 1	1.0	0.1875	0.19	7.7 lb/ft	$1.5 \times 10^{-2}/5.5 \times 10^{-4}$	$3.2 \times 10^{-2}/5.86 \times 10^{-3}$
	S S 7.5 Beam	3.0	—	2.21	7.5 lb/ft	2.93/0.59	1.95/0.47
	S S 10 Beam (Boxes 7 & 8)	5.0	—	2.94	10.0 lb/ft	12.3/1.22	4.92/0.81
	3 C 4.1	3.0	0.273	1.21	4.1 lb/ft	1.66/0.20	1.10/0.20
	1" ¢ Tube Leg (11 ga.)	1.0	0.12	0.33	1.1 lb/ft	3.2×10^{-2}	6.4×10^{-2}
	2-1/4" ¢ Tube Leg (11 ga.)	2.25	0.12	0.80	2.7 lb/ft	0.46	0.41
	Leveling Bolt 3/4" ¢	0.62	—	0.30	—	7.3×10^{-3}	2.3×10^{-2}
Glove Box Room Exhaust Ductwork	8" ¢ Sch. 10 Pipe	8.33	0.148	3.94	13.4 lb/ft	35.4	8.22
Room Exhaust Ductwork	36" x 30" Duct (22 ga.)	30	0.030	3.95	19.4 lb/ft	619/814	41.28/45.24
Air Supply Ductwork	34" x 44" Duct (22 ga.)	44	0.030	4.67	22.9 lb/ft	1410/957	64.09/56.30
Exhaust Stack	4'-0" ¢ 1/8"thk	48	0.125	18.80	64.0 lb/ft	5.4×10^3	2.2×10^2
Storage Container	4" ¢ Sch. 40 Pipe	4.5	0.237	3.17	10.8 lb/ft	7.23	3.21
Storage Rack Frame	2-8 [ ] 11.5	8.0	0.390	6.76	23.0 lb/ft	65.2/21.9	16.28/9.69
	4 C 5.4	4.0	0.296	1.59	5.4 lb/ft	3.85/0.32	1.93/0.28
	L 3 x 2 x 1/4	3.0	0.25	1.19	4.1 lb/ft	1.09/0.39	0.54/0.26
	2-6][13	6.0	0.343	7.66	26.0 lb/ft	34.8/4.12	11.6/1.91

TABLE 5-3. EQUIPMENT MATERIAL PROPERTIES (TENSILE UNLESS NOTED)

Equipment Component	Material Identification	Yield Strength				Ultimate Strength				Modulus of Elasticity - E, (ksi x 10 average)
		Min. Spec. (ksi)	Lower Bound (ksi)	Median (ksi)	Upper Bound (ksi)	Min. Spec (ksi)	Lower Bound (ksi)	Median (ksi)	Upper Bound (ksi)	
Glove Box Structure and Attachments	Type 304 Stainless Steel	25 (0.2% offset)	30	34	38.5	70	81	85	89	28.3
Glove Box Support Stand, Storage Rack Frame	ASTM A36	36	40	44	48.5	58	64	68	73	29.0
Glove Box Support Stand Pipe Legs & Storage Containers	ASTM A53 Grade B	35	39.5	43	47	60	65	69	74	29.0
Glove Box Leveling Bolts, Pipe and Duct Supports, Miscellaneous Bolting and Connections	ASTM A307	36	40	44	48.5	58	64	68	73	29.0
Glove Box Window	3/8" Plexiglass	—	—	—	—	—	12**	16**	21**	0.45 (0.35-0.50)
Glove Box Welded Studs Ultimate Tensile Load	Type 304 Stainless Steel	—	—	—	—	—	2400*	2800*	3300*	—
Maximum Shear Load		—	—	—	—	—	1800*	2100*	2500*	—
Exhaust Duct	ASTM A446 Grade A	33	38	41	45	45	49.5	54.5	60	29.0
Glove Box Support Stand Tie Down to Floor	OMARK Powder Actuated Fasteners	—	—	—	—	Pullout	844	1003	1211	—
						Shear	1170	1404	1658	

* KIPS

** Flexural Modulus of Rupture

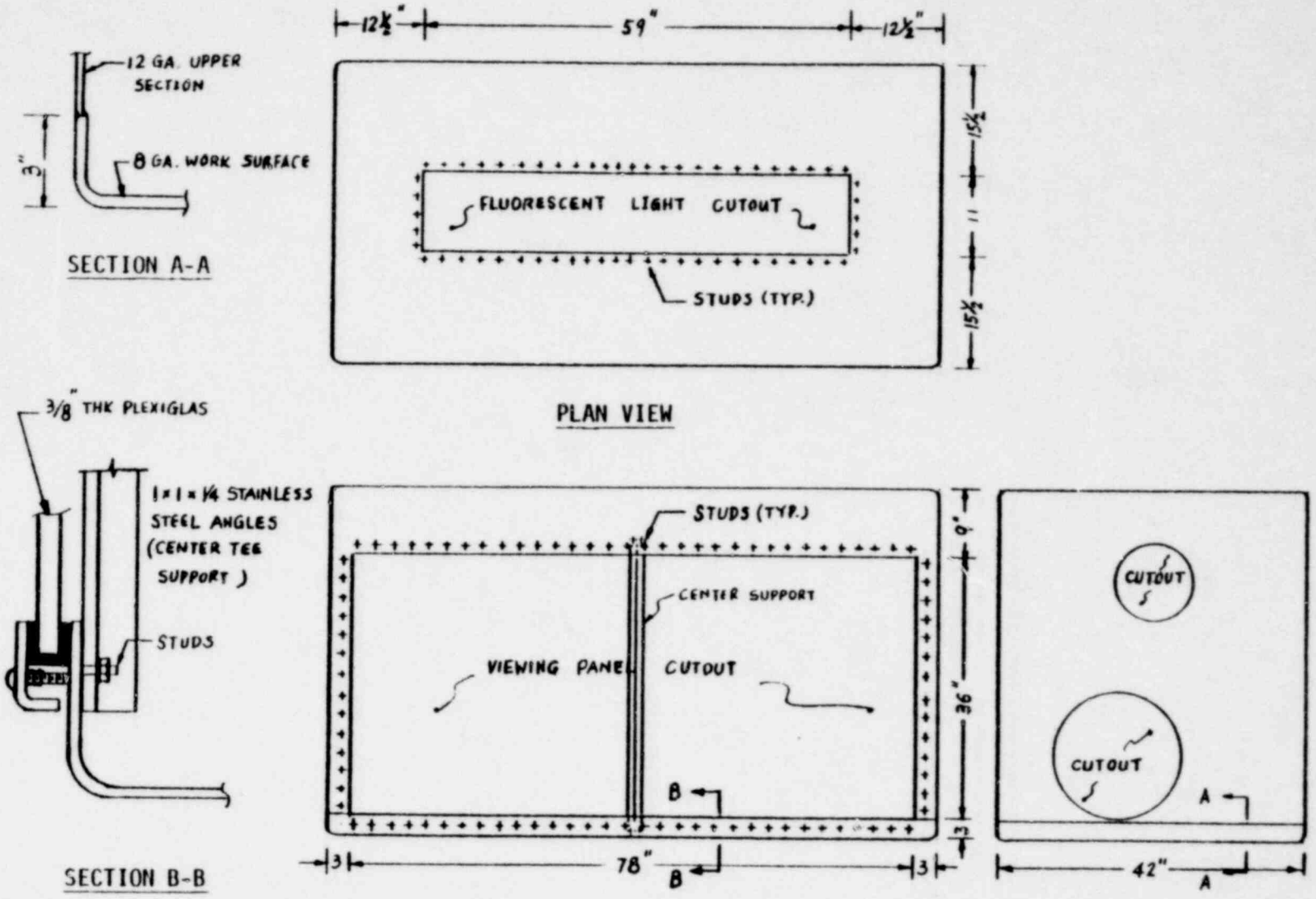

FIGURE 5-4. BASIC GLOVE BOX STRUCTURE AND DETAILS

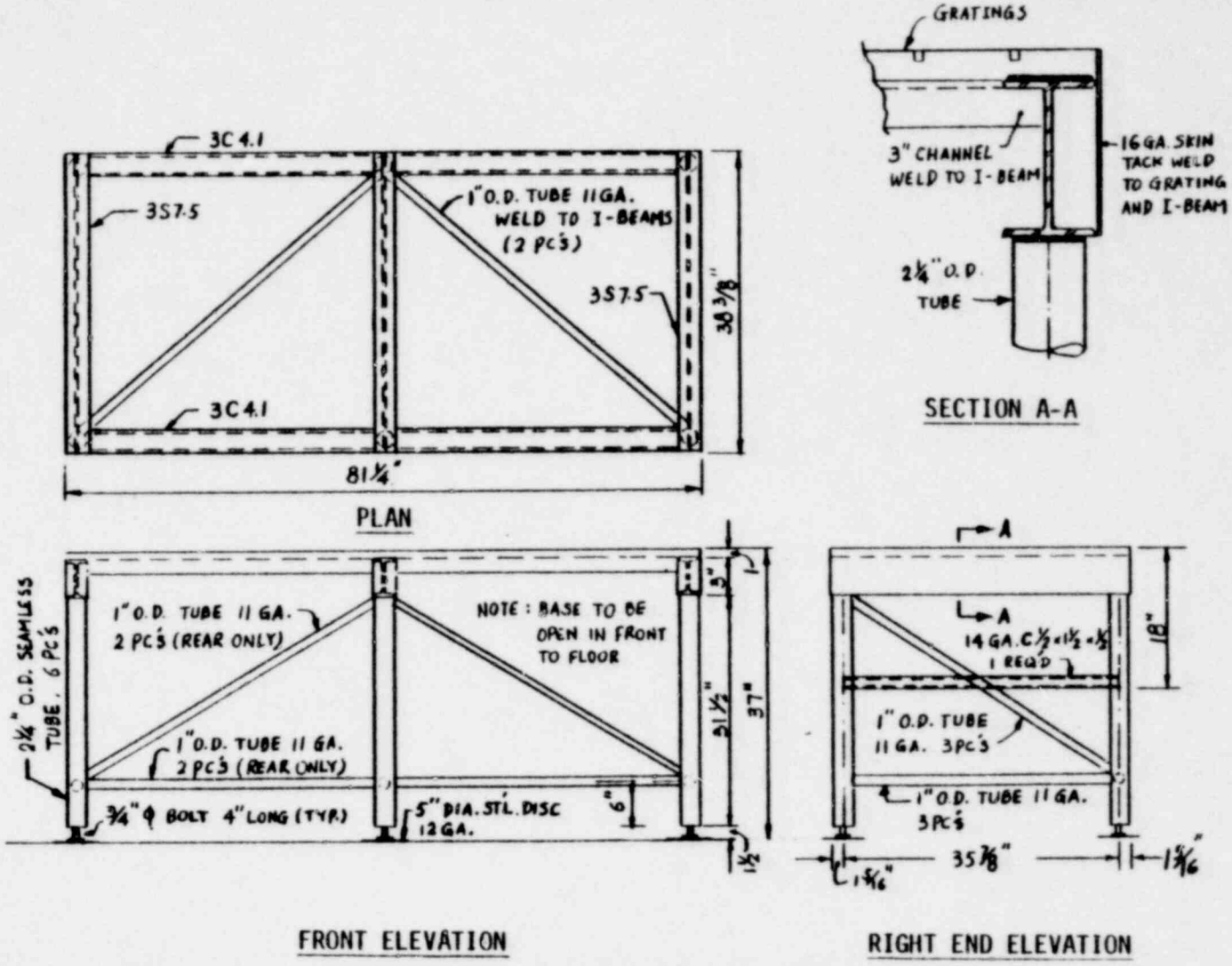

FIGURE 5-5. GLOVE BOX SUPPORT FRAME

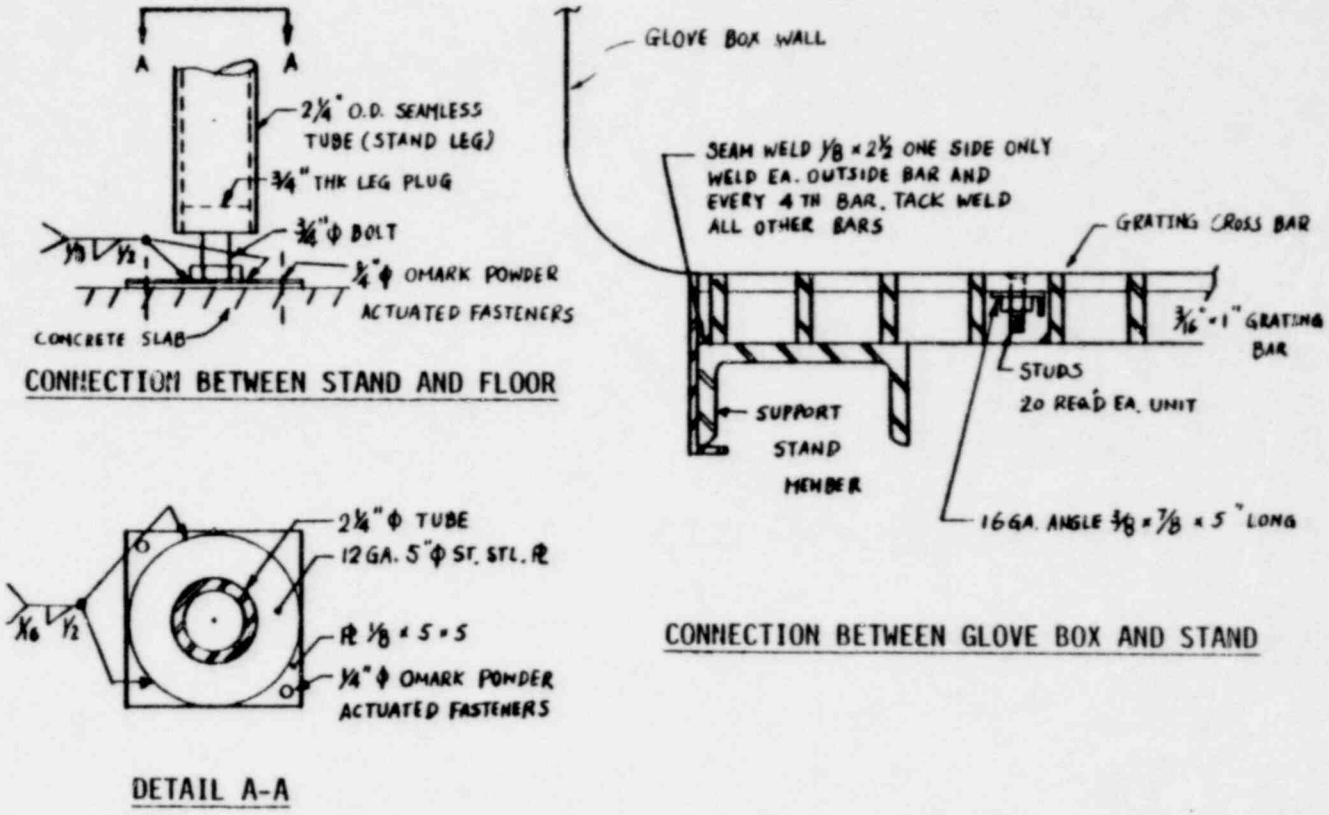

FIGURE 5-6. GLOVE BOX AND SUPPORT FRAME ANCHORAGE DETAILS

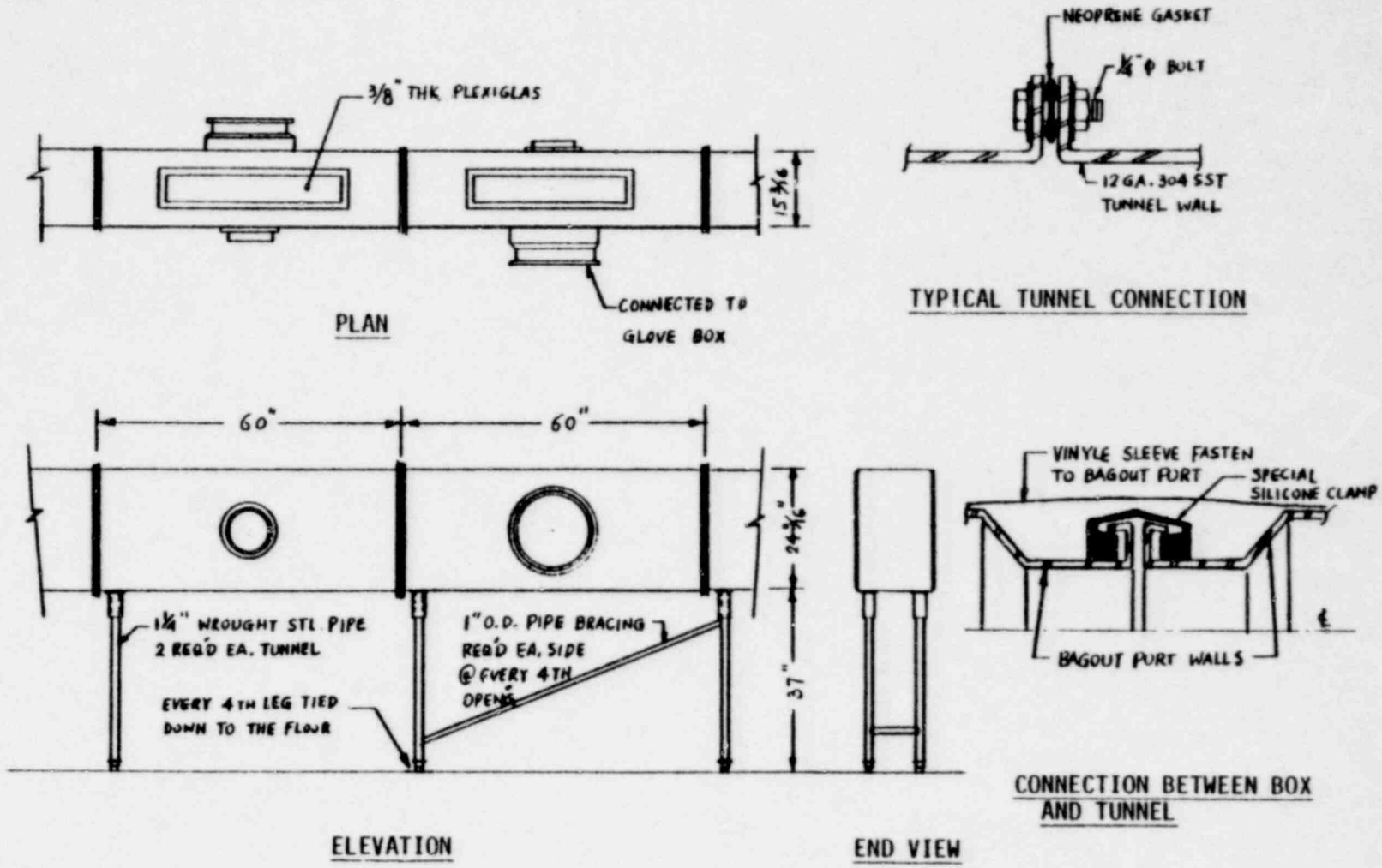

FIGURE 5-7. TRANSFER TUNNEL ASSEMBLY AND DETAILS

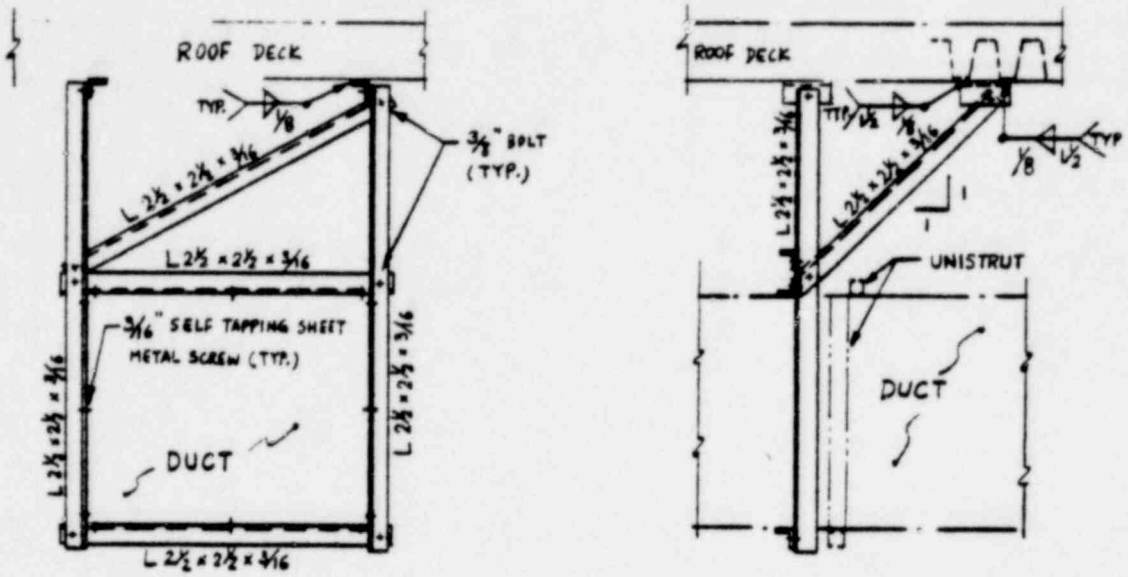

FIGURE 5-9. DUCTWORK SUPPORT AND BRACING

1361 527

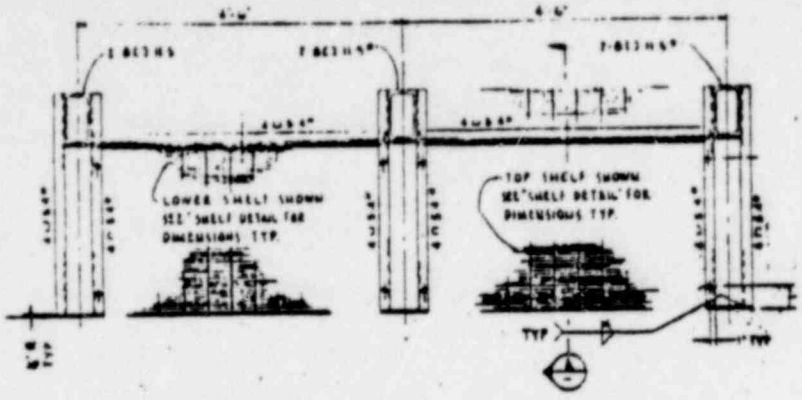

TOP PLAN

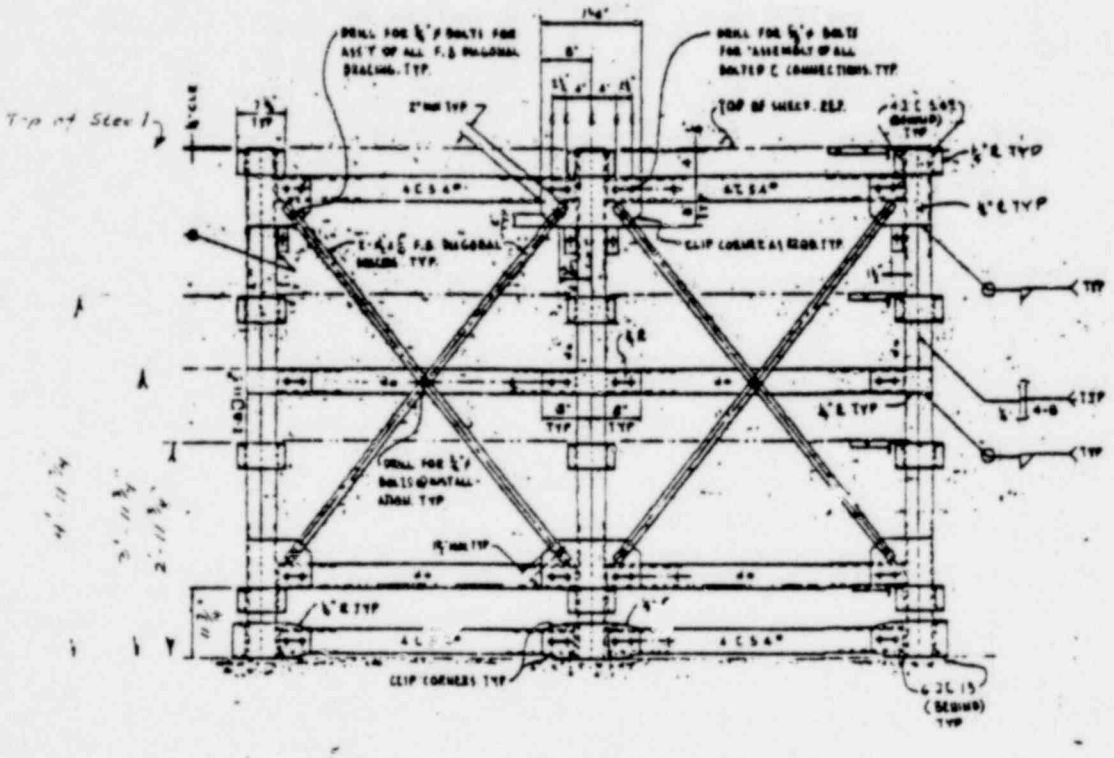

FRONT ELEVATION

VAULT STORAGE RACK

DETAILS

1361 323

EDAC

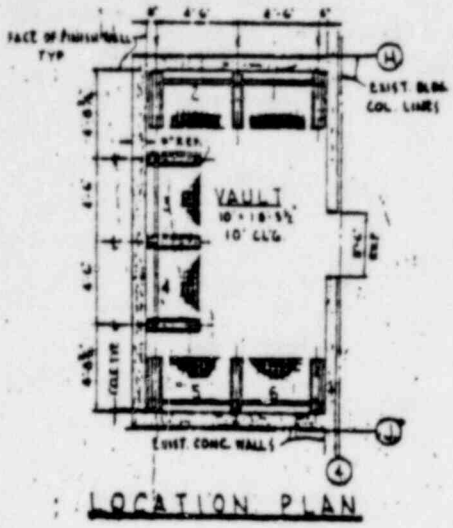

LOCATION PLAN

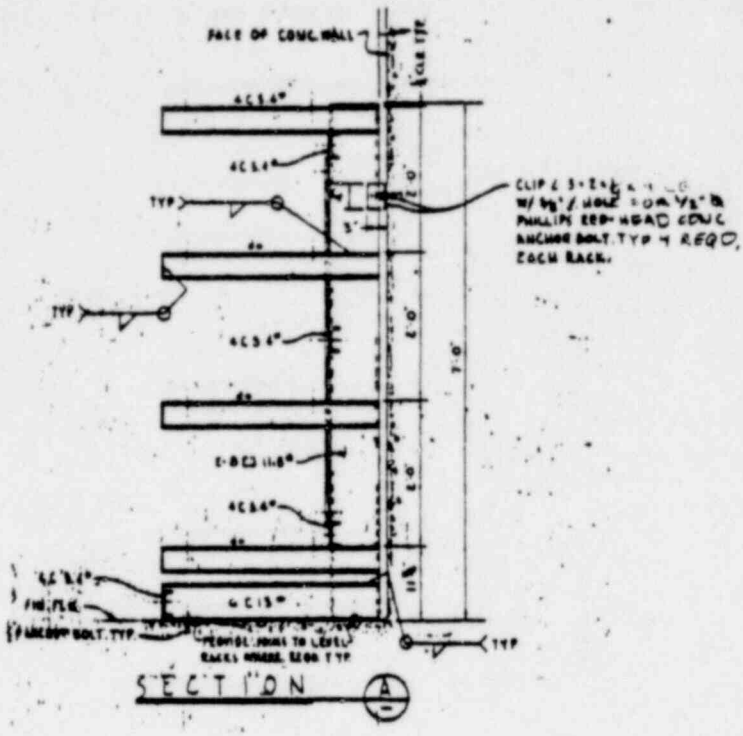

SECTION A

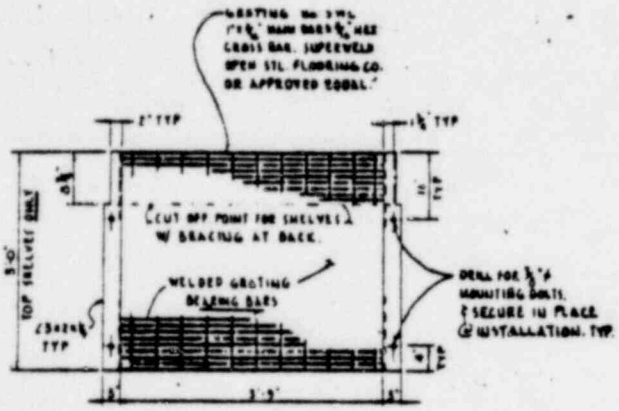

PLAN

SHELF DETAIL

VAULT STORAGE RACK DETAILS

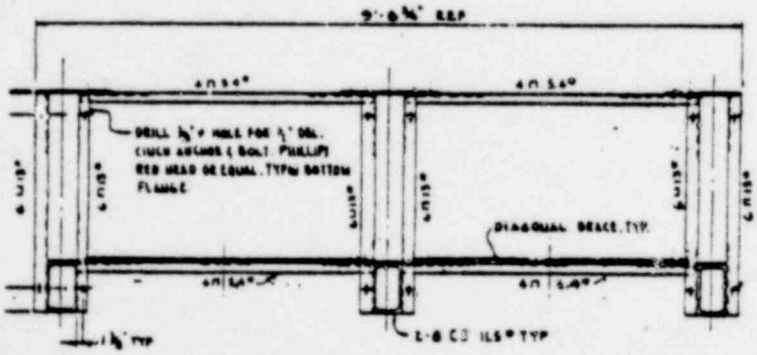

BOTTOM PLAN

1361 329

EDAC